Variation of the mechanical properties of the natural rubber used in bridges' bearings and seismic isolators in Canada

by

Mohammadreza YAVARITAJ

THESIS PRESENTED TO ÉCOLE DE TECHNOLOGIE SUPÉRIEURE
IN PARTIAL FULFILLMENT FOR A MASTER'S DEGREE
WITH THESIS IN CONSTRUCTION ENGINEERING
M.A.Sc.

MONTREAL, AUGUST 12, 2024

ÉCOLE DE TECHNOLOGIE SUPÉRIEURE
UNIVERSITÉ DU QUÉBEC

BOARD OF EXAMINERS

THIS THESIS HAS BEEN EVALUATED

BY THE FOLLOWING BOARD OF EXAMINERS

Mr. Lotfi Guizani, Thesis Supervisor
Department of Construction Engineering at École de technologie supérieure

Mr. Gabriel Lefebvre, President of the Board of Examiners
Department of Construction Engineering at École de technologie supérieure

Mr. Amar Khaled, Member of the jury
Department of Construction Engineering at École de technologie supérieure

THIS THESIS WAS PRESENTED AND DEFENDED

IN THE PRESENCE OF A BOARD OF EXAMINERS AND PUBLIC

ON JULY 30, 2024

AT ÉCOLE DE TECHNOLOGIE SUPÉRIEURE

ACKNOWLEDGMENTS

First, I would like to extend my heartfelt thanks to my research director, Mr. Lotfi Guizani, for granting me the opportunity to work within the framework of his research programs. His scientific expertise, along with his availability and advice, has been invaluable throughout this journey.

I am also deeply grateful to the Jacques Cartier and Champlain Bridges Incorporated (JCCBI) for their financial support and to Goodco Z-Tech, a Division of Canam Bridges, for providing some of the specimens essential for this research.

My sincere thanks go to the ETS DRSR Heavy Structures and LCMB Laboratories' technicians, Mr. Jonathan Auger and Mr. Francis Bilodeau, for their help, availability, and expert advice during the testing phases.

Lastly, I would like to express my deepest gratitude to my parents for their constant support and encouragement. Your unwavering belief in me has been a source of inspiration and strength throughout this journey. Your love and guidance have been invaluable, and I am eternally grateful for everything you have done to help me achieve this milestone. I love you more than words can express.

Variation des propriétés mécaniques du caoutchouc naturel utilisé dans les appuis et isolateurs sismiques pour ponts au Canada

Mohammadreza YAVARITAJ

RÉSUMÉ

L'isolation sismique de la base est un système antisismique largement utilisé pour protéger les structures des dommages induits par les tremblements de terre, en se concentrant sur l'atténuation de la demande sismique au lieu d'augmenter uniquement la capacité de résistance sismique de la structure. Les isolateurs à base d'élastomères sont l'un des systèmes couramment utilisés dans l'isolation sismique des ponts. Les élastomères utilisés dans les isolateurs sont principalement classés en deux catégories principales: Le polyisoprène (caoutchouc naturel) et le polychloroprène (caoutchouc synthétique connu sous le nom de néoprène). Les propriétés mécaniques de ces élastomères jouent un rôle crucial dans les performances et le comportement du système d'isolation. Cependant, ces propriétés sont variables et sont influencées par plusieurs facteurs, notamment les basses températures, le vieillissement, ainsi que la fabrication et la source des matériaux. L'exposition à de basses températures augmente la rigidité et l'hystérésis des élastomères, provoquant des variations dans leurs propriétés mécaniques clés qui modifient la réponse sismique des isolateurs sismiques et affectent la performance sismique de la structure.

Dans cette étude, la variation des propriétés mécaniques du caoutchouc naturel, couramment utilisé dans les applications d'isolation sismique et les appuis laminés pour les ponts au Canada, est étudiée expérimentalement. Quatre sources différentes de caoutchouc naturel, y compris le caoutchouc vieilli provenant des appuis récupérés du pont Champlain d'origine et le caoutchouc neuf, sont considérées pour établir la variation des propriétés mécaniques en fonction de la source, de l'âge, de la durée du conditionnement, de la température d'essai ainsi que de la fréquence des cycles. Les échantillons de chaque source de caoutchouc naturel sont conditionnés à différentes températures, à savoir 23ºC, -8ºC et -30ºC, pour différentes durées, allant de 1 heure à 28 jours. Des essais expérimentaux sont effectués, aux températures de conditionnement, sur des échantillons à quadruple cisaillement. Ils consistent à imposer une séquence de trois cycles de cisaillement d'une amplitude de déformation croissante allant de 25 à 150 %. Les essais ont été réalisés à différentes fréquences (0,1, 0,25 et 0,5 Hz). Les résultats des essais sont utilisés pour extraire les propriétés caractéristiques clef de l'hystérésis, notamment le module de cisaillement effectif et l'amortissement visqueux équivalent, en fonction des paramètres étudiés et de l'amplitude des déformations. Des courbes de raidissement instantané et de cristallisation sont construites. Les effets des paramètres étudiés sont étudiés et des distributions statitiques des propriétés mécaniques du caoutchouc naturel sont identifiées. Les résultats expérimentaux montrent que l'augmentation du temps de conditionnement intensifie le raidissement du caoutchouc naturel. Cependant, cet effet est minime à -8ºC mais plus prononcé à très basse température (-30ºC). La fréquence des cycles a un effet négligeable, dans la plage étudiée tandis que le vieillissement induit un raidissement notable du caoutchouc. De plus, l'analyse statistique montre que les variations des propriétés mécaniques due aux sources et aux basses températures (-30ºC), en particulier pour un temps

de conditionnement prolongé, sont statistiquement significatives. Enfin, on constate que les distributions de valeurs extrêmes généralisées et log-normales sont les mieux adaptées aux distributions des propriétés mécaniques (module de cisaillement) du caoutchouc naturel à température ambiante (23 °C) et à basses températures (-8 °C et -30 °C).

Mots-clés: caoutchouc naturel, isolation sismique, ponts, propriétés hystérétiques, basse température, cristallisation, fréquence, vieillissement, source, distribution statistique

Variation of the mechanical properties of the natural rubber used in bridges' bearings and seismic isolators in Canada

Mohammadreza YAVARITAJ

ABSTRACT

Seismic base isolation is a widely used earthquake-resistant system to protect structures from earthquake-induced damage, focusing on mitigating the seismic demand. Elastomer-based isolators are one of the common systems used in seismic bridge isolation. Elastomers used in the isolators are mostly classified into two main categories: Polyisoprene (natural rubber) and polychloroprene (synthetic rubber known as neoprene). The mechanical properties of these elastomers play a crucial role in the performance and behaviour of the isolation system. However, these properties are variable, being influenced by several factors, notably low temperatures, aging, as well as fabrication and material source. Exposure to low temperatures increases the stiffness and hysteresis of elastomers, causing variations in their key mechanical properties, which alter the seismic response of the seismic isolators and affect the seismic performance of the structure.

In this study, the variation of mechanical properties of natural rubber, commonly used in seismic isolation applications and laminated bearings for bridges in Canada, is experimentally studied. Four different sources of natural rubber, including aged rubber extracted from recuperated laminated bearings of the original Champlain Bridge and new rubber, are considered to establish the variation of mechanical properties due to source, age, conditioning duration, and test temperature as well as the frequency of cycling. Specimens from each source of natural rubber are conditioned at different temperatures, namely 23ºC, -8ºC, and -30ºC, for different durations, going from 1 hour to 28 days. Experimental tests are conducted, at the conditioning temperatures, on quadruple shear samples. They consist of imposing a sequence of three cyclic shear loading at an increasing strain amplitude ranging from 25 to 150%. Tests were conducted at different frequencies (0.1, 0.25, and 0.5 Hz). Test results are used to extract the key characteristic properties of hysteresis, notably the effective shear modulus and the equivalent viscous damping, as a function of the studied parameters and shear deformation level. Instantaneous stiffening and crystallization curves are constructed. The effects of the studied parameters are investigated and statistical distributions of the mechanical properties of natural rubber are identified. The experimental results show that increasing conditioning time intensifies the stiffening of natural rubber. However, this effect is minimal at -8ºC but more pronounced at very low temperatures (-30ºC). The frequency of cycling has a negligible effect, within the studied range, while aging induces a notable stiffening of the rubber. Additionally, statistical analysis shows that the variations of mechanical properties due to sources and low temperatures (-30ºC), specifically for prolonged conditioning time, are statistically significant. Finally, it is found that the generalized extreme value and lognormal distributions provide the best fit to the mechanical properties (shear modulus) of natural rubber at room (23ºC) and low (-8ºC and -30ºC) temperatures.

Keywords: natural rubber, seismic isolation, bridges, hysteretic properties, low temperature, crystallization, frequency, source, aging, statistical distribution

TABLE OF CONTENTS

LIST OF TABLES

Page

LIST OF FIGURES

Page

LIST OF ABREVIATIONS AND ACRONYMS

ANOVA	Analysis of Variance
BFREI	Bonded Fiber-Reinforced Elastomeric Isolators
CHB	Champlain Bridge Bearing
CHBDC	Canadian Highway Bridge Design Code
CSA	Canadian Standards Association
CV	Coefficient of Variation
DCFP	Double Concave Friction Pendulum
EDC	Energy Dissipated per Cycle
EPDM	Ethylene Propylene Diene Monomer
EQS	EradiQuake
EV	Extreme Value Distribution
FPS	Friction Pendulum System
FREB	Fiber-reinforced Elastomeric Bearings
GEV	Generalized Extreme Value Distribution
HDNR	High Damping Natural Rubber
HDRBs	High Damping Rubber Bearings
IRHD	International Rubber Hardness Degree
KS	Kolmogorov-Smirnov test
LOGN	Lognormal Distribution
LRB	Lead-core Rubber Bearing
LTRB	Lead Thick Rubber Bearings
NORM	Normal Distribution
NR	Natural Rubber
NRB	Natural Rubber Bearing
PBFREI	Partially Bonded Fiber-Reinforced Elastomeric Isolators
PDFs	Probability Distribution Functions
PTFE	Polytetrafluoroethylene
SD	Standard Deviation
SMAs	shape Memory Alloys

SREB	Steel-Reinforced Elastomeric Bearings
TNRB	Thick Natural Rubber Bearing
UFREI	Unbonded Fiber-Reinforced Elastomeric Isolators

LIST OF SYMBOLS

Lowercase Latin alphabet

t_r	Thicknesses of a single block of rubber
t_{20}	Aging time at the standard temperature of 20°C
t_s	Time to expose sample to an accelerated aging temperature

Uppercase Latin alphabet

A_r	Bonded rubber area
D	Displacements
E	Young's modulus
E_a	Kinematic energy
E_{lu}	Elongation in percent
F_y	Elastic force limit
F_{max}	Maximum force
F^+	Maximum positive forces
F^-	Minimum negative forces
G	Shear modulus
G_{eff}	Effective shear modulus
G_{sec}	Secant shear modulus
K	Bulk modulus
K_{eff}	Effective stiffness
K_d	Post-elastic stiffness
K_u	Elastic stiffness
P	Hydrostatic pressure
Q_d	Characteristic resistance
R	Gas constant
T_r	Total thickness of rubber
T_{20}	Standard temperature (20°C)

T_s	Arbitrary aging temperature
V_0	Initial volume of elastomer
W_d	Enclosed area of the stress-strain curve in a cyclic loading

Lowercase Greek alphabet

τ_{max}	Maximum stress
τ_{min}	Minimum stress
τ_0	Stress at zero strain
$\tau_0^{100\%}$	Stress at zero strain for 100% amplitude
v	Poisson's ratio
γ_{max}	Maximum strain
γ_{min}	Minimum strain
$\xi_{eq}^{100\%}$	Equivalent damping ratio for 100% amplitude

Uppercase Greek alphabet

Δ_{max}	Maximum displacement
Δ_u	Displacement limit
Δ^+	Maximum positive displacements
Δ^-	Minimum negative displacements

INTRODUCTION

0.1 Context and the problem

An earthquake is a natural phenomenon characterized by the sudden release of energy in the earth's crust, typically caused by the movement of plates along fault lines, resulting in the generation of seismic waves that propagate through the earth's surface, often leading to ground shaking, displacement, and potential damage to structures and infrastructure. When encountering seismic events, structures, including bridges, must possess the capacity to withstand these movements either without incurring damage, or restricting resultant damage according to the design criteria. One way to achieve this aim is to protect the structures from seismic forces through seismic isolation systems. These are specialized devices such as isolators or dampers strategically placed between the foundation and the superstructure, facilitating controlled movement and deformation during seismic events, thereby safeguarding the structural integrity and stability of the structure. A seismic isolation system is used to substitute the direct and stiff connection between the soil and structure with a laterally flexible linkage. The introduced flexibility extends the natural vibration period of the bridge in the isolated lateral direction, which reduces the seismic force demand the bridge must withstand (Guizani, 2007; Taylor and Igusa, 2004).

There are various seismic isolation systems available for bridges but elastomeric-based systems and friction-based systems stand out as the most prevalent choices, given their cost-effectiveness and performance (Guizani, 2007). Elastomeric-based systems are typically made of elastomeric laminated rubber bearings with or not modified construction details, introduced to achieve target hysteretic properties. An elastomeric rubber bearing is made of multi-layers of rubber assembled with separating thin plates, known as shims, typically made of steel and vulcanized to layers of elastomers utilized in the fabrication of bridge seismic isolators typically consisting of polyisoprene (natural rubber), or polychloroprene (synthetic rubber, known as neoprene) which is a synthetic polymer of chloroprene. Natural rubber is exclusively used in Canada (CSA, 2019) and is characterized by high elasticity and low hysteresis at low

strain amplitudes (Chen, 1995; Taylor and Igusa, 2004). The mechanical properties of natural rubber can be affected by several climatic and natural factors while manufacturing processes and technology can cause additional variations in these properties. Seismic analysis and design shall take into account such variations while reliability and probabilistic analyses and designs require statistical distributions of the hysteretic properties of seismic isolators (CSA, 2019; Nassar et al., 2022). The deconstruction of the original Champlain Bridge offered a unique opportunity to study the effect of site and non-controlled aging on the mechanical properties of natural rubber used in Quebec and Canada.

0.2 Objectives

The main objective of this research project is to experimentally assess the variation of hysteretic properties, under shear cycling, of the natural rubber commonly used in elastomer-based seismic isolators and bearings for bridges in Quebec and Canada, exposed to low temperatures. This overall objective is broken down into the following specific objectives:

1. assessing the effects of low temperatures and conditioning duration on the mechanical properties of four distinct sources of natural rubber including aged and new rubber, subjected to the shear cycling.
2. Developing curves for characterizing the effect of low temperatures on different sources of rubber as a function of strain amplitude and conditioning time, based on the results obtained.
3. Investigating the effects of other factors such as aging at room temperature under non-controlled conditions, the source of rubber as well as the cycling frequency.
4. Analyzing the statistical variation of mechanical properties and proposing probability distributions and statistical parameters that can be used to represent the hysteretic properties variation within the framework of probabilistic and reliability analyses.

0.3 Methodology

The methodology adopted to address the study's problem and accomplish the established objectives is outlined in the following step:

1. To comprehensively understand the research topic, a literature review was carried out. This review studied the types of bridge seismic isolators and their features, elastomeric materials, with a focus on the properties of natural rubber. Moreover, particular attention was given to factors influencing the properties of natural rubber, such as the impact of low temperatures, crystallization phenomena, aging effects including different types of aging, and pertinent findings from prior investigations.
2. An experimental program has been developed encompassing several key steps. The parameters to study experimentally are set, based on earlier research and gaps identified from literature review as well as the available testing facilities capacities. This experimental program included the design of a preparation procedure for original Champlain Bridge bearings and test specimens, from actual-size bearings to quadruple reinforced samples, which can be adopted in quality control and prototype characterization testing campaigns on real application projects or research projects. Also, it provides a cold conditioning process for samples at varying low temperatures, with differing exposure durations. The program details a cyclical shear testing plan for natural rubber specimens with various dimensions, conducted under three different frequencies at low temperatures. Natural rubber from four different sources and origins is used and tested in this study.
3. The specimens were exposed to cold temperatures, and the experimental program was carried out. The obtained results for each Series were analyzed and processed to characterize the mechanical properties of natural rubber and measure the effects of different studied parameters.
4. statistical analysis was employed to measure the variation of obtained data among four sources of natural rubber. Also, statistical tests including the ANOVA test were used

to compare the mechanical properties of four Series of natural rubber and assess if there are statistical differences among them.

5. Four different probability distribution functions were used in order to model the shear behaviour of each Series of natural rubber at room temperature and low temperatures. Also, Statistical tests including the Kolmogorov–Smirnov test (KS test) were conducted to validate the goodness of fit of probability distribution curves.

0.4 Organisation of the thesis

This dissertation comprises four chapters in addition to the introduction and conclusion. The first chapter provides a comprehensive literature review including seismic isolation systems and elastomeric rubber topics as well as a summary of previous studies related to the problem. Chapter two presents the preparation of samples, the experimental program, and the study parameters. Chapter three delves into the results of the experimental tests, along with their analyses and discussions. Chapter four focuses on the variation among series of rubber, emphasizing the statistical analysis of data and probability distribution modelling of natural rubber at low temperatures. Finally, the dissertation concludes with the main findings and recommendations for future research endeavours.

CHAPITRE 1

LITERATURE REVIEW

1.1 Seismic isolation systems

Seismic isolation systems, also known as base isolation systems, are engineering solution that involves placing flexible or sliding devices between a structure and its foundation. These systems aim to effectively decouple the horizontal movements of the ground from those of the structure. As a consequence of the utilization of base isolation systems, the susceptibility of the structure and its contents to damage during seismic events will be reduced (Taylor and Igusa, 2004).

1.2 Concept and fundament of seismic isolation

Due to the lateral flexibility provided by the isolation system, the fundamental period of the structure increases beyond the range of the predominant earthquake frequencies, thereby lowering the seismic forces transmitted to the structure (Taylor et al., 1992). Having a decrease in force enables, typically, the design of cost-effective bridges with elastic performance (no damage) in the seismic design (Constantinou et al., 2007). However, lateral flexibility within seismic isolation systems may lead to larger displacements. To address the potential drawbacks associated with increased displacements, energy dissipation mechanisms are employed to constrain displacements at the base level, by providing damping into the structure (Buckle et al., 2006). Energy dissipators effectively strike a balance between desired flexibility and acceptable displacement (Guizani, 2007). Hence, seismic isolation has many benefits, including reducing structural damage by replacing the hinge and inelastic zones of the structure with replaceable seismic isolation devices, improving structural safety, and reducing seismic design forces (Naeim, 2001). Figure 1.1 shows the influence of the increase in the period on the transmitted forces for typical bridges as well as on the displacement for variable damping (Constantinou et al., 2007).

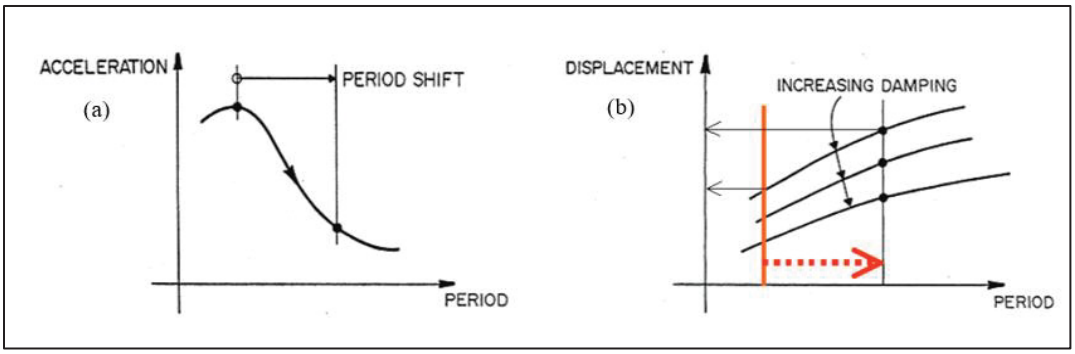

Figure 1.1 Effect of increasing in period on acceleration (a), and on the displacement (b)
Taken from Constantinou et al. (2007)

1.3 Features of base isolation systems

The main properties of base isolators are providing horizontal flexibility while being able to transmit vertical loads as a support, adding damping through integrated or parallel energy dissipation mechanism (damper) to control the seismic displacement, sufficient resistance, and stiffness under lateral service loads and non-seismic loads such as wind and braking (Guizani, 2007).

1.4 Types of bridge seismic isolators

In general, bridge isolation systems can be categorized into two widely used categories: slip-based and elastomer-based systems (Constantinou et al., 2007). Slip-based systems, also known as friction-based systems, typically employ a sliding interface made of stainless steel sliding against PTFE (Polytetrafluoroethylene) or other materials (Buckle *et al.*, 2006). The friction pendulum is the most widely used sliding isolation bearing among others such as the Izolatech and the Eradiquake (Guizani, 2007). The elastomer-based systems also known as laminated rubber bearings typically comprise rubber reinforced with steel plates. Low- and high-damping rubber bearings as well as lead-core bearings are three common types of elastomer-based systems (Constantinou et al., 2007). Hybrid isolation systems also are another form of seismic isolator made by a combination of sliding bearing and elastomeric bearing.

Hybrid isolators can provide a variety range of energy dissipation and stiffness (Buckle et al., 2006). Furthermore, the combination of smart materials, especially shape memory alloys (SMAs), with conventional bearings is a new type of isolation system designed to improve laminated bearing performance. SMAs can exhibit large hysteretic deformations without engaging in plastic deformation due to stress-induced phase transformations at the microscopic level. Additionally, they can serve to improve re-centring capabilities, reduce forces, decrease relative displacements transmitted from the substructure to the superstructure, and energy dissipation (Hedayati .D, 2015). Mechanical features of SMAs, particularly the super elasticity and hysteresis properties, enable them to be used with laminated rubber bearings (Bhuiyan and Alam, 2013).

1.4.1 Sliding-base systems

Friction-based isolation systems rely on the dissipation of seismic energy primarily through a frictional surface. This surface is typically made of polytetrafluoroethylene (PTFE) and is available on a curved or flat surface. Curved sliding systems are capable of creating restoring forces due to their geometric properties. while in the case of flat sliders, the restoring force needs to be created by additional devices such as spring components known as mass energy regulators (MER). These MER elements not only provide the sliding system with the required energy to return the bearing and structure to their initial positions by reserving part of the seismic energy but also restrict the excessive displacement (Fatemi and Conklin, 2019).

1.4.1.1 Friction pendulum bearings (FPS)

Friction pendulum bearings or friction pendulum systems (FPS), shown in Figure 1.2, are composed primarily of a concave stainless-steel plate and an articulated slider. The concave spherical plate can be oriented either upward or downward. To minimize frictional resistance, the contact surface of the articulated slider in contact with the curved spherical plate is coated with a low-friction composite material, typically polytetrafluoroethylene (PTFE), commonly known as Teflon (Buckle et al., 2006). The radius of curvature of the slip surface as well as

the friction of the involved surface serve as crucial parameters to control the isolation period and the dissipation of energy during an earthquake (Guizani, 2007). The double concave friction pendulum (DCFP) bearing, shown in Figure 1.3, is an alternative version of the single concave bearing, particularly advantageous when seeking significant displacement capacity.

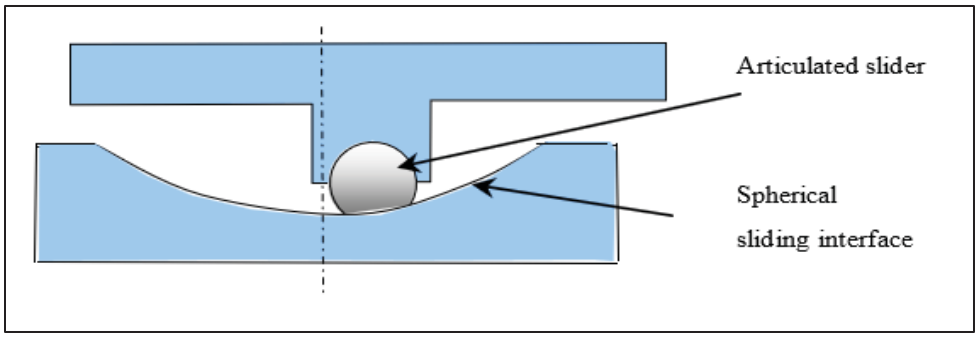

Figure 1.2 Friction pendulum system
Taken from Guizani (2007)

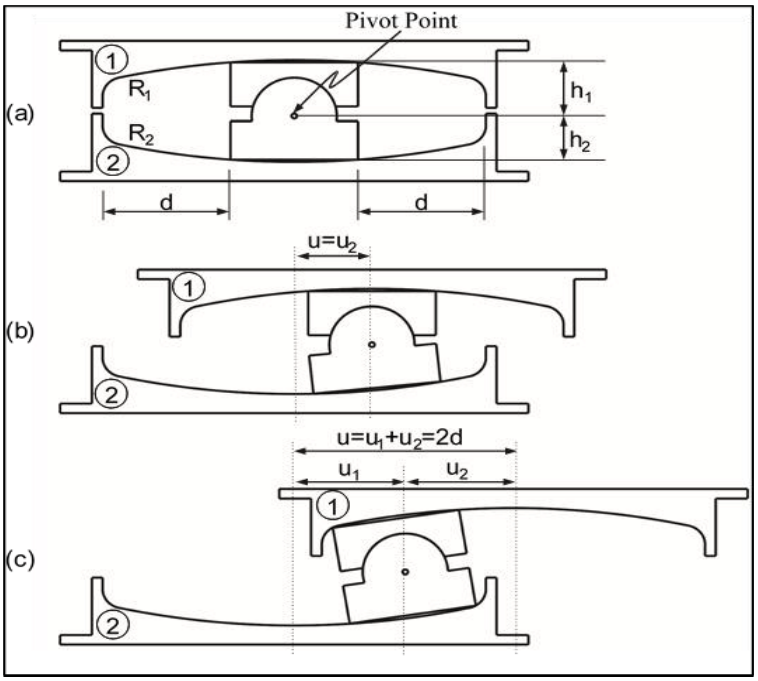

Figure 1.3 Double concave friction pendulum bearing
at different moving conditions
Taken from Constantinou et al. (2007)

The DCFP bearing comprises two opposing concave stainless steel surfaces; the upper and lower concave surfaces may have distinct radii, allowing for customization based on specific requirements (Constantinou et al., 2007).

1.4.1.2 EradiQuake (EQS) bearings

The EradiQuake system operates based on a similar principle as the friction pendulum, but with a distinct feature of a flat friction interface. EQS system, shown in Figures 1.4 & 1.5, employs the sliding interaction between stainless steel and PTFE surfaces to introduce flexibility and friction, facilitating energy dissipation. The system's restoring capacity is achieved through the utilization of two orthogonal springs, which transmit lateral forces from the movable component to the base. A rotation disc installed at the isolator's base ensures the system's rotational capacity. Energy dissipation occurs through friction at the interface between the movable and fixed components. The system's high initial stiffness is attributed to the coefficient of static friction between the two friction surfaces. The notable advantage of the EradiQuake system over alternative seismic isolation devices lies in its ability to vary the system's flexibility in different directions. The system's flexibility can be adjusted independently in each direction, as the two springs function autonomously (Olivier et al., 2014).

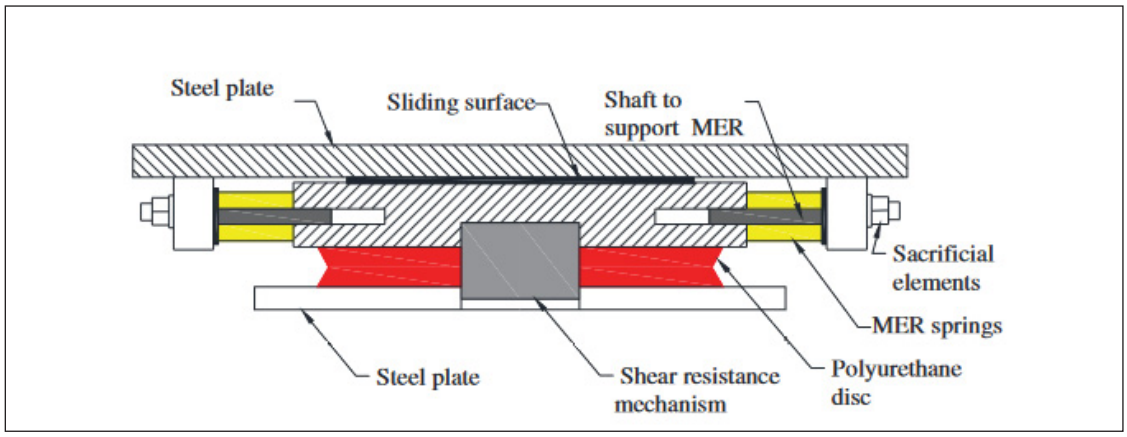

Figure 1.4 Transversa section of EQS system
Taken from Fatemi and Conklin (2019)

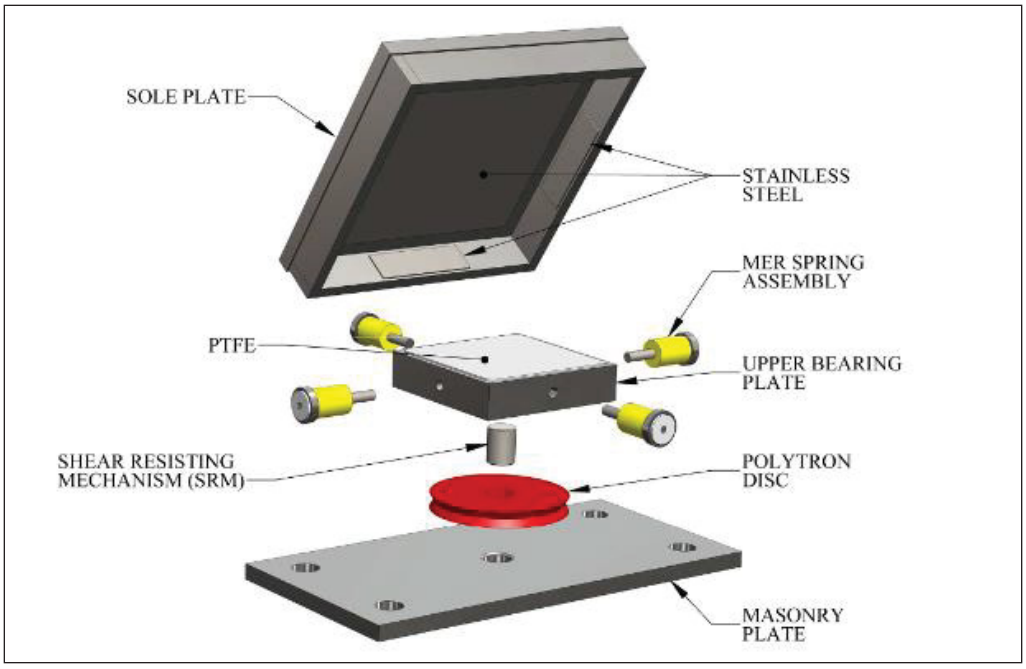

Figure 1.5 Elements of a typical multi-way EradiQuake system (EQS)
Taken from Fatemi and Conklin (2019)

1.4.1.3 Izolatech isolator

The Izolatech isolator is the first seismic isolation system developed in Quebec. This system was developed by the Goodco Z-Tech company of the Canam-ponts group, in collaboration with Canadian partners. The Izolatech isolator includes a confined elastomer bearing, a special stainless steel-Teflon sliding interface, and a recentering system made of steel springs, which is shown in Figure 1.6. The sliding interface provides energy dissipation and initial resistance. Also, the recentering system enables the isolator to return to its initial position while preserving the necessary lateral rigidity. The behaviour of the Izolatech isolator can be modelled by the bilinear force-displacement curve (Guizani, 2007).

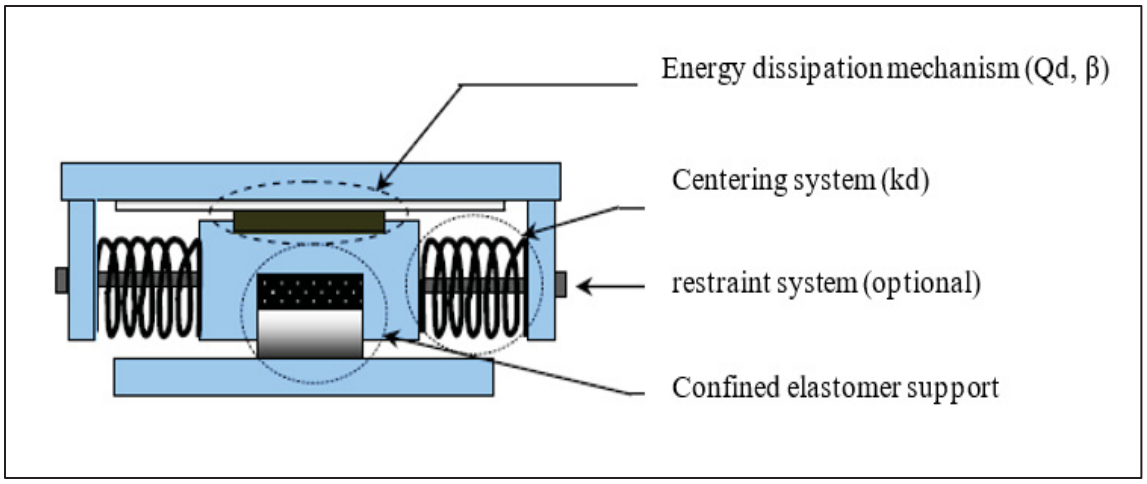

Figure 1.6 Izolatech seismic isolation system
Taken from Guizani (2007)

1.4.2 Shape memory alloy-based rubber bearings (SMA-RB)

Characteristics of shape memory alloy (SMA) make them ideal for application in structures subjected to a range of dynamic forces with varying magnitudes and frequencies. Under light external loads, such as wind or minor seismic activity, SMA-based rubber bearings serve as an effective means of establishing a rigid connection between the substructure and superstructure, thereby mitigating potential damage to structural elements. During moderate seismic events, SMA-based components, shown in Figure 1.7, enhance the damping capacity of rubber bearings, further improving the structure's resilience. In the event of strong ground motions, these SMA elements not only contribute to additional hysteretic damping but also serve as an effective controller by restricting the relative displacement of the superstructure. This effect is facilitated by the stiffness hardening exhibited by the SMA after completing the phase transformation process (Hedayati .D, 2015).

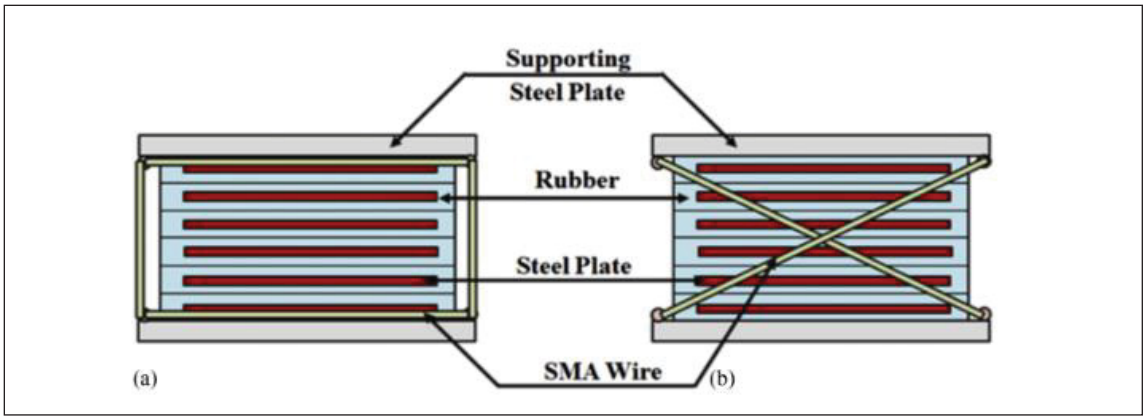

Figure 1.7 Rubber bearing with shape memory brace: (a) front view; (b) side view
Taken from Mishra et al. (2016)

1.4.3 Steel-reinforced elastomeric bearings (SREB)

Elastomeric bearings for seismic isolation applications consist of alternately multi-layers of rubber and thin steel plates, also known as shims. Shims are aimed at constraining the outward bulging of rubber layers when the isolator experiences axial load. Shims allow the bearings to withstand greater axial load and increase the axial stiffness of the bearings without exerting an influence on the lateral stiffness of the bearing (Taylor and Igusa, 2004). The Canadian Highway Bridge Design Code (CSA, 2019) specifies that steel strips must have a minimum elastic strength of 230 MPa and also must have a nominal thickness of at least 3 mm to be used in seismic isolators. There are three main types of steel-reinforced elastomeric bearings (SREBs) based on rubber material properties and energy dissipation capacity. These include low-damping natural rubber bearings (NRB), lead core rubber bearings (LRB), and high-damping rubber bearings (HDRB). SREBs are commonly used on bridges and high-rise buildings (Hedayati .D, 2015).

1.4.3.1 Natural rubber bearings (NRB)

Natural rubber bearings (NRB), also known as low-damping rubber bearings, are fabricated through a vulcanization process in which steel shims are bonded to rubber layers to enhance

compressive capacity (Hedayati .D, 2015). Figure 1.8 shows a laminated rubber bearing. The process of vulcanization or curing is the chemical conversion of raw rubber, explained in the following sections (Constantinou et al., 2007). Steel plates can be added to the top and bottom of the bearings to securely connect them to the structural elements using bolts, as well as to facilitate the mounting of the rubber bearings more easily. Taking into account that NRBs have low damping rates resulting from their mechanical properties, additional elements such as damper devices are required in order to improve damping properties (Naeim and Kelly, 1999).

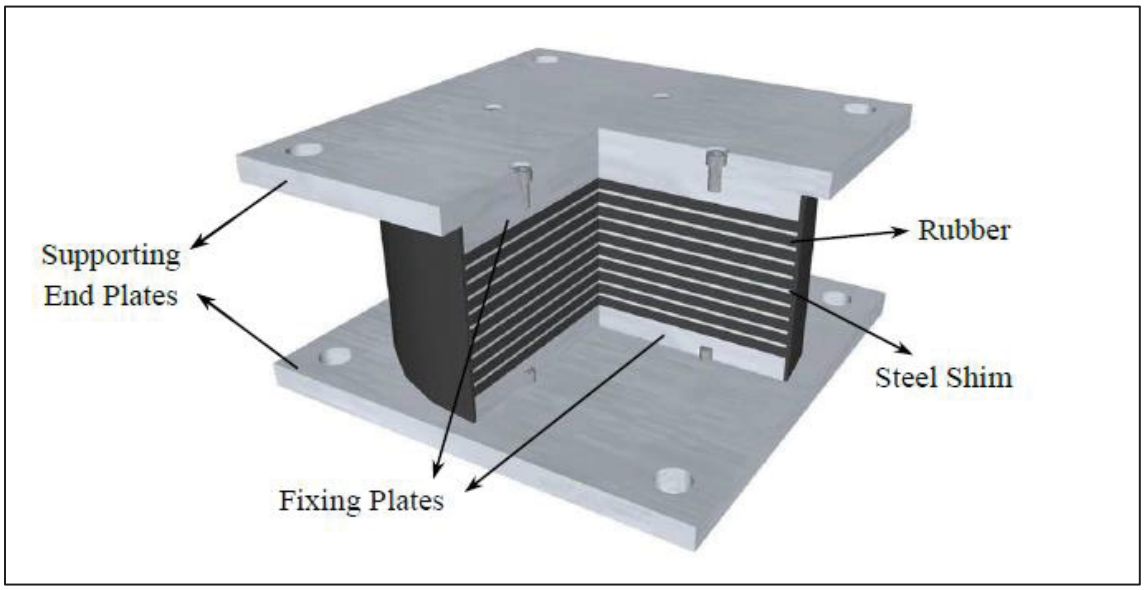

Figure 1.8 Scheme of a laminated rubber bearing
Taken from Hedayati (2015)

1.4.3.2 High-damping rubber bearings (HDRB)

High-damping rubber bearings (HDRBs), as with NRBs, are reinforced with steel shims but use high-damping rubber for dissipating energy. HDRBs have high energy dissipation and damping characteristics as a result of the addition of oils, resins, or black carbon to the natural rubber during the curing process (Naeim and Kelly, 1999). The damping capacity of HDRBs varies between 8 and 16% of critical damping (Taylor and Igusa, 2004). HDRBs exhibit highly nonlinear and complex behaviour and it is possible for them to experience large levels of shear

strain, up to 400% (Hedayati, 2015). However, at moderate shear strains (up to approximately 200%), high-damping rubber bearings typically demonstrate a bilinear force-displacement relationship. And, at very large displacement, these bearings undergo significant stiffening resulting in a trilinear curve (Clark, 1996).

1.4.3.3 Lead-core rubber bearings (LRB)

Lead-core rubber bearings (LRBs) are commonly fabricated using elastomers with low damping properties, coupled with lead cores featuring diameters that typically are between 15% and 33% of the bonded diameter of the bearing. The elastomer functions as the isolation component and provides lateral flexibility, while the lead core serves as the energy dissipater under seismic force. The maximum shear-strain range for LRBs exhibits variation as per manufacturer specifications. However, it typically falls within the range of 125% to 200% (Constantinou et al., 2007). Figure 1.9 shows the scheme of a lead-core rubber bearing.

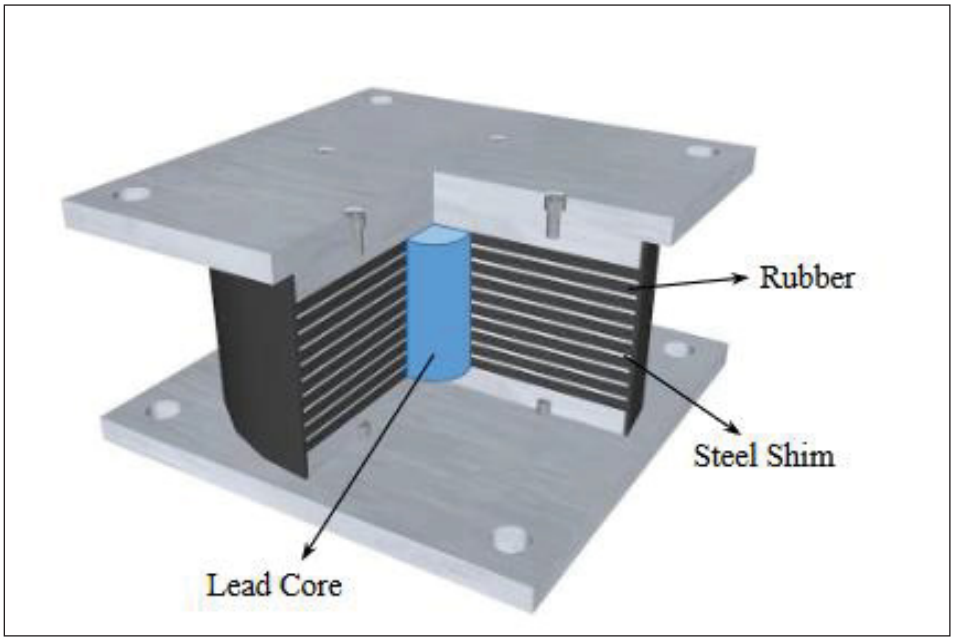

Figure 1.9 Scheme of a lead-core rubber bearing
Taken from Hedayati (2015)

1.4.4 Fiber-reinforced elastomeric bearings (FREB)

Fiber-reinforced elastomeric bearings (FREBs) have a configuration similar to that of steel-reinforced bearings, except that steel shims are replaced by fiber plates. By substituting steel shims with fiber plates, not only does the weight of bearings decrease, but the production cost also reduces by eliminating the high-cost process of vulcanization. Cold vulcanization, as an alternative, provides a cost-effective bonding between the elastomer and the fiber-reinforced plates. Moreover, FREBs can be manufactured in the form of long rectangular strips and then cut to the desired dimensions (Kelly, 1999). Reduction in the cost of fabrication and weight of conventional bearings through fiber reinforcement enables their application to expand into residential and public buildings. This is the main goal of designing and manufacturing fiber-reinforced bearing (Hedayati, 2015). Among fibers used in FREBs, carbon fibres are the ideal material for reinforcing the elastomeric bearings due to their mechanical properties, which include a high elastic modulus, a high tensile strength (Moon et al., 2002).

1.5 Elastomeric materials used in seismic isolators

Elastomers are a class of polymers that exhibit a remarkable degree of resilience. In polymers, many identical molecules are connected to form a long chain. The molecule chains are bound by relatively low-strength intermolecular forces of attraction. Their properties are determined by the arrangement of their atoms and molecules. When subjected to stress, these materials exhibit a high degree of elasticity, allowing them to be elongated to multiple times their initial length. Furthermore, they possess the ability to revert back to their original shape once the stress is relieved. Elastomers possess a diverse array of industrial applications. Seismic isolation bearings for bridges are among the various applications in which they are utilized. Two examples of elastomers include natural rubber and neoprene. Rubbers are resilient material that falls within the category of elastomers (Qayyum, 2016). In terms of chemical science, rubbers can be defined by their high molecular weight compounds made from low molecular weight units known as monomers. A rubber chain typically consists of a range of 1,000 to 20,000 similar units of monomers (Barlow, 1993). In rubber compounding, various

additives are employed to achieve specific effects and optimize the final product's performance. For instance, accelerators are utilized to expedite the vulcanization process by reducing heating duration or lowering the required heat levels. Additionally, fillers play a crucial role in modifying the mechanical properties of the rubber. Among these additivities, carbon black is the most commonly used filler, effectively altering hardness, stiffness, elongation at break, creep and relaxation characteristics, as well as the fatigue life of the rubber (Constantinou et al., 2007).

1.5.1 Natural rubber

The primary source of natural rubber (NR) is obtained from the latex of trees named Hevea. Cis-1,4-polyisoprene is the chemical composition of natural rubber, which is a linear polymer consisting of elongated chains with recurring isoprenoid units (C5H8), shows a density of 0.93 at a temperature of 20°C (Barlow, 1993). Vulcanization is a chemical process that transforms raw rubber from a plastic state to a highly elastic state through chemical crosslinking. During this process, specific agents such as sulfur, peroxide, or urethane are introduced into the raw rubber, while heat and pressure are applied. This curing exerts a significant influence on the properties of rubber, including strength, elasticity, resistance to solvents, and relative insensitivity to temperature fluctuations (Constantinou et al., 2007). Natural rubber is characterized by high elasticity and low hysteresis at low strain amplitude. Due to the molecule chain which is a double bond, natural rubber is an unsaturated polymer making it vulnerable to ozone attack and the development of cracks under excessive strain beyond its threshold limit (Chen, 1995). However, Anti-ozone as an additive, find application in safeguarding the product against ozone-induced cracking through delay in degradation, thereby mitigating aging effects.(Constantinou et al., 2007).

1.5.2 Synthetic Rubber

Neoprene with the scientific name of polychloroprene is the most known synthetic polymer of chloroprene. The first development of neoprene can be attributed to DuPont during the 1930s,

wherein it was produced by using a polymerization process of chloroprene monomers (Barlow, 1993). Neoprene exhibits considerably greater heat and ozone degradation resistance compared to natural rubber. However, natural rubber provides better performance in terms of mechanical properties such as shear and compression at low temperatures. The Canadian Highway Bridge Design Code indicates that in cold regions where temperatures are predicted to drop below -25°C for extended periods only natural rubber should be used for bridge bearings (CSA, 2019).

1.6 Mechanical properties of natural rubber

Hardness

The concept of hardness can be described as the measure of a material's ability to resist indentation. The durometer is a device utilized for measuring the level of indentation. Hand-held durometers equipped with spring-loaded mechanisms are frequently employed in various applications. However, their susceptibility to operator error is a notable concern (Schaefer, 2010). Figure 1.10 shows the scheme of a durometer.

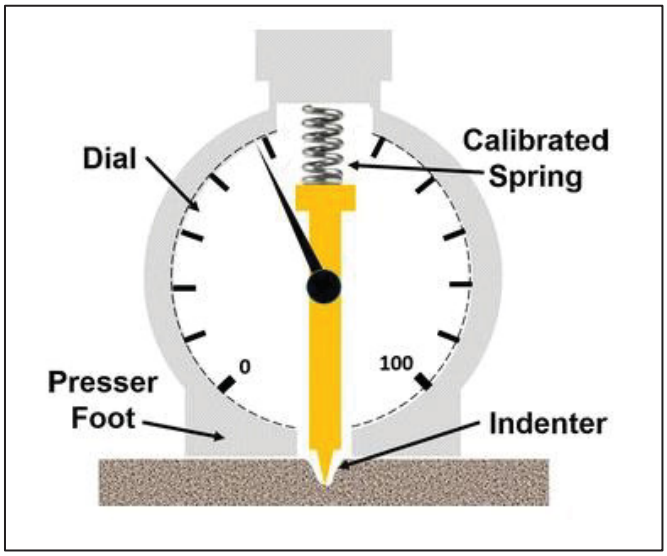

Figure 1.10 Scheme of a durometer
Taken from Broitman (2016)

The durometer gauge quantifies the depth of penetration to the surface resulting from indentation. The durometer is comprised of several components, including a reference presser, an indenter, an indicator device, and a calibrated spring responsible for applying force to the indenter. The test is commonly conducted within a time frame of 1 to 3 seconds and is characterized by its destructive nature. The purpose of a hardness test is to quantify the reaction of rubber to minor surface stress, primarily employed for the purpose of differentiating between various rubber materials (Qayyum, 2016).

The international rubber hardness degree (IRHD) introduces four definitions for measuring hardness, namely normal-hardness, high-hardness, low-hardness, and micro. Generally, they measure the difference between the depth of ball indentation on a rubber surface. According to the hardness of the rubber, the diameter of the indenting ball and the magnitude of the indenting force vary between the tests. In the IRHD scale, 0 represents the hardness of a material with Young's modulus of 0 and 100 represents a material with an infinity-based Young's modulus. A typical IRHD test requires approximately 35 seconds and is non-destructive, which means it does not leave a permanent imprint on the product (Shirazi, 2010). However, there are numerous limitations to this test. The durometer test can only measure the hardness of the exterior layer. Additionally, properties of interest to engineers, notably the shear modulus, are not well determined by this test. According to the Canadian Highway Bridge Design Code (2014), elastomeric bearings were required to have a hardness of 55 Shore A, with a tolerance range of ±5 (CSA, 2014). However, the latest version of the code (CSA-S6:19) specifies the shear modulus instead of hardness. As a result, rubbers used in elastomeric bearings are required to have a shear modulus of 0.81 MPa, with a tolerance range of ±0.15 MPa (CSA, 2019).

Elastic modulus

The response of rubber to uniaxial tensile stress is characterized by a roughly linear behaviour at low strains, followed by nonlinearity as strains increase, and subsequently transitioning to another linear response at higher strains. Figure 1.11 shows the uniaxial tensile stress-strain

curve of rubber. The determination of a singular tensile modulus value is unfeasible due to this intricate mechanical profile. The established approach involves the assessment of the tensile modulus via the utilization of the secant modulus, specifically within the domain of low strains (Constantinou et al., 2007). However, the modulus of elasticity varies with temperature and strain levels; for instance, decreasing temperature corresponds to an increase in the modulus of elasticity (Ciesielski, 1999).

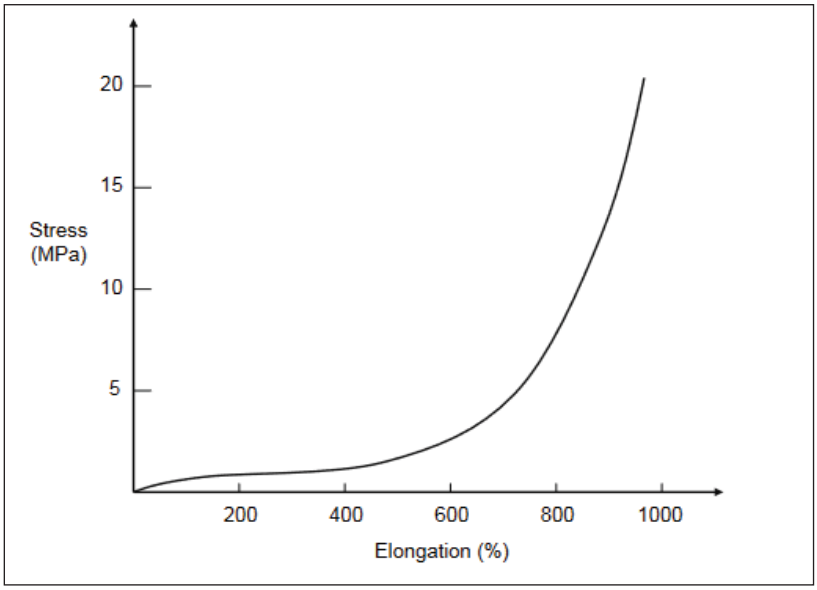

Figure 1.11 Uniaxial tensile stress-strain curve of rubber
Taken from Constantinou et al. (2007)

Bulk Modulus, *K*

The bulk modulus of a material can be defined as its resistance to volume change when compressed (Shirazi, 2010). The bulk modulus of rubber is mostly characterized within the range of 1000 to 2000 MPa, largely exceeding the corresponding values associated with the elastic modulus (1 to 10 MPa). These considerable coefficients signify the near-incompressibility of rubber material, thereby allowing the approximation of a Poisson's Ratio of 0.5 (Buckle et al., 2006). However, the compressibility of rubber may become significant

based on its geometry, such as its size and shape (Qayyum, 2016). The bulk modulus, *K*, can be described using the equation (1.1) :

$$K = P/\varepsilon_v \tag{1.1}$$

where *P* is the hydrostatic pressure and ε_v is equal to the change in volume (ΔV) divided by the initial volume of the material (V_0) . A decrease in volume indicates a positive volumetric strain (Shirazi, 2010). The bulk modulus of rubber can be calculated as:

$$K = E/3(1 - 2v) \tag{1.2}$$

where v is Poisson's ratio (≈ 0.5), and *E* is the Young's modulus.

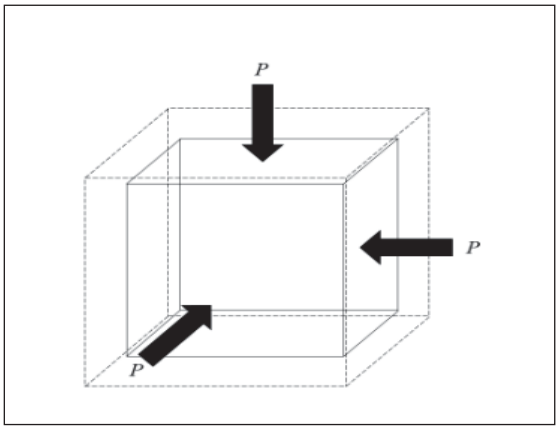

Figure 1.12 Compressibility of rubber
Taken from Qayyum (2016)

Shear modulus, *G*

Since elastomers have a non-linear strain-stress relation, the shear modulus varies according to the level of imposed strain as well as other parameters including temperature. There are two experimental methods for evaluating the shear modulus of rubber, the first one is a non-destructive test conducted on a set of complete bearings and the second one is a quad shear test

performed on small rubber samples extracted from a bearing and afterwards affixed to inflexible plates via a cold-bonding process (Yura et al., 2001). A full-scale shear test involves the application of a continuous compressive force to the sample, which is maintained throughout the duration of the test. Horizontal shear deformation is implemented on the central plate in order to represent the movement experienced by a bridge. Bearing samples can be subjected to shear in either one-way or two-way direction. The measured shear modulus varies by 7 percent depending on whether it is based on one direction or both directions (Yura et al., 2001).

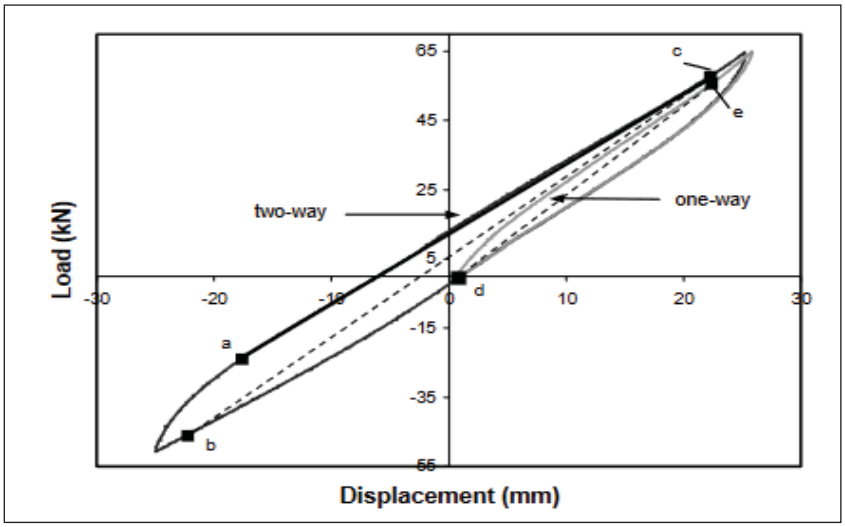

Figure 1.13 Typical load-displacement response for shear deformation applied in one-way and two-way directions
Taken from Yura et al. (2001)

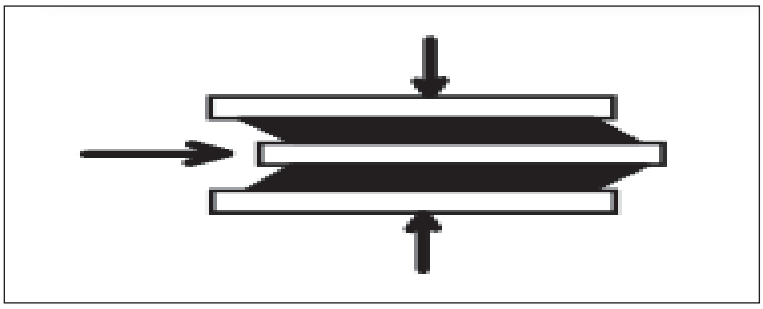

Figure 1.14 Full-scale shear test to find the shear modulus
Taken from Yura et al. (2001)

ASTM D4014 provides a standard procedure to determine the shear modulus of scaled-down specimens which consist of four blocks of rubber with the same dimensions sandwiched between three rigid plates. The steel plates located at the centre experience uniaxial tensile pressures, resulting in the shear deformation of the elastomer blocks. Six loading cycles are employed until reach deformation equivalent to the average thickness of the rubber blocks. The determination of the shear modulus value is thereafter obtained from the shear stress-strain curve associated with the sixth load cycle (ASTM D4014-03, 2018).

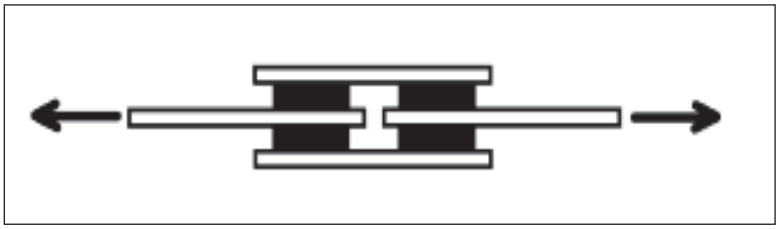

Figure 1.15 Standard quad-shear specimen
Taken from Yura et al. (2001)

Tensile strength

The tensile strength of rubber is the maximum stress under which it can be stretched before it breaks. The tensile strength of rubber depends on the composition of the rubber and the vulcanization process used. Elastomers can also vary in their tensile strength due to external factors such as temperature; for instance, natural rubber will offer a tensile strength of 30 MPa at 23°C while it will only exhibit about 22 MPa at 80°C (Ciesielski, 1999). It is required that elastomers used in the construction of seismic isolators meet a minimum tensile strength of 17.0 MPa under the Canadian Highway Bridge Code (CSA, 2019).

Ultimate elongation

Ultimate elongation also known as elongation at break is the deformation in which rupture occurs under continued tensile stress, as defined by the equation (1.3) (ASTM D412-16, 2021).

$$E_{lu} = 100(l - l_0)/l_0 \quad (1.3)$$

Where E_{lu} is the elongation in percent, l is observed distance between benchmarks on the extended specimen, and l_0 is original distance between benchmarks (ASTM D412-16, 2021). Rubber's elongation at break is dependent on its chemical composition and its rigidity (Ciesielski, 1999). The latest version of the Canadian Highway Bridge Design Code specifies that a minimum elongation at break of 400% for elastomers to be used in seismic isolators (CSA, 2019).

1.7 Force-displacement bilinear model of elastomer-based seismic isolators

The modelling of elastomer isolation bearings involves the key factors that characterize the bearing's behaviour. Although its simplicity and limitations, the bilinear model is widely employed to describe the force-displacement relation of elastomer-baaed bridge bearings and seismic isolators including natural rubber bearings (NRB), low-damping rubber bearings (LDRB), and high-damping rubber bearings (HDRB), and lead-core bearings (LRB). However, there are some modifications in the case of LRB, which will be discussed in the following sections. The bilinear model for elastomeric bearings relies on K_u representing the elastic stiffness, K_d the post-elastic stiffness, and Q_d the force at zero displacement which is known as characteristic resistance.

Figure 1.17 presents the bilinear model in which F_y and F_{max} refer to the max force at the elastic displacement limit (Δ_u) and at the maximum displacement (Δ_{max}), respectively. The effective stiffness (K_{eff}), which is the secant stiffness at the maximum displacement, can be calculated by following the formula (Naeim and Kelly, 1999):

$$K_{eff} = K_d + \frac{Q_d}{\Delta_{max}} \quad (1.4)$$

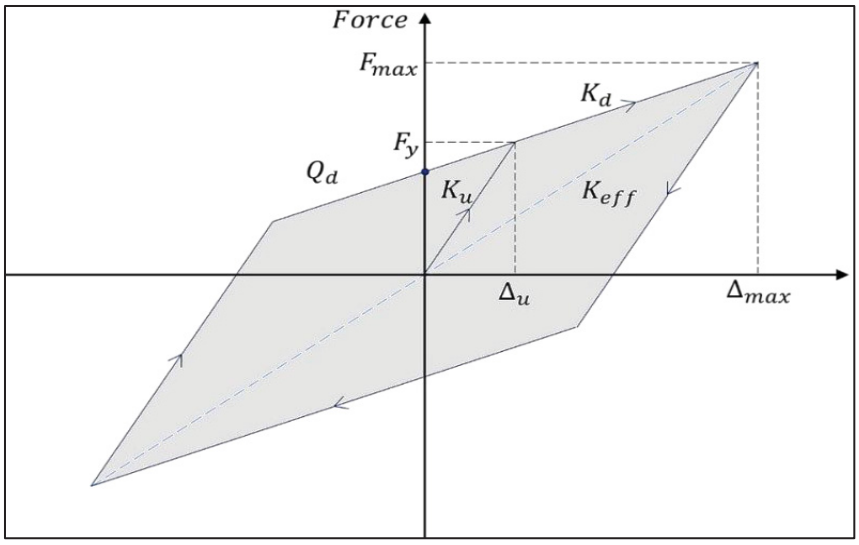

Figure 1.16 Bilinear model of force-displacement relationship
for elastomeric bearing and their crucial parameters
Adapted from Naeim and Kelly (1999)

Effective stiffness (K_{eff}), also can be calculated by equation (1.5) in which Δ^+ and Δ^- are the maximum positive and minimum negative displacements and F^+ and F^- are the maximum positive and minimum negative forces of the force-displacement curve (Constantinou et al., 2007).

$$K_{eff} = \frac{|F^+| + |F^-|}{|\Delta^+| + |\Delta^-|} \tag{1.5}$$

The energy dissipated per cycle (EDC) is the enclosed area of the force-displacement curve, and is expressed by the equation (1.6), where the Δ_u is derived from the equation (1.7) (Naeim and Kelly, 1999).

$$EDC = 4Q_d(\Delta_{max} - \Delta_u) \tag{1.6}$$

$$\Delta_u = \frac{Q_d}{K_u - K_d} \tag{1.7}$$

The equivalent viscous damping ratio is defined by the following relation (1.8) (Constantinou et al., 2007):

$$\xi_{eq} = \frac{2}{\pi}\left(\frac{EDC}{K_{eff}\,(\,|\,\Delta^{+}\,|\,+|\,\Delta^{-}\,|)^{2}}\right) \tag{1.8}$$

1.8 Factors affecting the properties of elastomer-based bearings

1.8.1 Creep And relaxation

Elastomeric materials exhibit time-dependent phenomena, such as creep and relaxation, when subjected to extended loading. Creep is an increase in strain level caused by continuous and constant loading, whereas relaxation is the decrease in stress caused by imposed constant and prolonged strain. Both phenomena have a logarithmic correlation with time (Yura et al., 2001). The creep behaviour varies among different elastomeric compounds, usually being noticeable in stiffer elastomers or those with a higher shear modulus. However, the impact of creep is typically negligible when, under moderate stress, using high-quality materials. This is because the limits for deflection are usually chosen based on serviceability rather than the total load, as specified by (AASHTO, 2020).

Based on the results of a creep study on the long-term behaviour of laminated rubber bearings, Kim et al. (2017) reported that, under compression creep tests at 7.5 and 8.37 MPa and actual environmental conditions, the maximum creep deformation is about 0.3% to 1.92 % of the total rubber thickness. In their study, the impact of shear modulus and shape factor on the creep has been evaluated. The authors determined that when the section property and shape factor (*s*) are constant, an increase in shear modulus (*G*) results in a corresponding increase in creep, as shown in Figure 1.17. Moreover, as the shape factor rises, the vertical stiffness increases while the degree of creep decreases, as shown in Figure 1.18, (Oh and Kim, 2017).

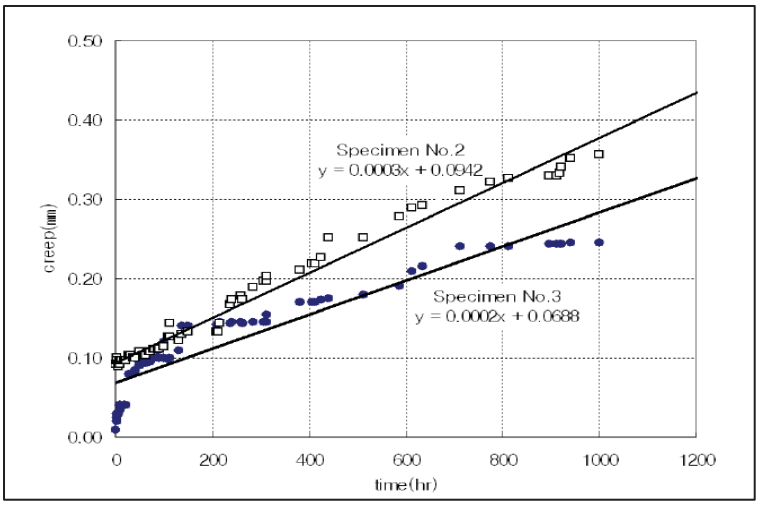

Figure 1.17 Creep for different specimens with varying shear modulus
Taken from Oh and Kim (2017)

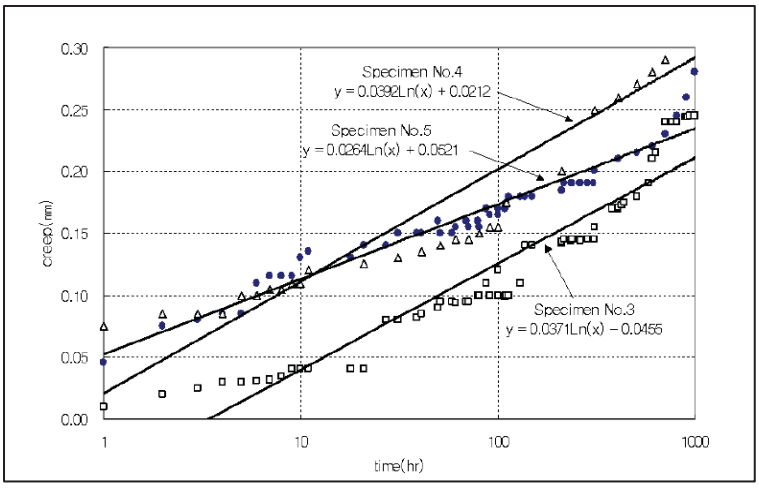

Figure 1.18 Creep for different specimens with different shape factor
Taken from Oh and Kim (2017)

1.8.2 Aging

Aging is a natural phenomenon that causes changes in elastomers' mechanical characteristics over time (Morgan et al., 2001). Generally, there are two main types of aging of rubber. The first type is due to vulcanization continuation in time, which is rooted in the resumption of the

vulcanization process. This process is irreversible and causes the material to stiffen, leading to an increase in the shear modulus. The second type is environmental impact, which changes the mechanical properties of rubber. Environmental factors that effectively contribute to the deterioration of rubber properties include ozone, heat, oxygen, sunlight, and humidity. However, these impacts can be mitigated through the utilization of wax or the integration of anti-degradation chemical agents, such as antioxidants (Yura et al., 2001).

1.8.2.1 Thermal Aging

To assess the performance of an aged elastomeric material, one of the effective approaches involves conducting an accelerated heat deterioration test, also known as a thermal aging test. In this test, the sample is exposed to intensified heat conditions to accelerate its inherent aging progression. Estimating the accelerated aging of the sample involves applying Arrhenius law, enabling the prediction of the material response based on temperature and time. Arrhenius law is formulated as follows (Toopchi-Nezhad et al., 2019):

$$\ln\left(\frac{t_{20}}{t_s}\right) = \left(\frac{1}{T_{20}} - \frac{1}{T_s}\right)\left(\frac{E_a}{R}\right) \tag{1.9}$$

Where t_{20} represents the aging time at the standard temperature of 20°C, t_s is the required time to expose the sample to an accelerated aging temperature, T_{20} is the standard temperature, here 20°C, T_s is the arbitrary aging temperature, E_a is the kinematic energy (31.7 kcal/mol), and R is the gas constant (2cal/mol. ºC). For instance, one day condition time at a temperature of 70°C is equivalent to gradually aging during 7.3 years for a sample preserved at the standard temperature of 20°C (Toopchi-Nezhad et al., 2019).

Using Arrhenius law, He et al. (2023) investigated the aging impacts on the mechanical properties of circular laminated rubber bearings. In this study, the performance of laminated rubber bearings at 10, 15, 20, and 25 years of age with different shape factors has been

evaluated by using thermal aging tests. In total 21 circular bearings according to the Chinese guidelines were chosen and categorized into 7 groups based on their shape factor and age. Groups A, C, F, and G with the same age,15 years old, were selected to establish the influence of the aged shape factor. Groups B, C, D, and E which had the same shape factor of 9.06 were selected to study the influence of aging time. To simulate the aging effect and to have samples with the desired age, samples were subjected to heat in the electric blast drying oven for period of time calculated by equation (1.9). The heating process was applied to make an equivalent aging effect on samples. Shear modulus and compression modulus before thermal aging were obtained from the production certificate provided by the manufacturer and after the aging process, compression and shear tests were conducted on the aged specimens to characterize their mechanical properties of samples and to find out the influence of aging. As presented in Figure 1.19, the compression modulus shows a more significant increase than the shape factor, when the thermal aging period increases (He et al., 2023).

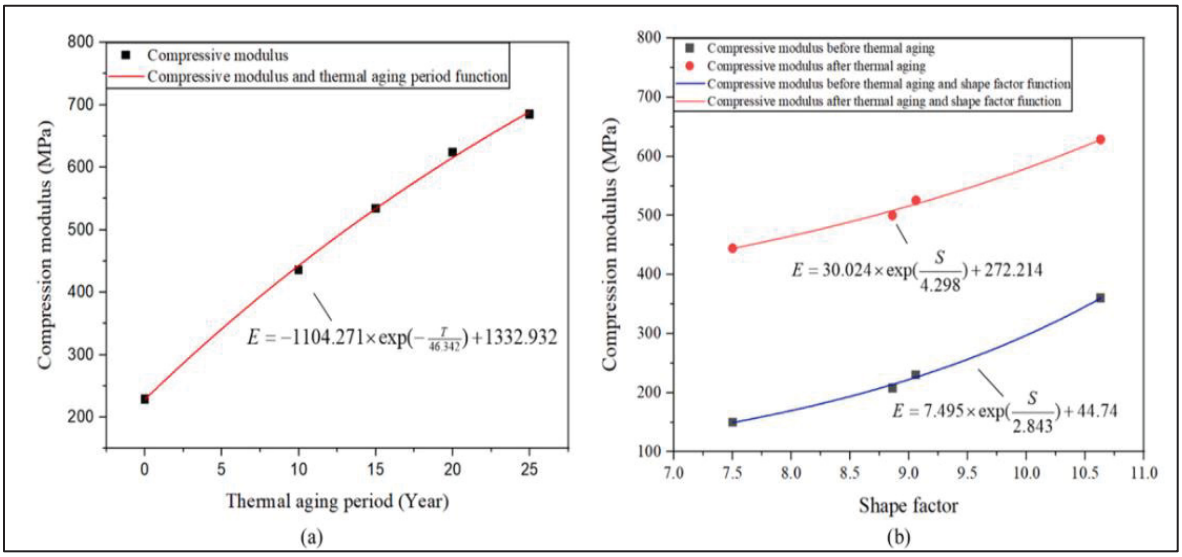

Figure 1.19 Compression modulus relationship with (a) thermal aging; (b) shape factor
Taken from He et al. (2023)

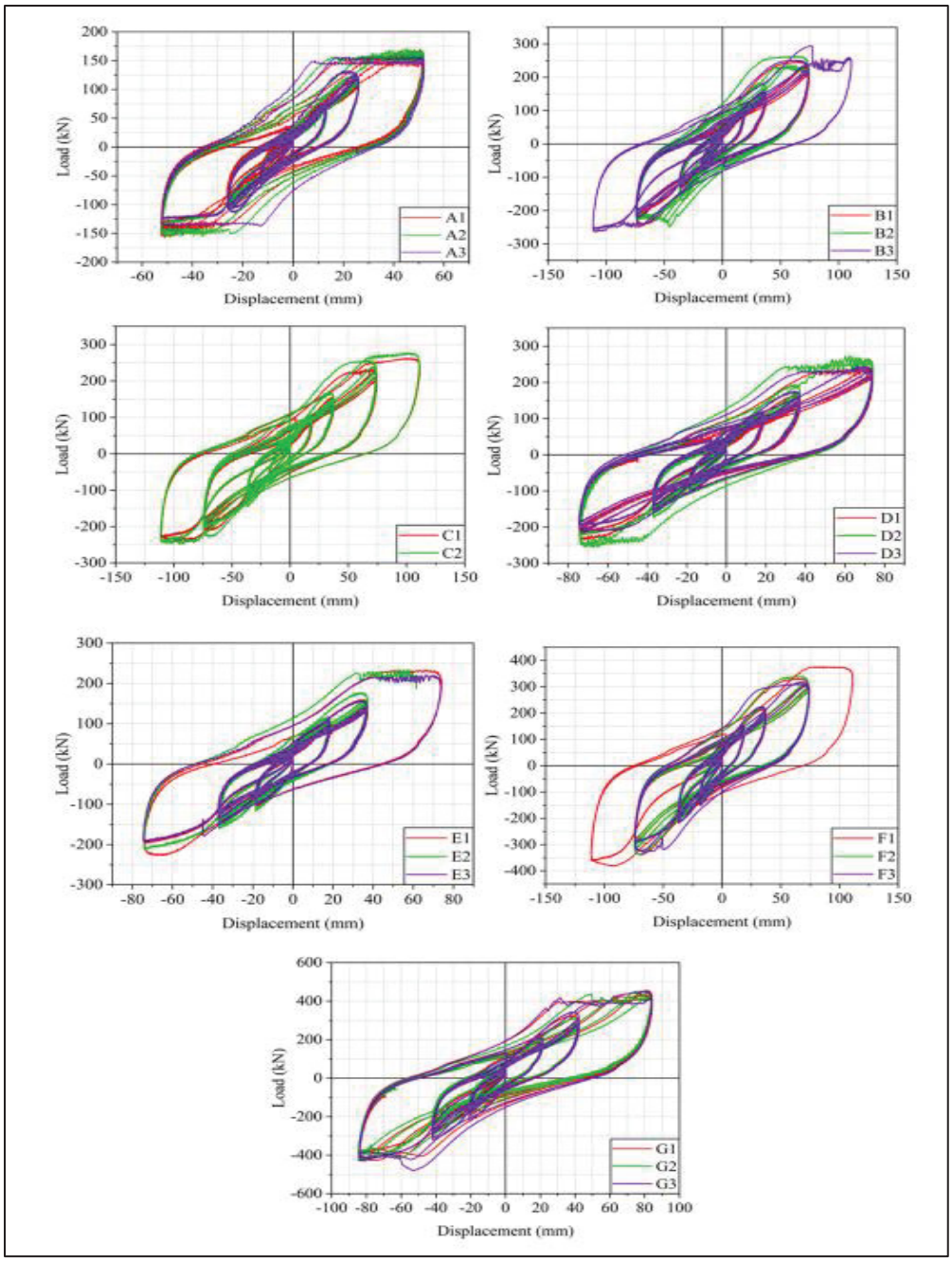

Figure 1.20 Load-displacement relationships of groups A to F specimens
Taken from He et al. (2023)

Figure 1.20 shows the shear force-displacement curve of groups A to F. Figure 1.21 also reveals that shear modulus experiences a decrease when the applied thermal aging period increases. Also, it shows that samples with higher shape factors provide greater shear modulus.

Also, After the thermal aging test, it was found that the frictional coefficients increased as the equivalent aging period extended and after 10 years, the growth rate slowed down and stabilized (He et al., 2023).

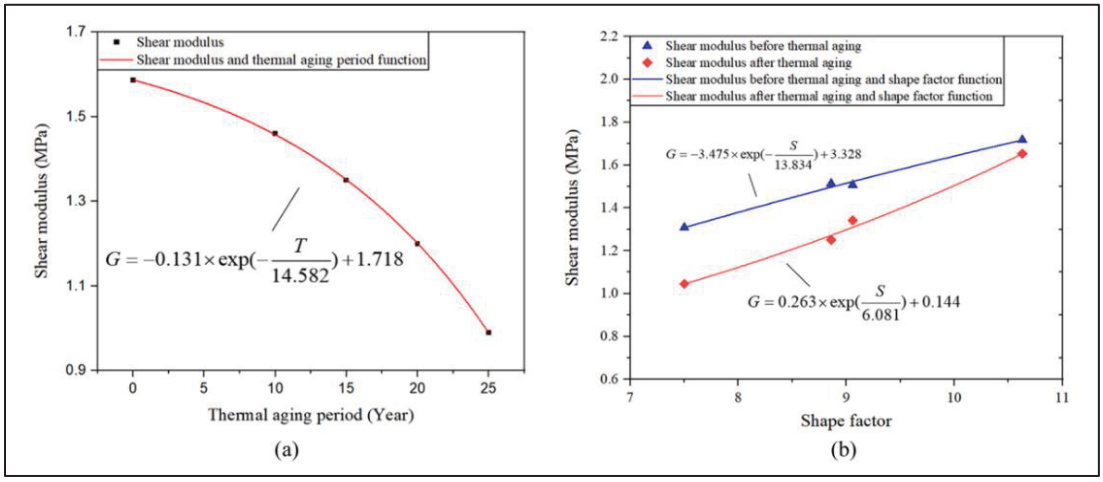

Figure 1.21 Shear modulus relationship with thermal aging (a) and shape factor (b) Taken from He et al. (2023)

1.8.2.2 Dry-wet cyclic aging

Laminated rubber bearings used in sea-crossing or offshore bridges are highly susceptible to the effects of dry-wet cycles induced by weather conditions, including rain, sun, and other environmental factors commonly found in coastal areas (Ma et al., 2019). The environmental conditions in coastal regions have the most detrimental effect on bearings used in offshore bridges, making the aging effect the primary degradation factor (Ma et al., 2016). To establish the influence of marine environment on performance of rubber, Ma et al. conducted seawater dry-wet cycles test. The performance deterioration law of rubber bearings was investigated through experimental tests and accelerated testing using the Arrhenius law. In the experimental tests, different specimens were regularly immersed in seawater and subsequently dried in a thermal aging box. During the seawater dry-wet cycles test, the specimens were dried for twice the duration of their soaking period. The dry-wet circulation mechanism for the immersion test was determined based on the annual ratio of sunny days to rainy days in coastal cities in China.

The test results, as depicted in Figures 1.22 &1.23, reveal that the horizontal and vertical stiffness of rubber increased by 23% and 7%, respectively, after a 60-day test period. Furthermore, both horizontal and vertical stiffness exhibited a linear increase with the duration of the seawater dry-wet cycles test (Ma et al., 2019).

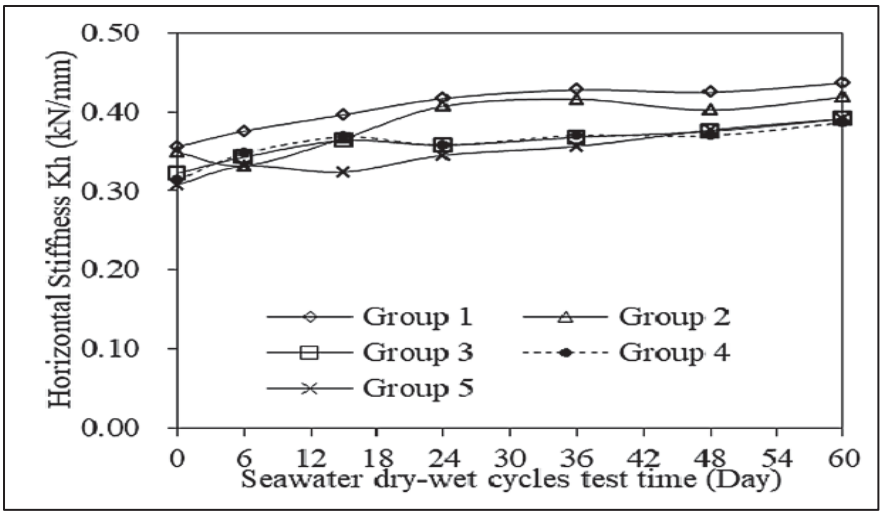

Figure 1.22 The variation trend of vertical stiffness among five groups over the duration of seawater dry-wet cycle testing
Taken from Ma et al. (2019)

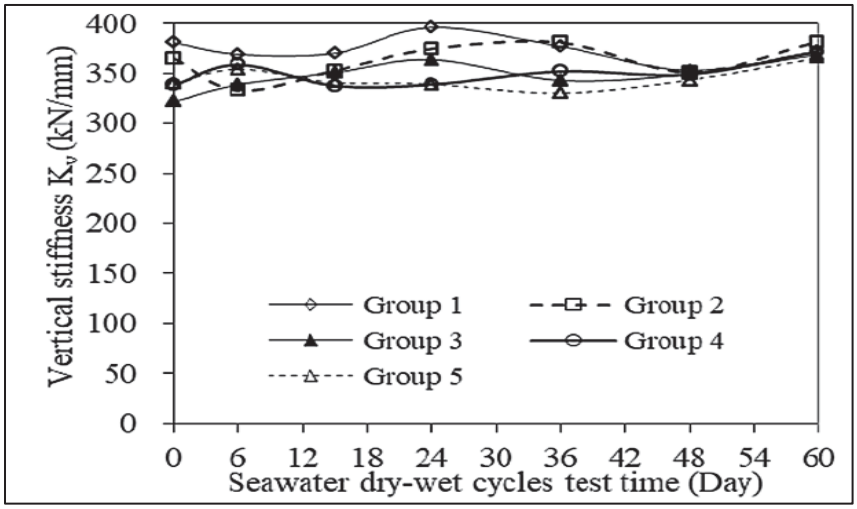

Figure 1.23 The variation trend of vertical stiffness among five groups over the duration of seawater dry-wet cycle testing
Taken from Ma et al. (2019)

In the Ma et al. (2019) study, seawater dry-wet cycle tests were conducted on NRBs to assess their performance degradation characteristics. The evolution of tensile stress and strain of the rubber material over the testing period is depicted in Figure 1.24. It is observed from Figure 1.26 that the tensile stress of the rubber material increased over the testing duration across different tensile strains. Notably, after 60 days of testing, the tensile stress at specific strains of 50%, 100%, 200%, and 300% experienced increases of 58.20%, 86.39%, 118.02%, and 115.05%, respectively. These findings underscore the significant impact of seawater dry-wet cycles on the performance of the rubber material (Ma et al., 2019).

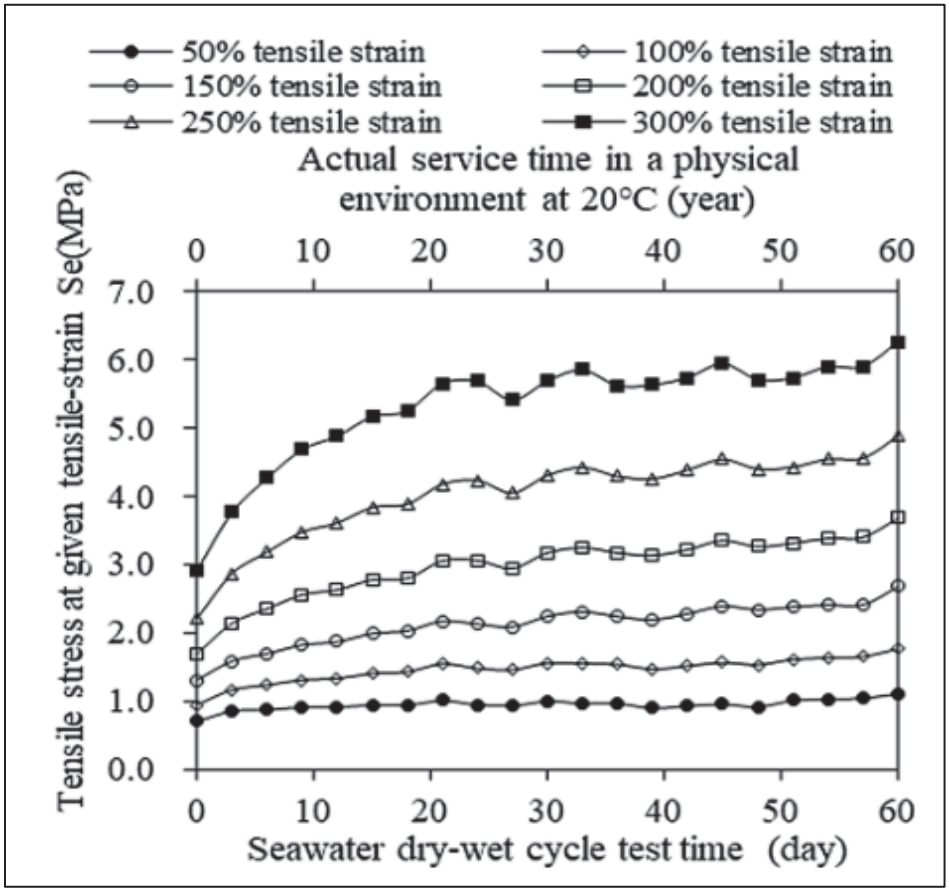

Figure 1.24 Impact of seawater dry-wet cycles on the tensile stress of natural rubber for various predetermined strains
Taken from Ma et al. (2019)

1.8.3 Effect of low temperatures on the mechanical properties of rubber

In response to low temperatures, the shear stiffness (modulus) of the elastomer increases. There are three phases in the stiffening process, two of which contribute significantly to the characterization of the mechanical properties of elastomers at low temperatures since the main increase in stiffness takes place in these two phases. Figure 1.25 illustrates the changes in elastomers' stiffness as a function of exposure time to low temperatures. In this figure, the first phase is instantaneous thermal stiffening, corresponding to the time (t_1) required for thermal equilibrium. The time demanded for thermal equilibrium varies with the dimensions of the bearings. Following this initial phase, a second phase takes place during the period of time between t_1 and t_2, and where stiffness remains roughly unchanged. This period called the induction period, and essentially depends on the temperature and the chemical composition of the elastomer. The last phase is crystallization stiffening, which is time-dependent and occurs due to the reorientation of the molecular structure of the elastomer. Exposure to very low temperatures also causes a glass transition, making the elastomer brittle and leading to a significant change in its mechanical and physical properties. The glass transition varies by material and is compound-dependent; for example, the glass transition temperature for natural rubber is approximately -55°C (Constantinou et al., 2007).

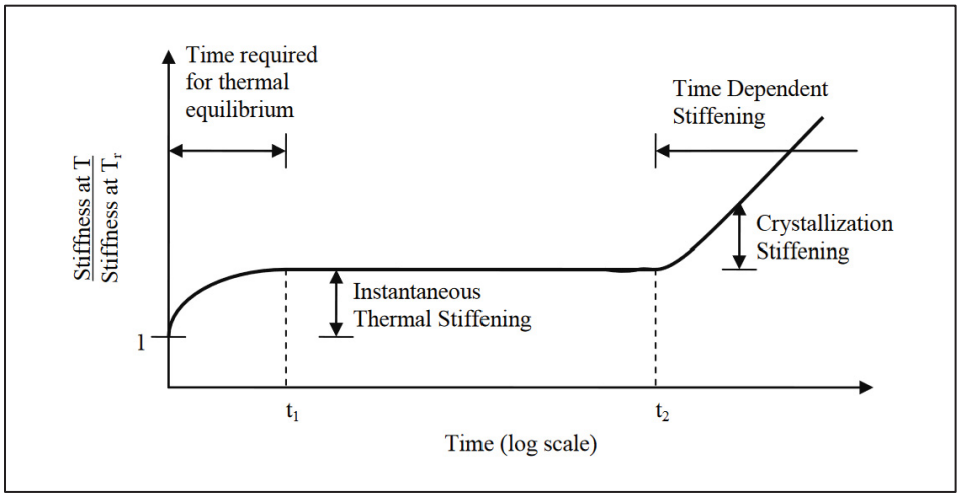

Figure 1.25 Behaviour of elastomers under low temperatures
Taken from Constantinou et al. (2007)

1.8.3.1 Instantaneous thermal stiffening

Instantaneous thermal stiffening refers to the rapid increase in the stiffness of elastomers when exposed to low temperatures. This phenomenon takes place within a time period required to achieve thermal equilibrium between the center of the block of elastomer and the surrounding temperature. Temperature and thickness of the elastomer block strongly influence this time period (Constantinou et al., 2007). Canadian Highway Bridge Design Code requires elastomers not to have a hardness greater than 3 times that measured at 20°C when subjected to the -40ºC (CSA, 2019).

1.8.3.2 Crystallization at low temperatures

Crystallization is the mechanism that occurs in elastomers when they are subjected to prolonged periods at low temperatures, after experiencing instantaneous thermal stiffening (Constantinou et al., 2007). The progressive stiffening of the elastomer depends on several parameters, such as temperature, period of exposure, and the specific type and chemical composition of the material. It is worth mentioning that natural rubber has a greater rate of crystallization as temperatures approaches -25°C, while neoprene reaches its maximum crystallization rate at approximately -10°C. The rates of crystallization for natural rubber and neoprene remain moderate at temperatures of their respective thresholds. It is crucial to recognize that crystallization is completely reversible and dissipates with an increase in temperature (Yura et al., 2001).

Figure 1.26, provided by Treloar in 1975, depicts the variation in the crystallization rate of natural rubber as a function of temperature. Experimental studies conducted by Fuller et al. reveal that polymer additives, such as vinyl-butadiene, when added to high-damping natural rubber (HDNR), can extend the induction period, leading to a delay in the occurrence of crystallization. As a consequence, the instantaneous thermal stiffening is considerably increased (Fuller et al., 2004, 1997).

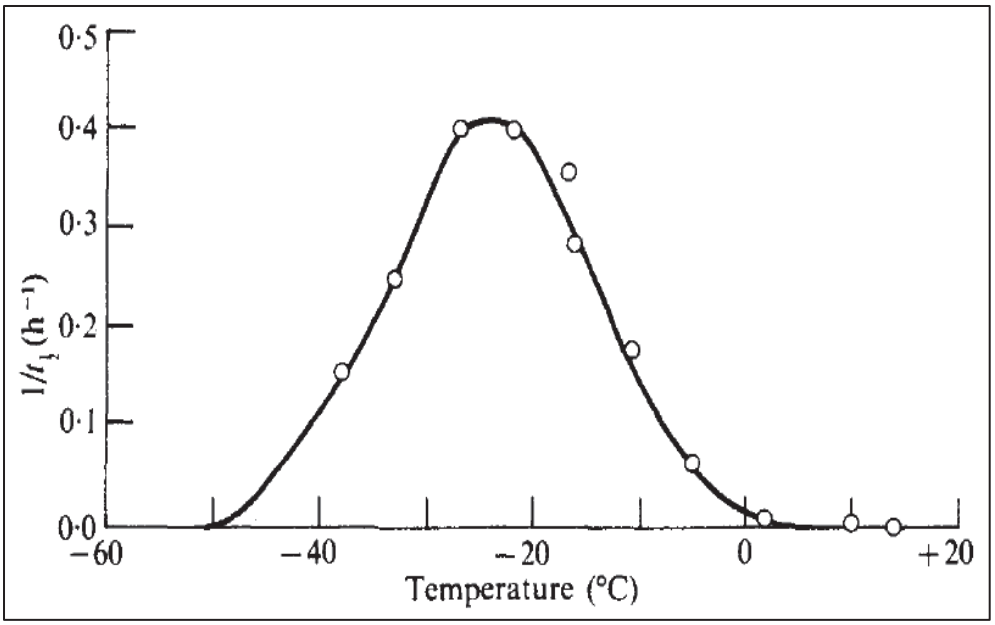

Figure 1.26 Crystallization rate of natural rubber based on temperature
Taken from Treloar (1975)

1.9 Study review

Gaetano Pianese et al. (2024)

Pianese et al. studied the performance of the fiber-reinforced elastomeric isolators (FREI) under bonded, partially bonded, and unbonded conditions. In this study, high-damping rubber composition made of natural rubber (NR) and ethylene propylene-diene monomer (NR-EPDM) supported by thin glass-fiber layers were used to produce the FREIs prototypes. Fiber layers have lower weight and can be manufactured through cold vulcanization, compared to the steel-reinforced elastomeric isolators. In this study, The FREIs were circular bearings with a diameter of 200mm, and a total height of 67mm, constituted by 15 layers of NR-EPDM rubber pads (4mm thick) and 14 glass fiber fabric laminas (0.5mm thick). The shape factor and the aspect ratio of the bearing were 2.50 and 2.98, respectively. To provide the bearings with partially bonded condition, a technique was applied wherein only segments of the bearing's contact surfaces were bonded to the steel endplates. This approach effectively preserves key attributes associated with the unbonded condition, like rollover deformation, and the bonded

condition, like the resistance to uplift forces and slip. The dynamic properties of the bearings were assessed through a cyclic shear test. FREIs were subjected to a vertical monotonic load, sustained at the design load throughout the shear test. Employing a horizontal actuator, the bearing underwent three fully reversed cycles of sinusoidal motion at a frequency of 0.2Hz. The amplitudes of displacement were set to 25%, 50%, 75%, and 100% shear strain. These tests were conducted under three different pressures: 1MPa, 2MPa, and 3MPa (Pianese et al., 2024).

As depicted in Figures 1.27 & 1.28, an increase in shear strain correlates with consistent decrease in horizontal stiffness of all the three configurations. Elevating the vertical load from 1Mpa to 3Mpa results in a similar downward trend in horizontal stiffness values for each configuration. Among all the configurations, the bonded isolator (BFREI) displays the highest horizontal stiffness values. Conversely, the unbonded isolator (UFREI) exhibits the lowest stiffness values. Also, the partially bonded isolator (PBFREI) occupies a middle position, exhibiting stiffness values between those of the bonded and unbonded isolators (Pianese et al., 2024).

Moreover, the damping capacity of the device escalates with an increase in vertical load. Specifically, the unbonded configuration demonstrates the highest damping capacity among all configurations (Pianese et al., 2024). Slip resistance tests were conducted by Pianese et al. to examine the frictional interaction between the bearing and the moving steel plates of the testing machine. In these tests, unbonded FREI was subjected to vertical loading, ranging from 1MPa to 3MPa while an increasing horizontal load was applied to the platform, inducing shear deformation in the isolator, and causing slip. The horizontal load was incrementally increased to assess slip resistance and determine slip load which is the maximum load that can be applied on the bearing before slipping occurs (Pianese et al., 2024).

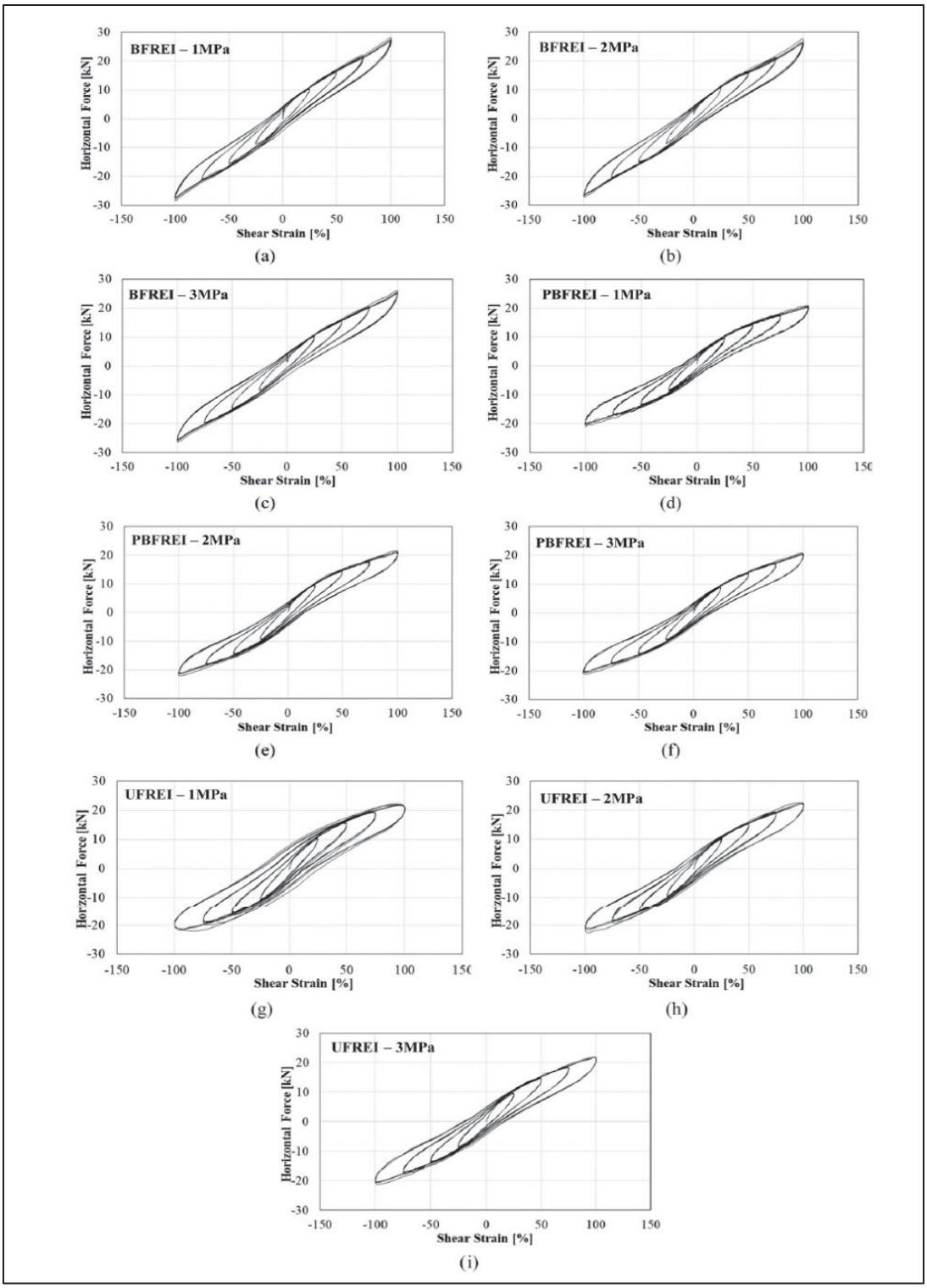

Figure 1.27 Force-strain curves of shear tests: (a-b-c) BFREI, (d-e-f) PBFREI and (g-h-i) UFREI
Taken from Pianese et al. (2024)

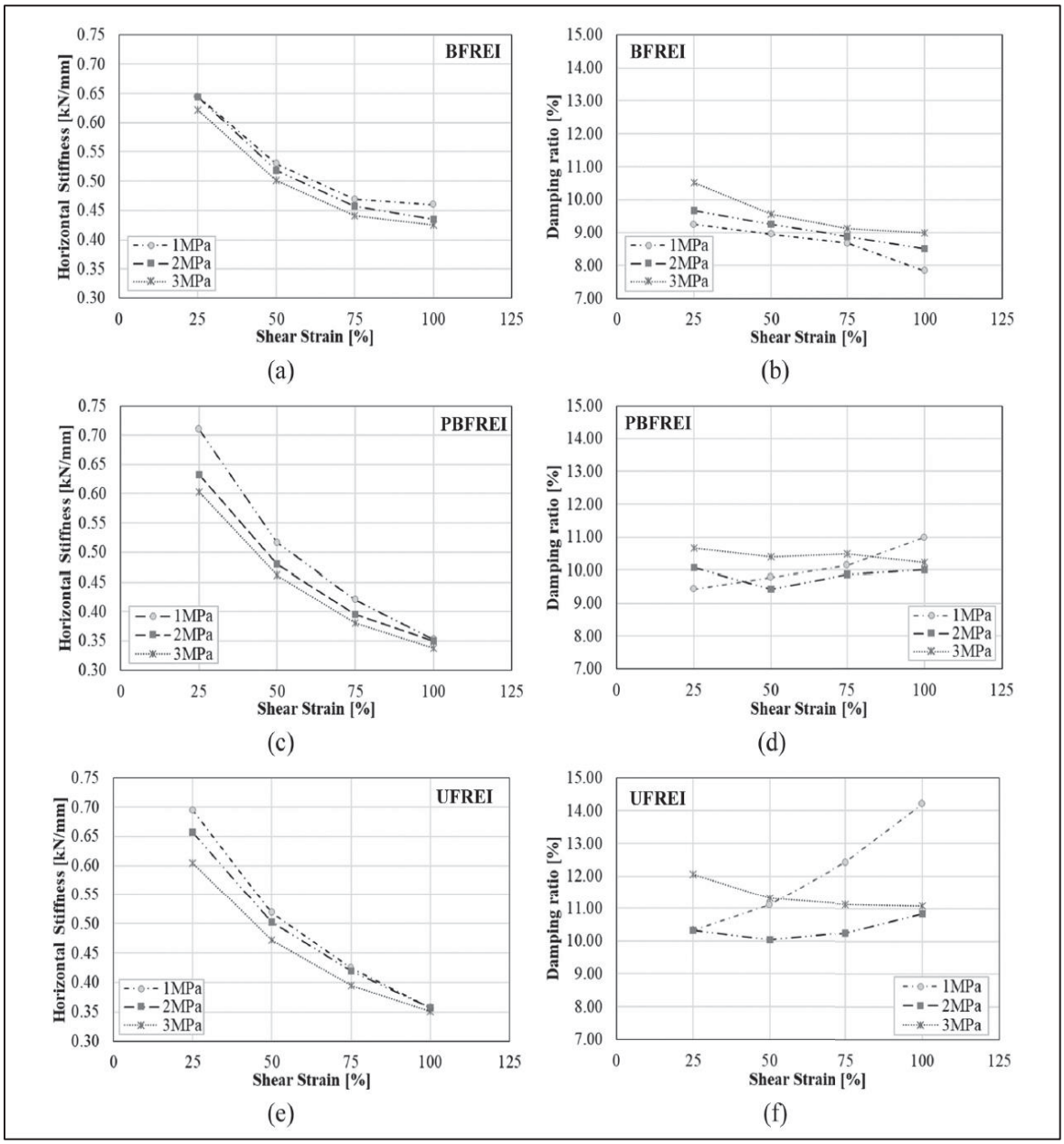

Figure 1.28 Shear test results: (a-c-e) horizontal stiffness and
(b-d-f) damping ratio as a function of shear strain
Taken from Pianese et al. (2024)

Various factors, including compressive load, type of rubber, and surface condition, impact sliding behaviour. However, this study specifically focused on investigating the influence of vertical (compressive) load. Force-displacement curves for different vertical loads are plotted

in Figure 1.29. The obtained results underscore that the minimum vertical load should exceed 1.25MPa if instability induced by slip is required to be prevented in the testing machine. The author suggests that, in structural applications, a vertical pressure of 1MPa may be suitable for a stable response due to the fact that the presence of concrete is expected to enhance friction (Pianese et al., 2024). However, the last version of the Canadian Highway Bridge Design Code (CSA, 2019) required positive attachment for pressures less than 3 MPa on a laminated bearing, under a serviceability limit state (SLS), to prevent bearing walking (displacement relative to the surface with which it is in contact) under bridge vibration.

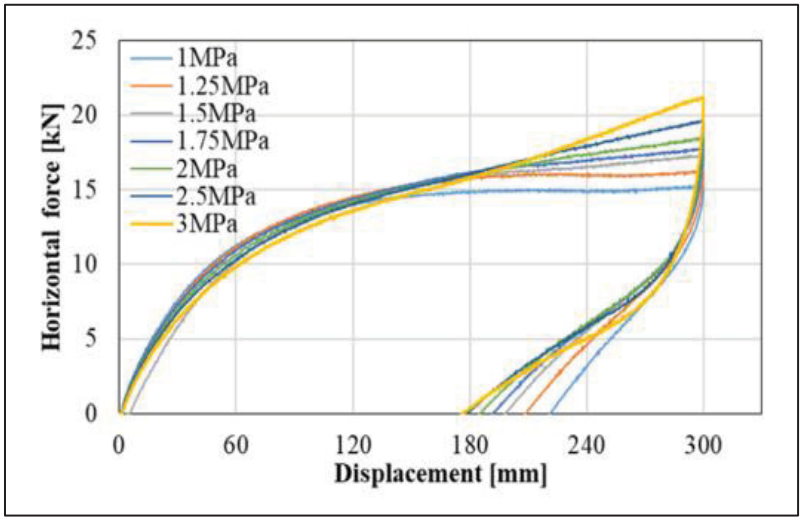

Figure 1.29 Results of slip resistance test
Taken form Pianese et al. (2024)

Zengde Zhang and Ying Zhou (2023)

Zhang and Zhou studied the mechanical behaviour of full-scale thick rubber bearings (TRBs). They conducted experimental and analytical evaluations on the horizontal behaviour of TRBs with differences in first and second shape factors (S1 and S2). In their study, eight full-scale thick rubber bearings including five full-scale thick natural rubber bearings (TNRBs) specimens (#1 to #5), and three lead-core thick rubber bearings (LTRBs) specimens (#1 to #3) were designed and tested under shear loading. The study delved into the influence of geometric parameters and loading conditions on these isolators. The employed rubber material exhibited

a secant shear modulus of 0.55 MPa, as determined under a shear strain of 100%. All specimens had a circular configuration with 800 mm diameter, the same thickness of rubber cover of 10 mm, and the thickness of steel shims of 10 mm. To facilitate heat conduction during the vulcanization process, a central hole with a diameter of 50 mm was provided for TNRB specimens. The specimens were subjected to constant vertical load and cyclic horizontal displacements with increasing amplitudes of 50%, 100%, 150%, and 200% of the strain. Three loading cycles were applied for each strain level. In future tests, various vertical loads also were applied to specimens by following this procedure (Zhang and Zhou, 2023).

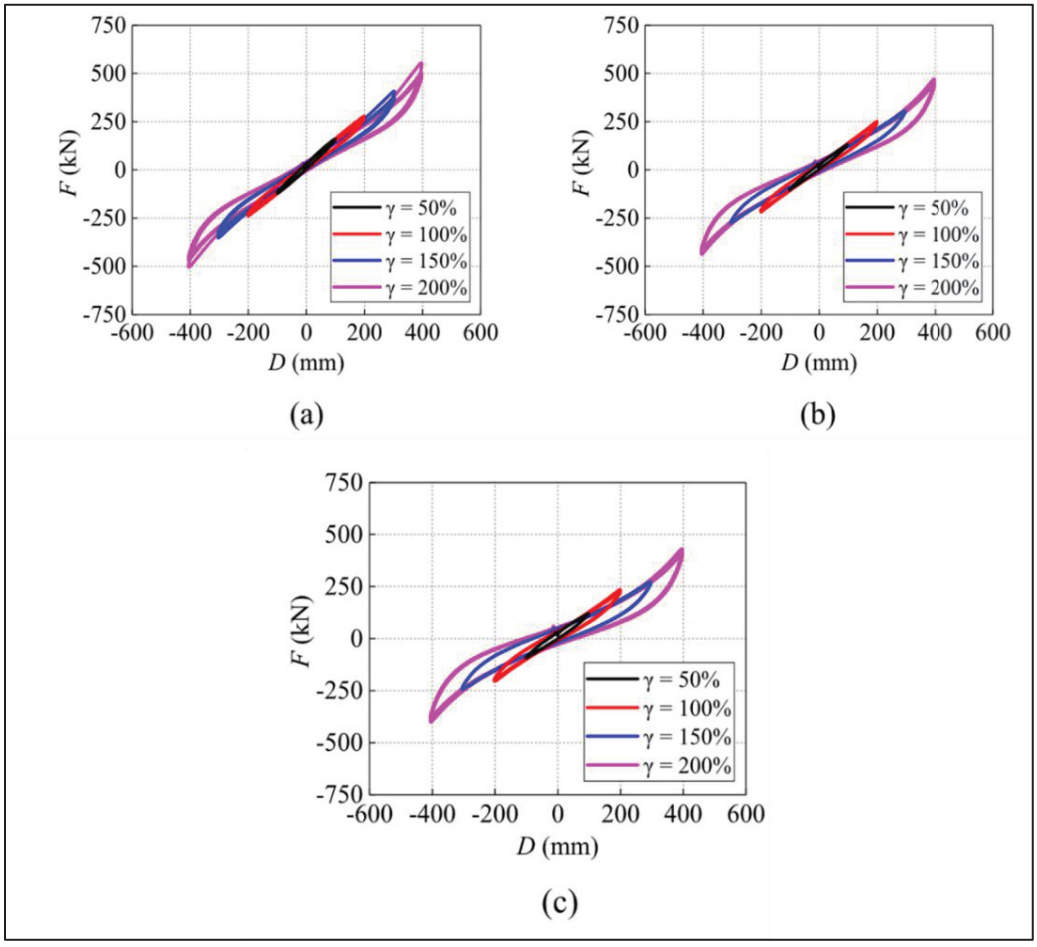

Figure 1.30 Force-displacement curves of TNRB #3 under different vertical pressures: (a) 6 MPa; (b) 8 MPa; (c) 10 MPa
Taken from Zhang and Zhou (2023)

In order to mitigate the influence of prior loading on the shear properties of the samples and to ensure a consistent loading temperature, time intervals of 20 minutes for TNRBs and 40 minutes for LTRBs were considered. They were applied between consecutive loadings performed under different vertical pressures. Throughout all tests, a sinusoidal input signal characterized by a frequency of 0.006 Hz was employed. The relationship curve between shear force (F) and lateral displacement (D) of TNRB and LTRB under vertical loads of 6 MPa, 8 MPa, and 10 MPa at different lateral displacements is illustrated in Figures 1.30 & 1.31. From this figure, the author found that both TNRB and LTRB exhibit increased horizontal softness as the vertical load is raised. The lead TRB specimen demonstrates a higher energy dissipation capacity compared to the Natural TRB, attributed to the presence of a plugged lead core (Zhang and Zhou, 2023).

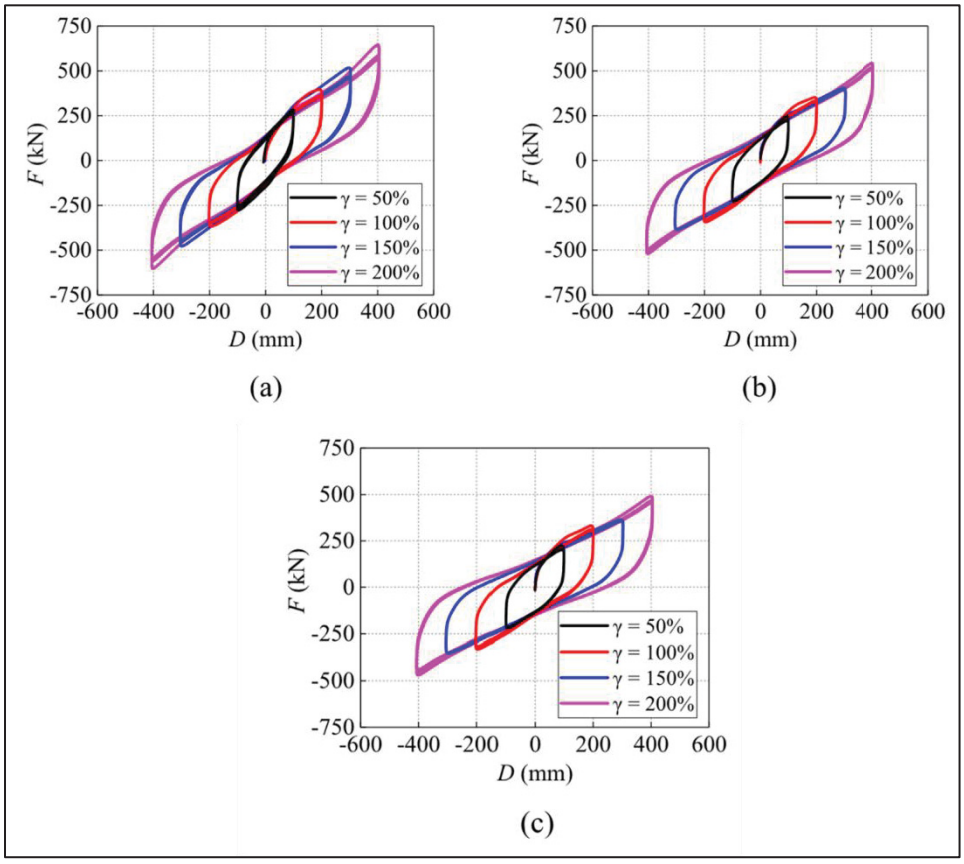

Figure 1.31 Force-displacement curves of LTRB #1 under different vertical pressures: (a) 6 MPa; (b) 8 MPa; (c) 10 MPa
Taken from Zhang and Zhou (2023)

Zhang et al. (2023) compared the effective stiffness (K_{eff}) of TNRBs with different values of shape factors S1 and S2, defined hereafter. The first shape factor denoted as S1, represents the ratio of the compressive area divided by the area of the lateral surface free to bulging deformation. According to Zhou and Zhang (2022), the first shape factor S1, as a design parameter, plays a crucial role in controlling the restraint influence exerted by the steel plate on the bulge, thereby impacting vertical stiffness and operational frequency. Additionally, the second shape factor S2, represents the aspect ratio and is obtained by the external diameter, d, divided by the total rubber thickness. S2 governs not only the stability (against buckling) but also the nonlinear behaviour of TRBs under both horizontal and vertical loads (Zhou and Zhang, 2022). As shown in Figure 1.32 (a), they found that bearings sharing the same S2 value of 4.00 exhibit a reduction in effective stiffness when the S1 value is altered from 12.18 to 9.38. However, this decline is less notable for bearings characterized by a higher S2 value of 5.00. In the comparison of bearings featuring an S1 value of 9.38, the reduction of S2 from 5.00 to 4.00 leads to a noteworthy decrease in the horizontal stiffness of the bearings. Consequently, the horizontal flexibility of natural TRBs manifests greater sensitivity to alterations in the S2 value, and slenderer TNRBs display increased flexibility in the horizontal direction. Also, bearings with a lower S2 value below 2.5 tended to exhibit instability. A moderately sized S2 value of approximately 4.0 appears to provide more stability and effectiveness for TRBs (Zhang and Zhou, 2023).

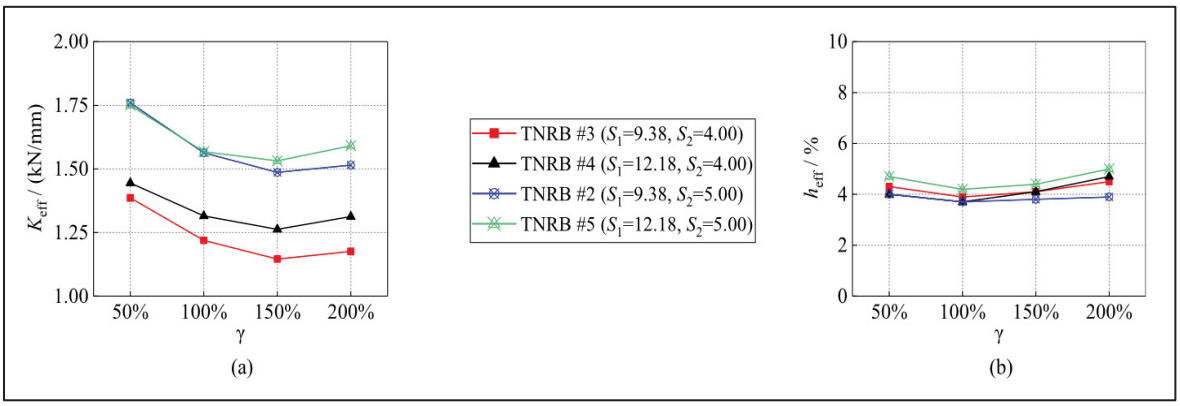

Figure 1.32 Influence of S1 and S2 on shear behaviour of TNRBs: (a) effective stiffness; (b) effective damping ratio[1]
Taken from Zhang and Zhou (2023)

Figure 1.32(b) shows the variation of the effective damping ratio (h_{eff})[1] of thick natural rubber bearings when shape factors are different. It reveals that the effect of S1 and S2 on the effective damping ratio of bearings (ranging from 3.7% to 5.6%) is negligible. Figure 1.33 shows the shear properties of LTRBs with different values of S1 and identical values of S2, including effective stiffness (K_{eff}), post-yield stiffness (K_d), characteristic strength (Q_d), and effective damping ratio (h_{eff})[1]. In this study Q_d is calculated by the average of maximum and minimum force at the zero strain. The stiffnesses (K_{eff} & K_d), and the damping ratio of LTRBs shows limited sensitivity to an increase in S1 from 10.00 to 12.99, while the characteristic strength of bearings rises by approximately 10% (Zhang and Zhou, 2023).

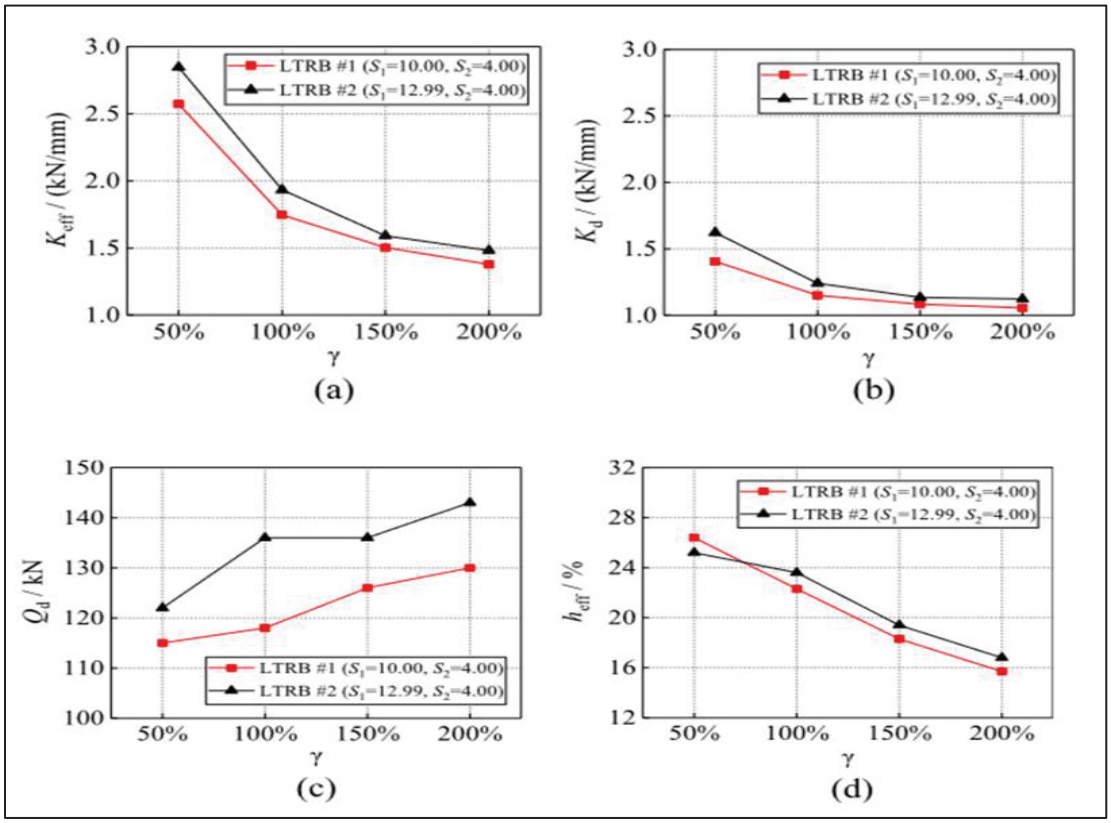

Figure 1.33 Influence of *S*1 on shear behaviour of LTRBs: (a) Effective stiffness; (b) Post-yield stiffness; (c) characteristic strength; (d) Effective damping ratio[1]
Taken from Zhang and Zhou (2023)

[1] Damping ratio in this thesis is denoted as ξ_{eq}

Changes in the effective stiffness (K_{eff}) and effective damping ratio (h_{eff})[1] of TNRB #3 as a function of strain amplitude for different vertical pressures are depicted in Figure 1.34 (a) & (c), showing that by increasing the vertical pressure, there is a decrease in effective stiffness and an increase in damping ratio. Figure 1.34 (b) & (d) show the variations in effective stiffness and effective damping ratio of TNRB #5 under varying vertical pressures. These figures highlight that the impact of vertical pressure on the shear properties of the bearings is not contingent upon their shape factors (Zhang and Zhou, 2023).

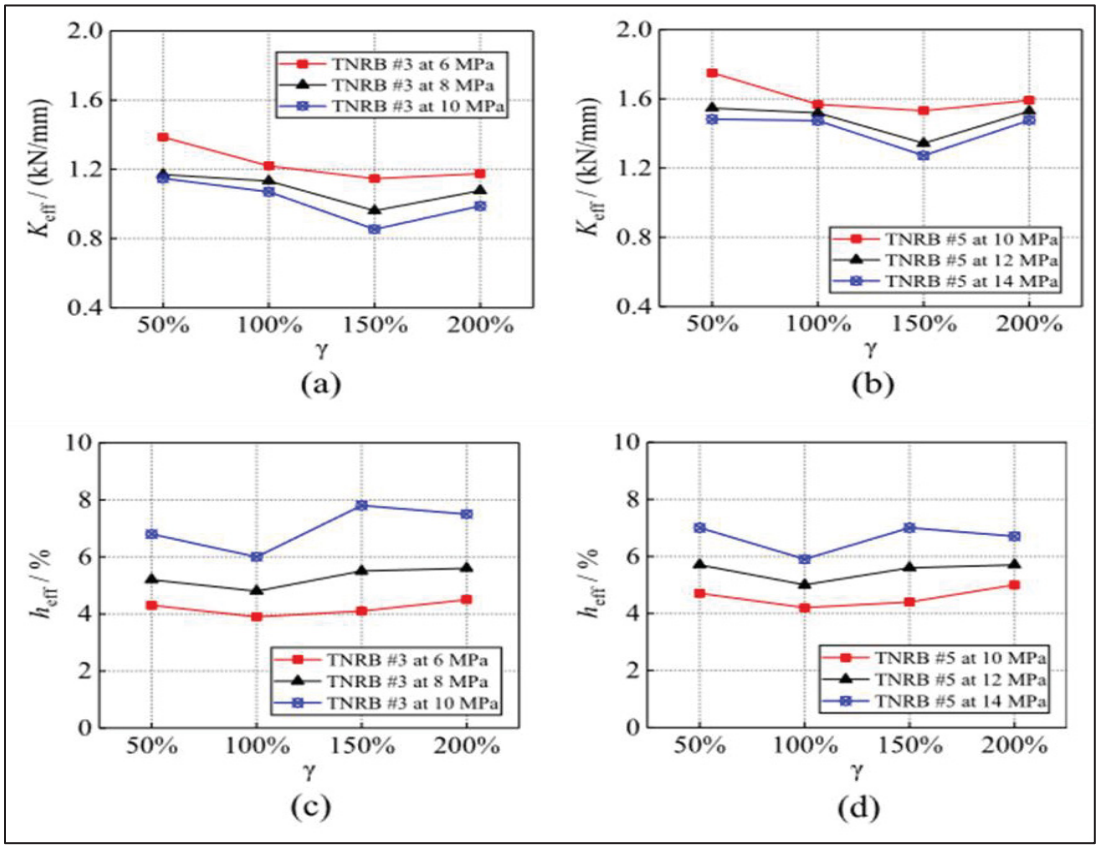

Figure 1.34 Loading conditions impact on shear properties of TNRB: (a) and (b) effective stiffness; (c) and (d) effective damping ratio[1] Taken from Zhang and Zhou (2023)

Figure 1.35 shows the influence of the vertical pressure on the shear behaviour of LTRBs. It revealed that by increasing the vertical pressure, shear stiffness decreases, while the characteristic strength and damping ratio experience an increase.

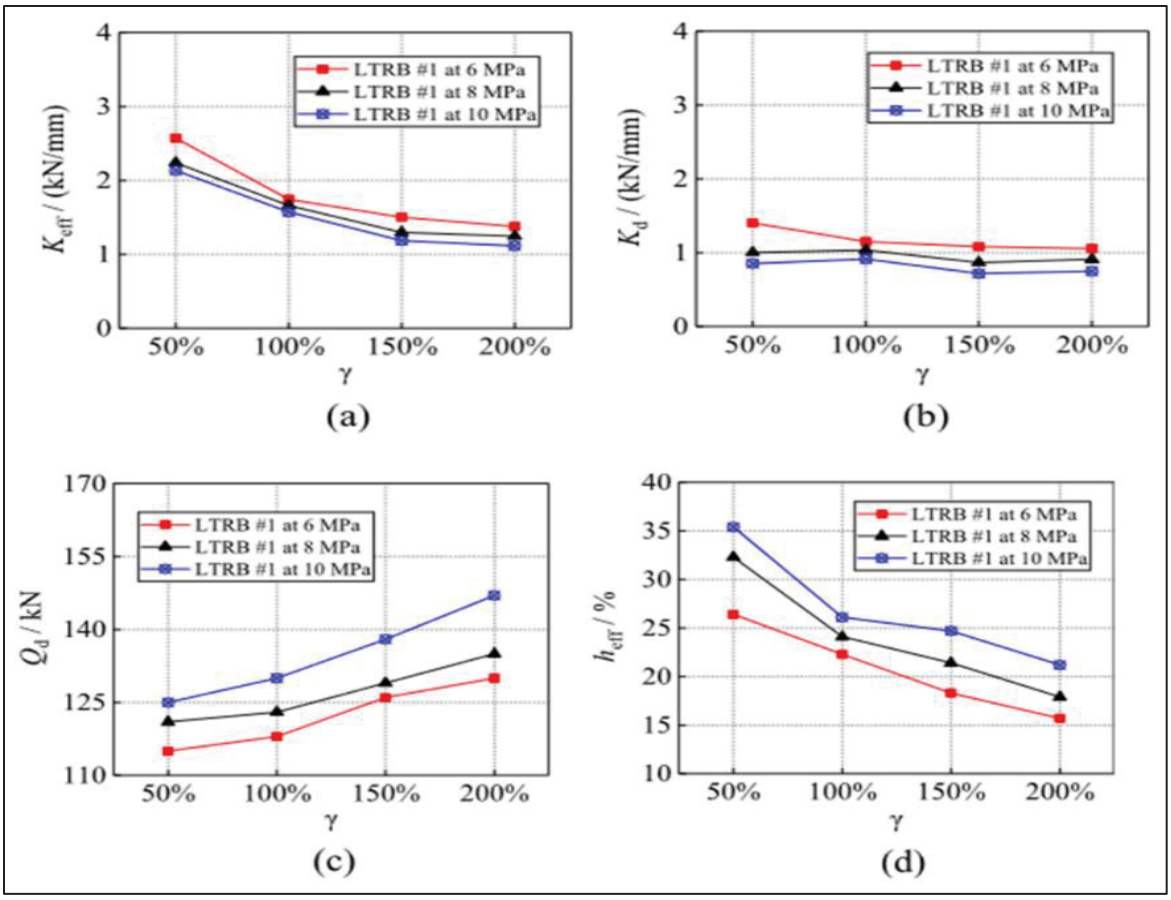

Figure 1.35 Loading conditions impacts on shear properties of LTRB #1:(a) effective stiffness; (b) post-yield stiffness; (c) characteristic strength; (d) damping ratio[1]
Taken from Zhang and Zhou (2023)

Muntasir Billah and Borislav Todorov (2019)

A study by Muntasir Billah and Borislav Todorov examined the low-temperature effects on the seismic response of a lead rubber-bearing isolated bridge. The research focused on a seven-span continuous highway bridge located in Montreal, QC. The bridge is classified as a major route bridge according to the Canadian Highway Bridge Design Code (CHBDC). It is composed of six multi-column pier bents, with the superstructure consisting of six simply supported precast concrete girders. Each pier and abutment are equipped with lead rubber bearings to address the longitudinal and transverse drift of the bridge deck induced by thermal loading and earthquake ground motions (Billah and Todorov, 2019).

The study utilized a finite element model to assess the isolated bridge's performance, considering the isolator force-deformation relationship and shear strain in the isolation bearings. The model accounted for material properties of bridge components and bearing properties at both summer and winter service temperatures, specifically addressing the low-temperature effects on the seismic response of LRB-isolated bridges. Dynamic time history analyses for the 10 selected earthquake records, scaled to match the CHBDC spectra, are performed to establish the seismic performance of the isolated bridges under summer and winter conditions (Billah and Todorov, 2019).

To assess the shear deformation of lead rubber bearings (LRBs) under diverse ground motions during hot and cold seasons (ranging from +35°C to -35°C), Billah and Todorov analyzed the shear strain (γ) of LRBs over time, as illustrated in the Figure 1.36. Upon comparing peak shear strain values in these two scenarios, a notable observation emerged. Specifically, as detailed in Figure 1.36 , under summer conditions, the maximum shear strain within the LRB surpassed 150%, while during winter conditions, shear strains consistently remained below 90%. This reduction in shear deformation (seismic displacement) is systematically observed for winter conditions, when compared to summer conditions, which indicates diminished effectiveness of the isolation system due to lower lateral flexibility during winter. The authors calculated an average reduction of 26% between the maximum shear deformation in summer and winter. This reduction underscores the impact of temperature variations on the shear behaviour of LRBs, highlighting the importance of considering such factors in the seismic performance evaluation of isolated structures (Billah and Todorov, 2019).

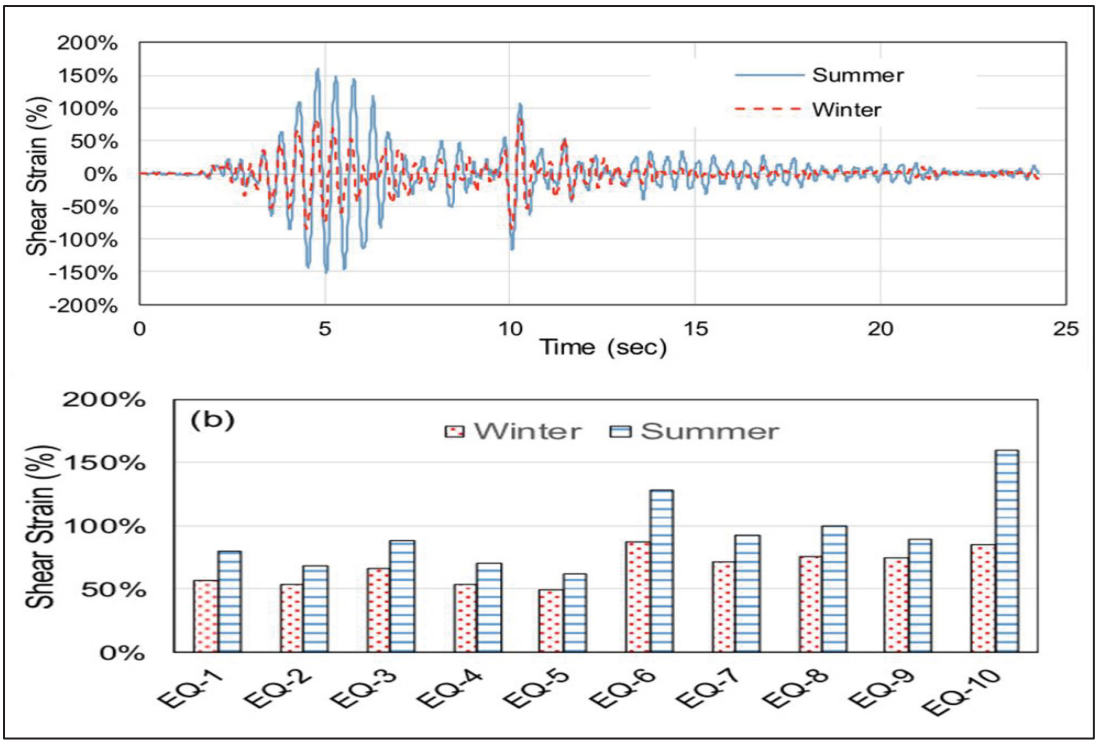

Figure 1.36 (a) Time history analysis of shear strain in the LRB bridge subjected ground motion #10, (b) comparison of LRB shear strain in summer and winter Taken from Billah and Todorov (2019)

Figure 1.37 illustrates the impact of low temperatures on the hysteretic response of LRBs when exposed to ground motion #10. It is evident from Figure 1.37 that, in colder conditions, not only bearing deformation but the hysteresis loop area experiences a significant decrease. The observed reduction in the hysteresis loop amplitude implied a decrease in the overall energy dissipated and higher seismic forces. In the case of the short pier (Figure 1.37 b), the total energy dissipated during summer and winter alters from 1830 kN.m to 1480 kN.m, respectively, indicating a 24% decrease in winter. Additionally, for longer pier (Figure 1.37 a), energy dissipation decreased by 42% in winter (Billah and Todorov, 2019).

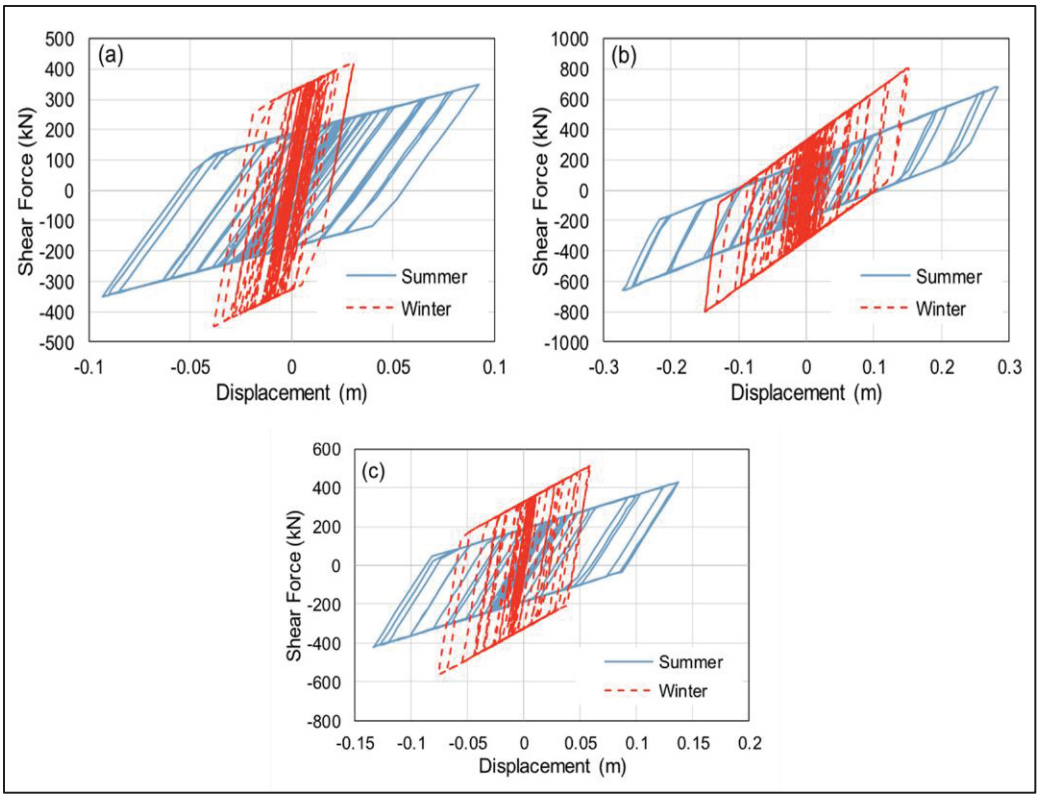

Figure 1.37 Hysteretic behaviour of LRBs in summer and winter for different piers; (a) long pier, (b) short pier, and (c) medium pier
Taken from Billah and Todorov (2019)

Djamel Ankik (2019)

Ankik studied the mechanical properties of two different compounds of high-damping rubber (B and E) and a low-damping natural rubber. In this study, vulcanized quadruple samples supplied by the Canadian company Goodco Z-Tech, of the Canam-Bridges group, were subjected to shear loading cycles at low temperatures after being continuously exposed to these low temperatures for a variable period. These samples all had the same size with dimensions of 25.4 mm x 25.4 mm and a thickness of 6 mm, as recommended by ASTM D4014. As experiment variables, temperature, strain rate, and conditioning time were key parameters. Based on the locality of Montreal and following the requirements of CSA 2014b, temperatures of -8ºC and -30ºC, as well as 20ºC, were chosen for testing the samples. Also, in order to study the effect of duration of exposure to the low temperatures on the low-damping and high-

damping rubber, conditioning times of 15 minutes, 30 minutes, 1 hour, 24 hours, 3 days, 7 days, and 14 days were considered. 15 minutes represented an estimate of the time required to reach thermal equilibrium in the tested specimens, based on the ASTM D832. In this study, samples were exposed to defined temperatures, -8ºC and -30ºC, for a specific duration, and then subjected to the cyclic shear load with a frequency of 0.5 Hz to gradually reach the desirable strain amplitude ranging from 25% to 150% with a step of 25%. Shear tests were carried out under controlled displacement by using the MTS press located at the ETS laboratory. Each strain amplitude repeats three times since the hysteresis curve essentially stabilizes at the third cycle and the properties of elastomers are often determined at this loading cycle. Results for low-damping natural rubber specimens (NAT55) tested at -8°C are shown in Figure 1.38, in terms of hysteresis responses, obtained after different conditioning times. They show an increase in the maximum stress and the area of the hysteresis loops compared to the specimen tested at 20°C. For example, the maximum stress at 100% strain increases by about 11% after 15 min of conditioning at -8°C, compared to a temperature of 20°C. Additionally, it was observed that there is no notable difference in the mechanical response of the natural rubber (NAT55) at -8°C when the conditioning time increased. For example, from 15 min to 14 days, approximately a 2% increase in the maximum stress at 100% deformation was experienced. However, hysteresis responses at -30°C, shown in Figure 1.39, indicate that the area of the hysteresis loops and maximum stress are considerably greater than those obtained at 20°C (Ankik, 2019). For instance, the maximum stress at 100% strain increases by about 35% after 15 min of conditioning at -30°C, compared to a temperature of 20°C. Moreover, notable differences between the hysteresis curves at -30°C were observed when the conditioning duration increased. For example, at 100% strain, the maximum stress increased by approximately 9% when the conditioning duration increased from 1 to 3 days, by approximately 10% when it increased from 3 to 7 days, and by approximately 27% when it increased from 7 to 14 days. Subsequently, the author found that the hysteresis responses of compounds B and E exhibit similar stress behaviours to NAT55 at low temperatures of -8°C and -30°C, but with higher sensitivity to the low temperatures and greater stress levels. For example, compared to 20°C the maximum stress of compounds B and E increased by approximately 32 % and 40%, respectively, after 24 hours of conditioning at -8°C for a strain

amplitude of 100%. Also, after 24 hours of conditioning at -30°, the maximum stress of compounds B and E increased by 139% and 148% after 24 hours of conditioning at -30°, compared to 20°C (Ankik, 2019).

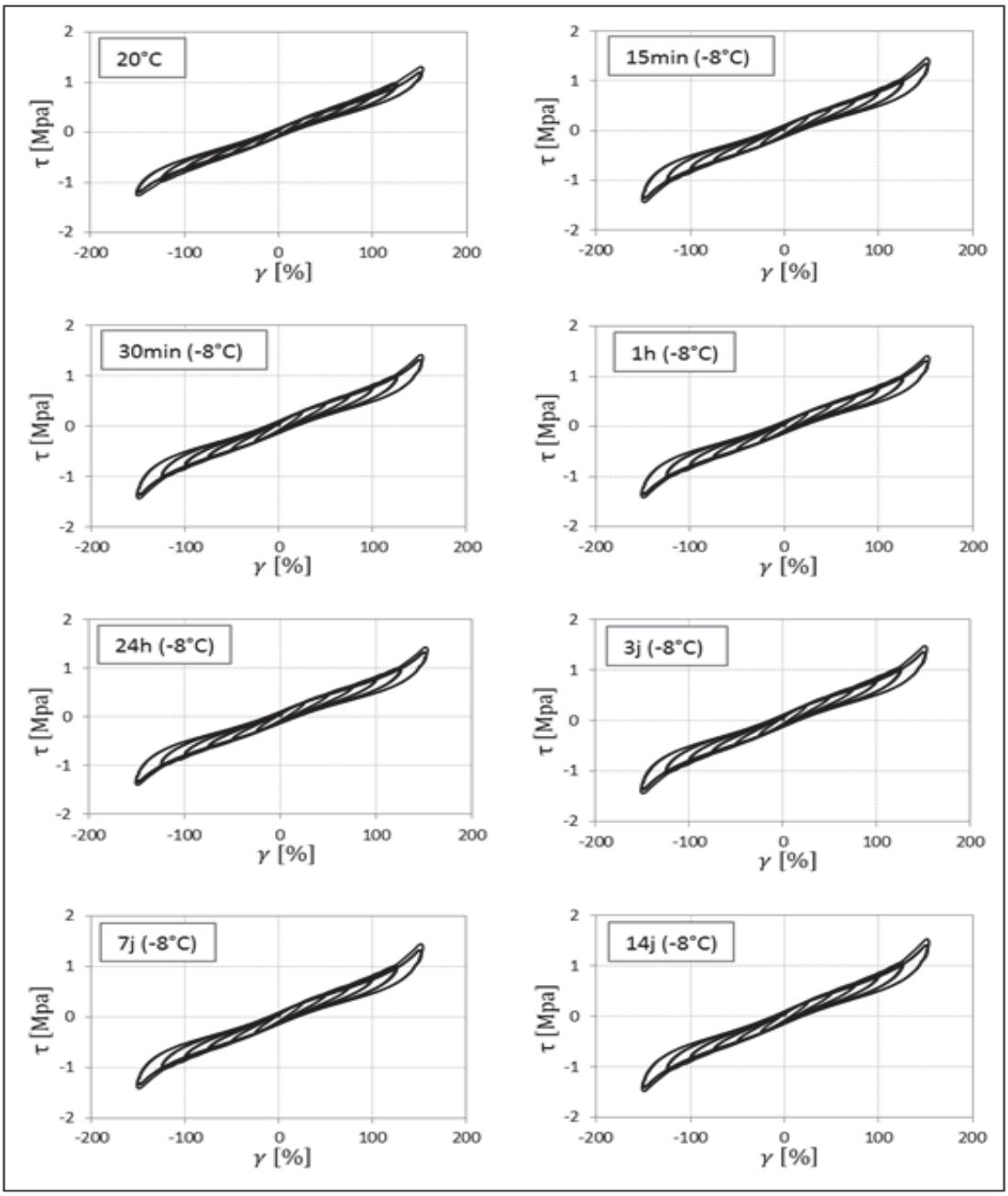

Figure 1.38 Hysteresis curves of the NAT55 compound at 20°C and -8°C for the different cold conditioning times from 15 min to 14 days
Taken from Ankik (2019)

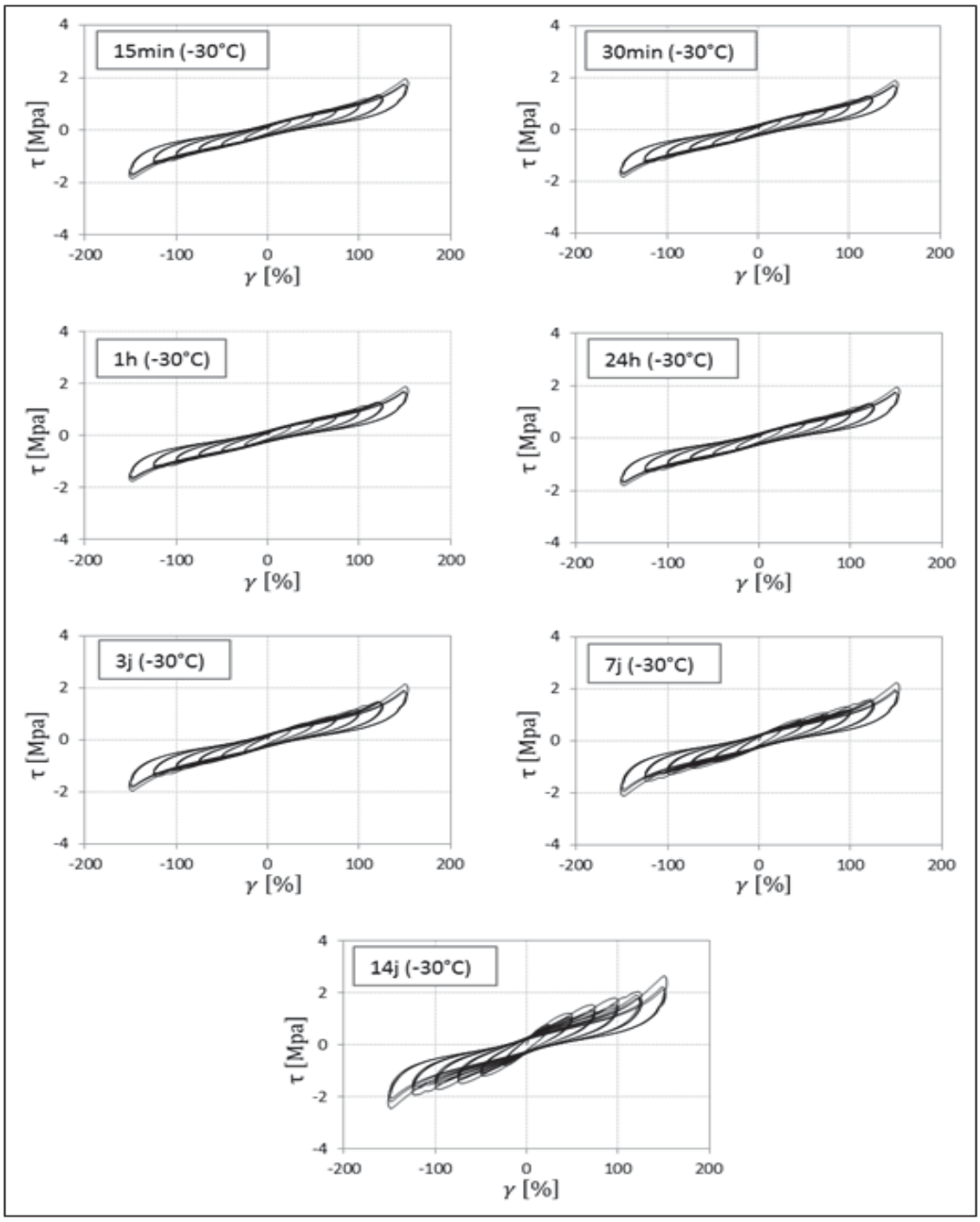

Figure 1.39 Hysteresis curves of the NAT55 compound at -30°C for the different cold conditioning times from 15 min to 14 days
Taken from Ankik (2019)

The mechanical properties of compound B including the effective shear modulus (G_{eff}), equivalent damping ratio (ξ_{eq}), and stress at zero strain (τ_0) as a function of the strain amplitude for the different conditioning times at -8°C and -30°C are shown in Figures 1.40 & 1.41, respectively. It is found that at a temperature of -8°C, when the conditioning duration increased from 15 min to 14 days, the variation of effective shear modulus is negligible. Additionally, at -30°C, a slight increase in G_{eff} is observed with the increase in the conditioning duration. For example, G_{eff} at 100% strain increased by approximately 6% when the conditioning duration increased from 15 min to 14 days. Subsequently, the author found that the effective shear modulus of NAT55 and compound E exhibit similar shear behaviours to compound B at low temperatures of -8°C and -30°C, but with different proportions and sensitivity to the low temperatures. For example, G_{eff} at 100% strain for compound E increased by approximately 6% when the conditioning duration increased from 15 min to 14 days while for NAT55 G_{eff} increased by approximately 1% between 15 min and 24 h, by 10% between 24 hours and 3 days, and by 40% between 3 and 14 days. Finally, it was concluded that low-damping natural rubber experiences less instantaneous and overall thermal stiffening compared to high-damping compounds (B and E), while it is more sensitive to the conditioning time (crystallization phenomenon) at very low temperatures (Ankik, 2019).

The equivalent damping (ξ_{eq}) is mathematically related to the area of the hysteresis loop and the effective shear modulus. Consequently, it was calculated that for NAT55, compound B, and compound E, the equivalent damping (ξ_{eq}) hardly varies when the conditioning time increased from 15 min. to 14 days, at both temperatures, -8°C and -30°C, also ξ_{eq} decreased almost linearly with increasing strain amplitude from 25 to 150% (Ankik, 2019).

Regarding the τ_0, small variations in τ_0 was indicated when conditioning time was extended from 15 min to 14 days. It was observed that τ_0 increased when the overall shear strain increased from 25% to 125%. Moreover, an atypical decrease in τ_0 between the strain amplitudes of 125% and 150% was observed (Ankik, 2019).

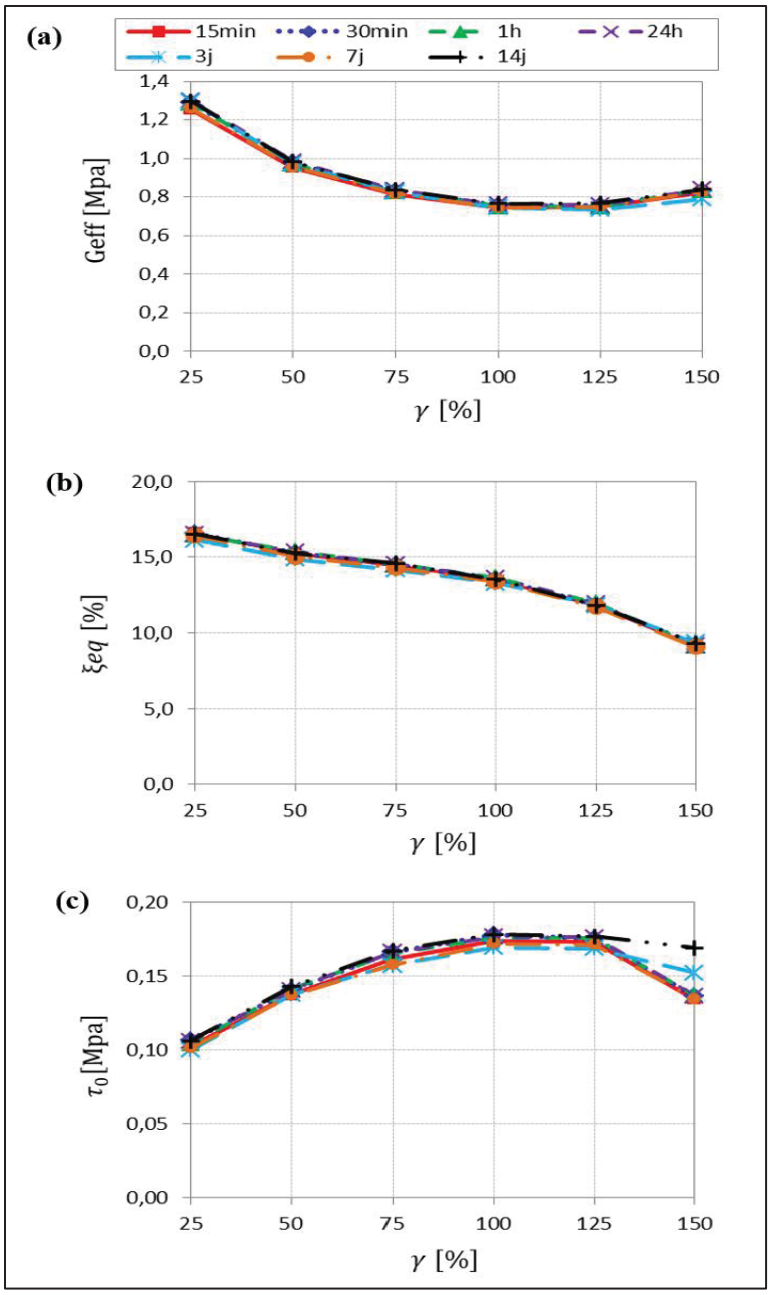

Figure 1.40 Effect of conditioning times on the mechanical characteristics of compound B tested at -8°C
Taken from Ankik (2019)

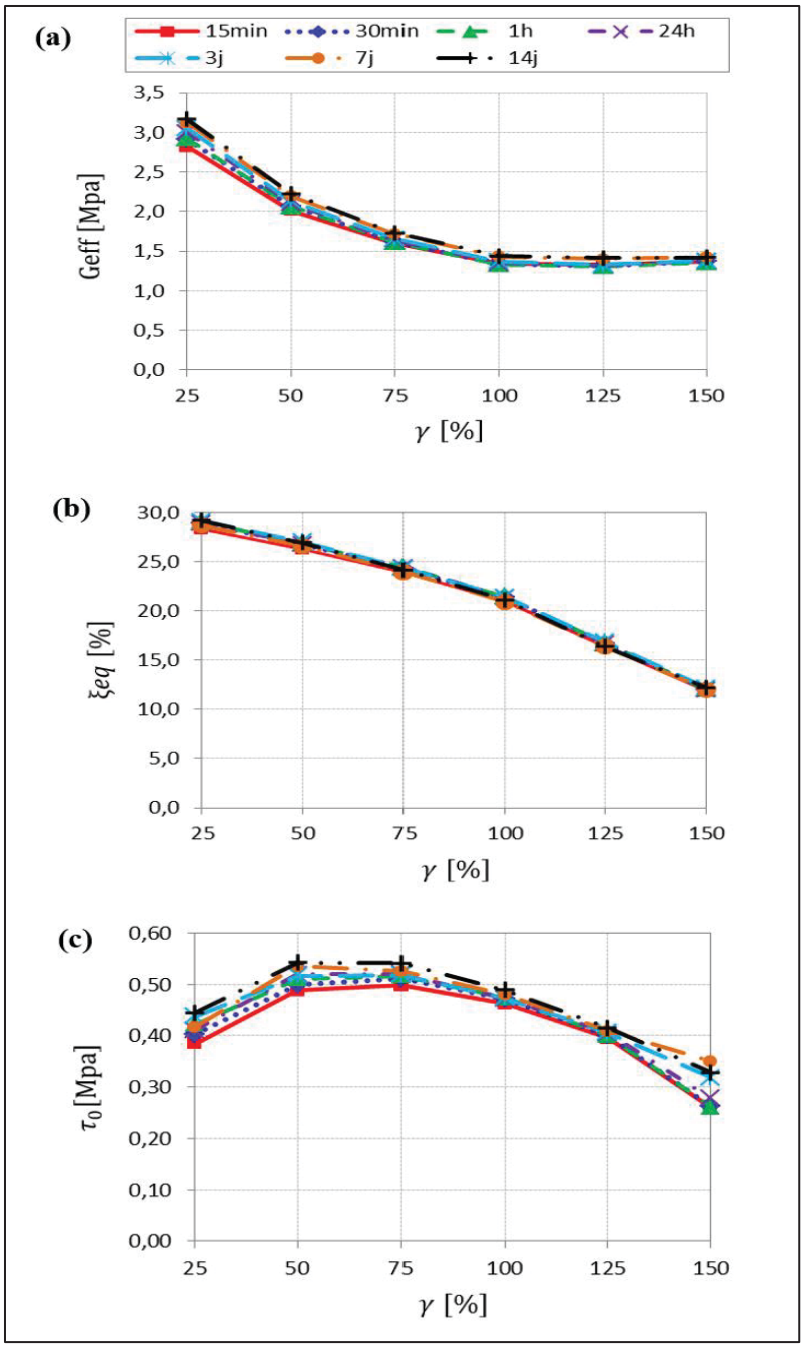

Figure 1.41 Effect of conditioning time on the mechanical characteristics of compound B tested at -30°C
Taken from Ankik (2019)

Cardone and Gesualdi (2012)

In their 2012 study, Cardone and Gesualdi investigated the low-temperature cyclic shear behaviour of elastomers utilized in seismic isolator construction. The study involved testing six elastomer chemical compositions sourced from two distinct manufacturing plants in Italy. The elastomers were categorized into three groups based on their hardness: hard (H), normal (N), and soft normal (SN). Additionally, the factory of origin was designated by 1 or 2, resulting in the following groups: H1, N1, SN1, H2, N2, and SN2.

The dynamic shear modulus of the elastomers was measured at a temperature of 20°C and a strain of 100%, ranging from 0.5 to 1.2 MPa. The specimens used in the tests were elastomer blocks with plan dimensions of 35 mm x 35 mm and a thickness of 10 mm. To ensure a secure attachment, these blocks were affixed on each side to steel plates that matched the dimensions of the elastomer blocks. In the initial phase of the research, specimens underwent exposure to temperatures ranging from 40°C to -20°C. The exposure durations varied between 30 and 60 minutes. This experimental setup aimed to assess the performance of elastomers under diverse air temperature conditions (Cardone and Gesualdi, 2012).

In the subsequent phase, the elastomers were subjected to temperatures of -10°C and -20°C, with conditioning times ranging from 1 to 24 hours. This part of the study focused on investigating crystallization phenomena at low temperatures. Three loading cycles, completely reversed, were applied. The strain amplitude increased from 25% to 125%, with increments of 25%, and the frequency was set at 0.5 Hz. The stress-strain curves obtained from these tests were analyzed to determine mechanical characteristics, including the secant shear modulus, equivalent damping ratio, shear stress at zero cyclic deformation, and maximum shear stresses. These parameters were examined to gain insights into the elastomer's behaviour under different temperature and loading conditions (Cardone and Gesualdi, 2012). Figures 1.42 to 1.44 show the stress-strain curves for elastomers H1, N1, and SN1. The findings indicate that when the temperature decreases, both the maximum stress levels and the area enclosed by the hysteresis curves exhibit an increment. For instance, when the test temperature descended from 20°C to

-10°C and -20°C, stress increased by 1.5 to 2.5 times at 100 % shear strain. This underscores the influence of low temperatures on the mechanical response of the elastomers (Cardone and Gesualdi, 2012).

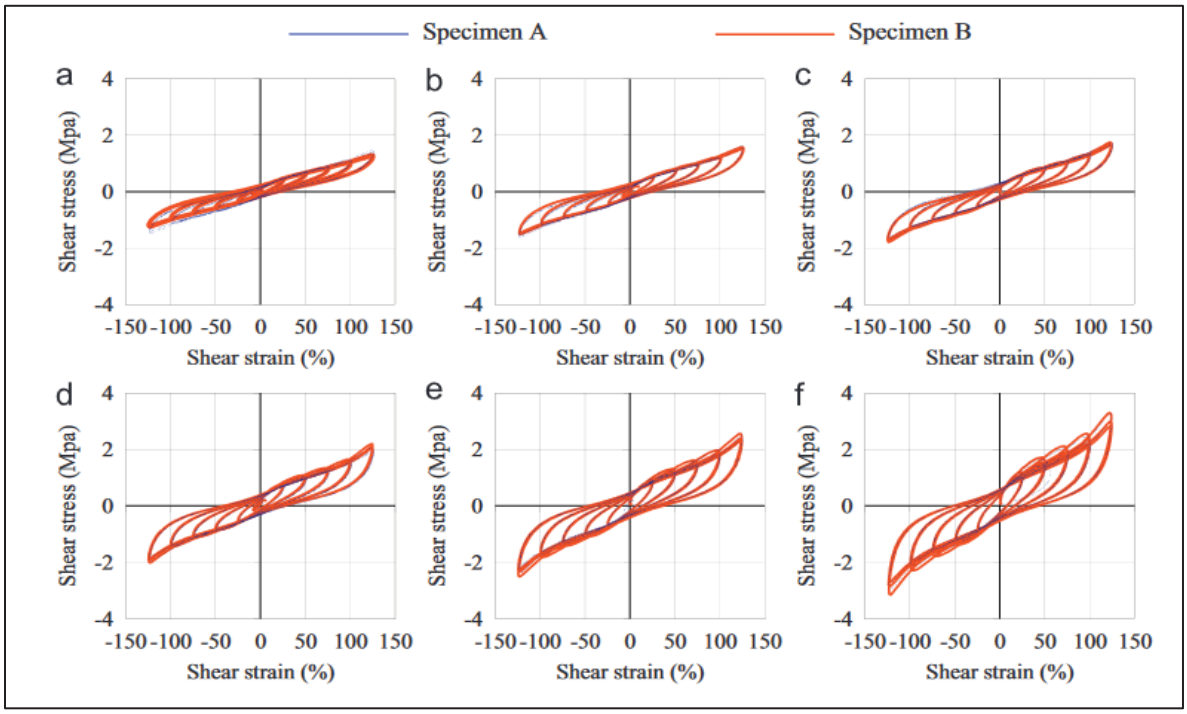

Figure 1.42 Stress-strain curves of elastomer H1 at temperatures:
(a) 40ºC, (b) 20ºC, (c) 10ºC, (d) 0ºC, (e) -10ºC and (f) -20ºC
Taken from Cardone and Gesualdi (2012)

Figure 1.45 shows the variation in mechanical characteristics for elastomers H1, N1, and SN1 concerning exposure temperature for various amplitudes of imposed deformations, corresponding to the third load cycle. The findings indicate that the secant shear modulus (G_{sec}) remains relatively constant for temperatures above 20ºC but increases for temperatures below 0ºC. The equivalent viscous damping (ξ_{eq}) experiences an increase with decreasing temperature in the case of H1 and N1 elastomers, while it remains nearly unchanged for the SN1 elastomer. Additionally, both the stress at zero strain (τ_0) and the maximum shear stress (τ_{max}) exhibit approximately linear increases as the temperature decreases for all three elastomers (Cardone and Gesualdi, 2012).

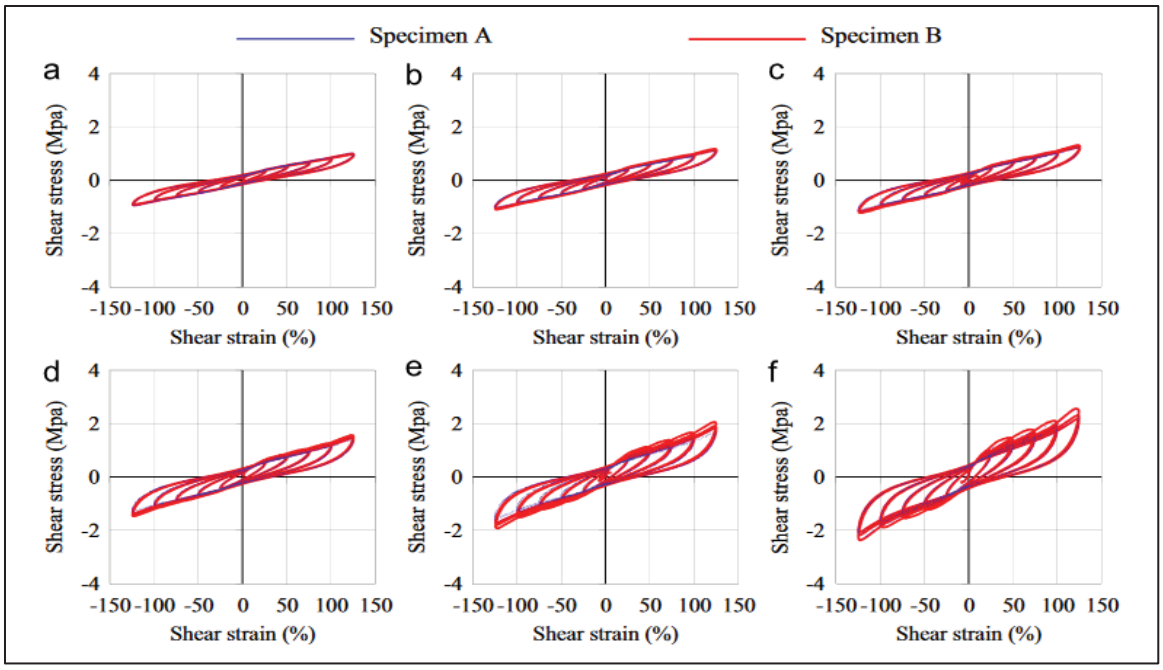

Figure 1.43 Stress-strain curves of elastomer N1 at temperatures: (a) 40ºC, (b) 20ºC, (c) 10ºC, (d) 0ºC, (e) -10ºC and (f) -20ºC
Taken from Cardone and Gesualdi (2012)

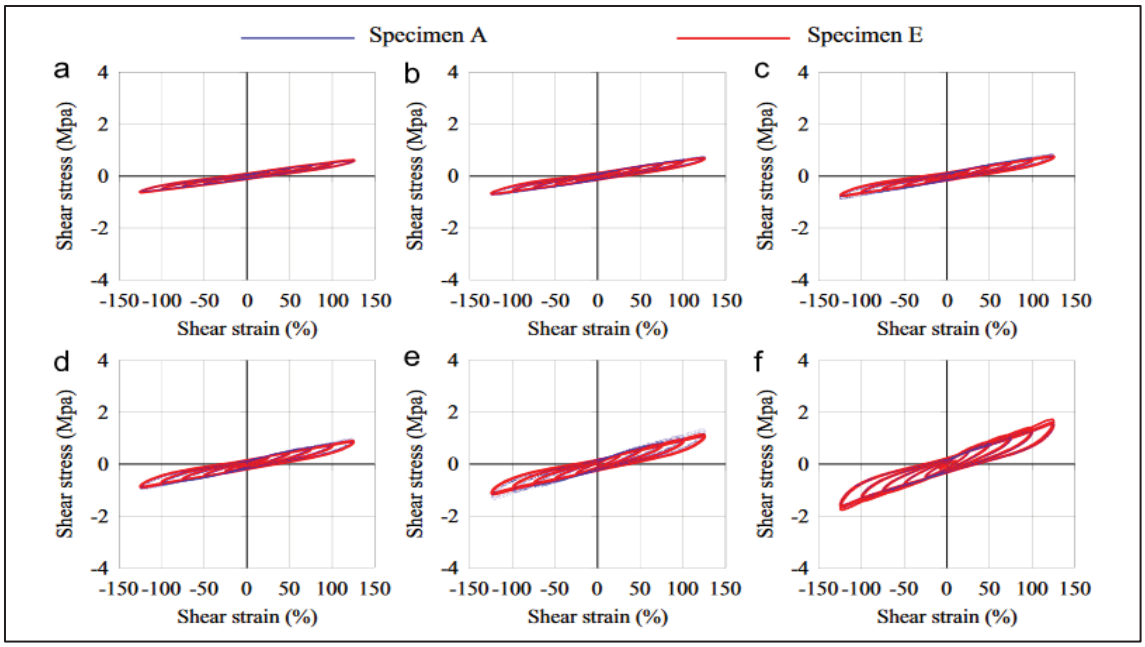

Figure 1.44 Stress-strain curves of SN1 elastomer at temperatures: (a) 40ºC, (b) 20ºC, (c) 10ºC, (d) 0ºC, (e) -10ºC and (f) -20ºC
Taken from Cardone and Gesualdi (2012)

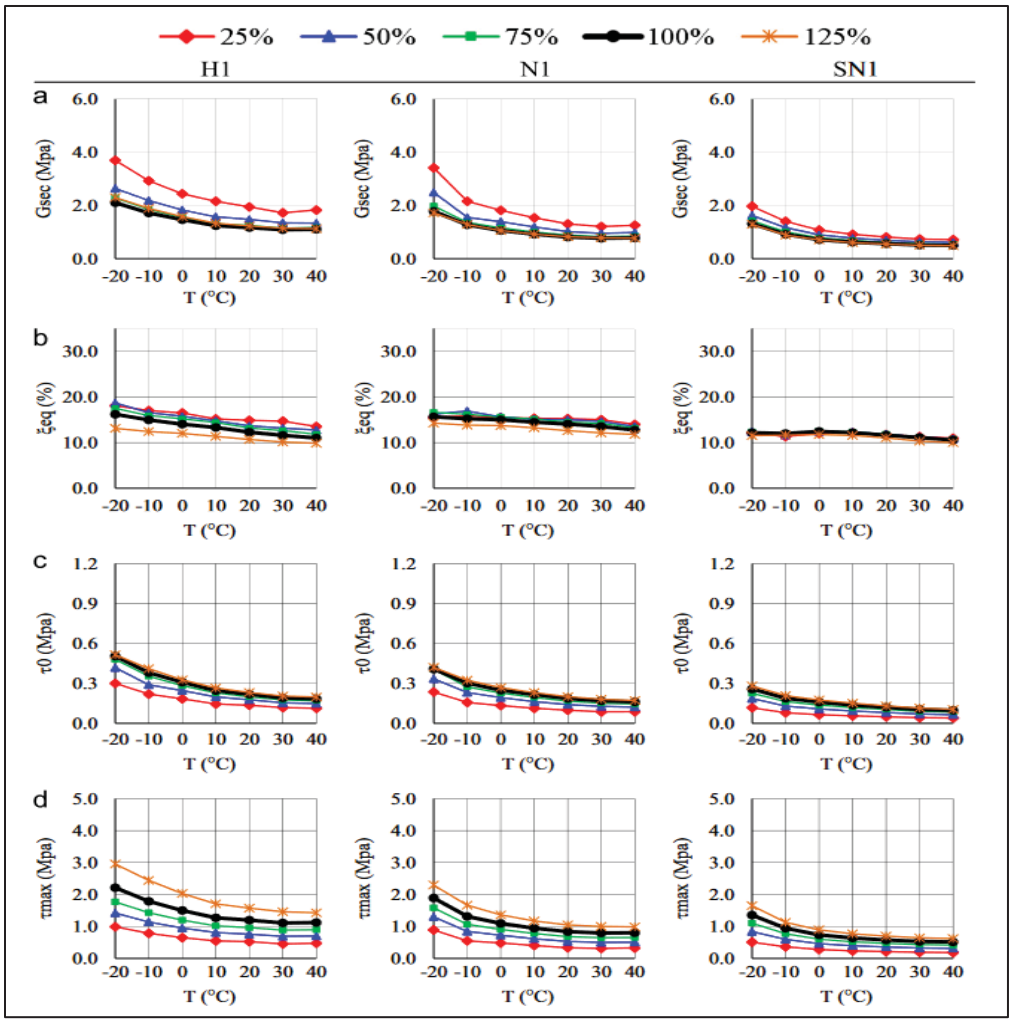

Figure 1.45 Variation of the mechanical properties of H1, N1, and SN1 based on the temperature and different amplitudes of strain
Taken from Cardone and Gesualdi (2012)

In Figure 1.46, the variation of mechanical characteristics as a function of deformation amplitude is depicted for elastomers H1, N1, and SN1, corresponding to the third load cycle at different temperatures. The results reveal that the secant shear modulus (G_{sec}) exhibits a decrease with increasing strain amplitude. Notably, this reduction is more pronounced at low strains (25% to 50%) compared to larger amplitudes (100% and 125%). For instance, at 25% strain, G_{sec} is on average 60 to 80% larger than that calculated at 100% strain. The damping ratio (ξ_{eq}) for H1 and N1 decreases with the rise in amplitude of deformation, while it remains practically constant for the SN1 elastomer. Lastly, the stress at zero strain (τ_0) and the

maximum shear stress (τ_{max}) demonstrate an almost linear increase as the strain amplifies for all elastomers (Cardone and Gesualdi, 2012).

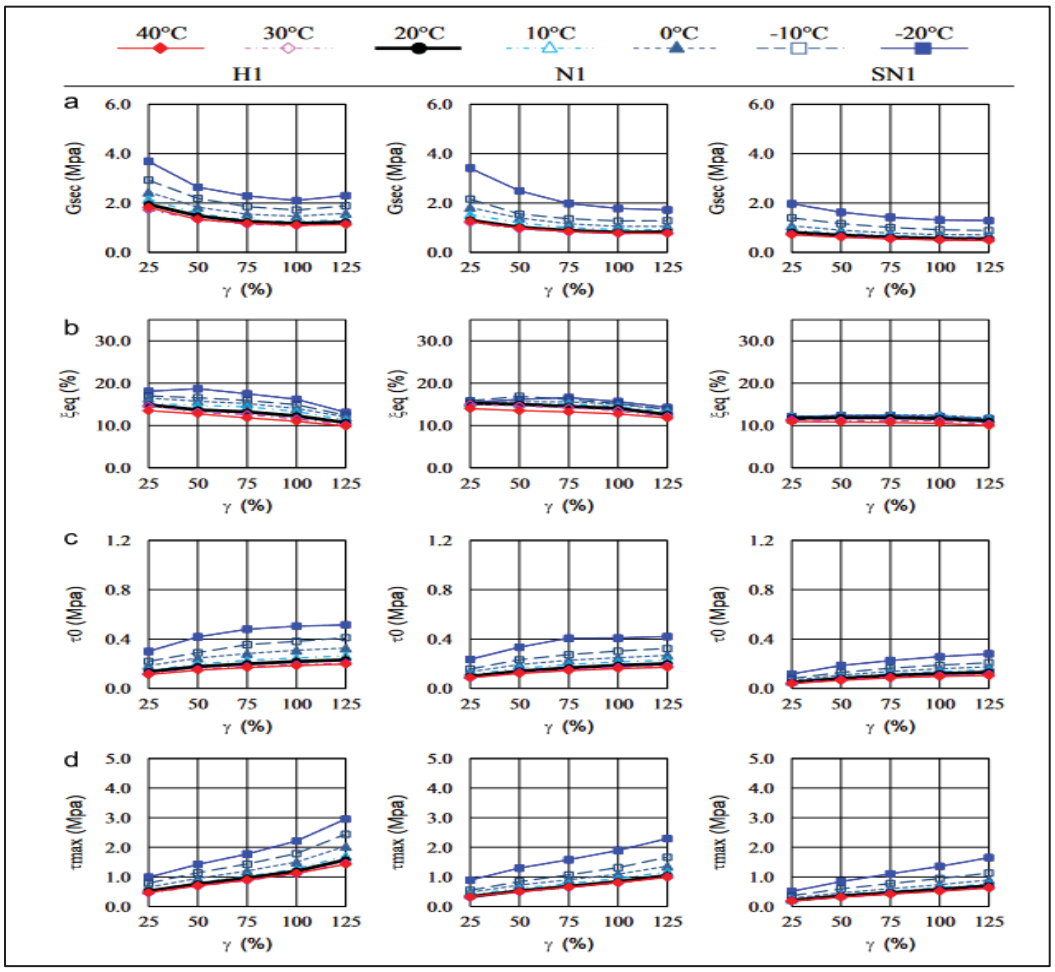

Figure 1.46 Variation in the mechanical properties of H1, N1, and SN1 as a function of the amplitude of deformation at different temperatures Taken from Cardone and Gesualdi (2012)

In Figure 1.47, the variation of mechanical characteristics is presented as a function of conditioning time at -20°C for elastomers H1, N1, and SN1. The data corresponds to the third load cycle and encompasses various deformation amplitudes. The results reveal that the secant shear modulus (G_{sec}) experiences an increase with prolonged conditioning time at -20°C. Particularly, when compared to 20°C, this increase ranges from 50% to 150% after 24 hours

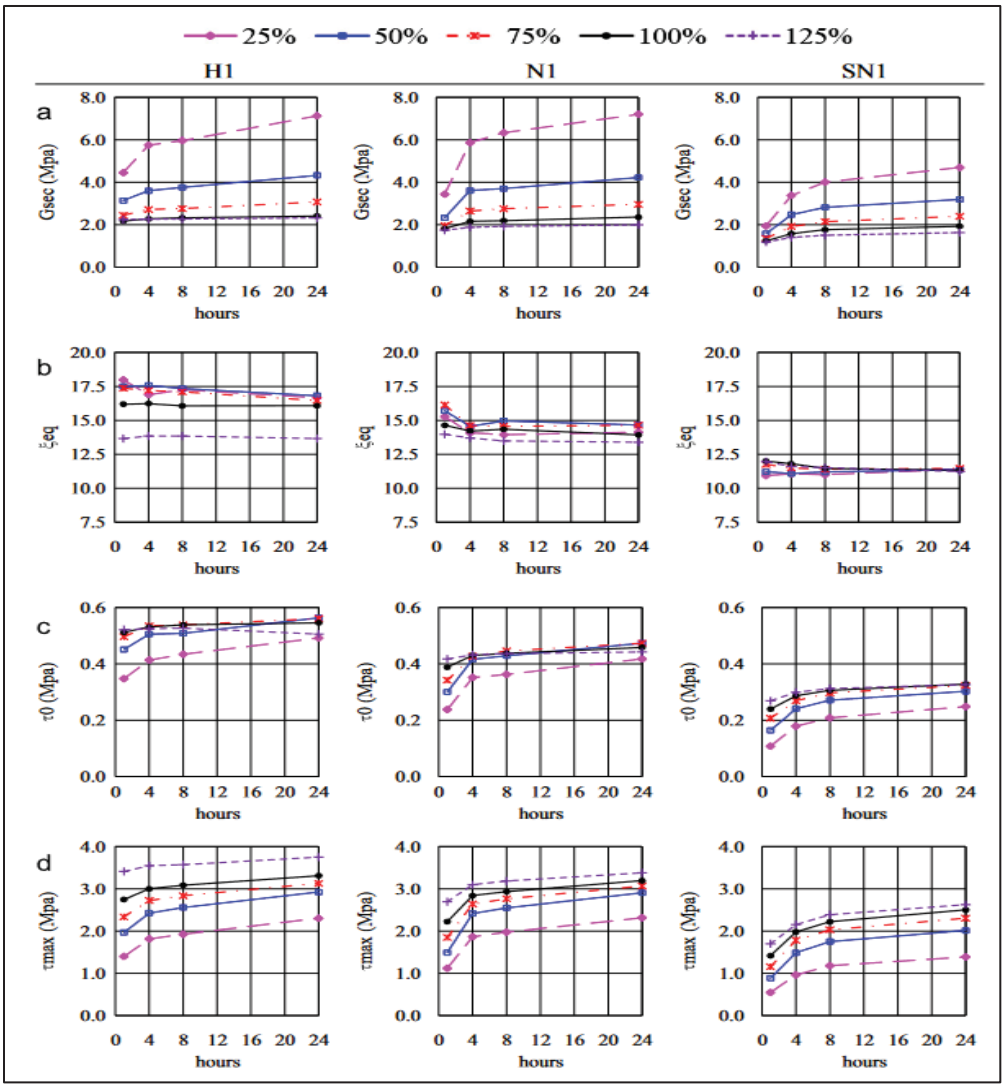

Figure 1.47 Variation of the mechanical properties of H1, N1, and SN1 as a function of conditioning time at -20°C for different deformation Taken from Cardone and Gesualdi (2012)

of exposure to -20°C for lower deformation levels (25% to 50%). However, for larger deformation amplitudes (100% and 125%), the increase does not exceed 30%. The damping rate (ξ_{eq}) exhibits no significant change with the duration of conditioning for all considered strain levels. Lastly, both the stress at zero strain (τ_0) and the maximum shear stress (τ_{max}) demonstrate substantial increases between 1 hour and 4 hours of conditioning, followed by a gradual but slight rise to 24 hours of conditioning (Cardone and Gesualdi, 2012).

CHAPITRE 2

EXPERIMENTAL PROGRAM

2.1 Introduction

To determine the mechanical properties of elastomeric natural rubbers used for bridge bearings, an experimental program including experimental tests at room temperature and low temperatures is conducted in this research. These tests aim to characterize the mechanical properties of natural rubber used in bridge bearings, including the shear modulus (G_{eff}), equivalent damping (ξ_{eq}), and stress at zero strain (τ_0). The objective is to measure the variation of such mechanical properties among the natural rubbers and examine their variability under low temperatures. To elaborate further, various sources of elastomeric natural rubbers have been subjected to cyclic loads under low temperatures to not only specify their cyclic and dynamic shear behaviour but also assess the variation among the different sources of natural rubber manufactured by different bridge bearing suppliers in Quebec and Canada, known as cold temperatures regions. In this research, the influence of low temperatures, the duration of exposition to these low temperatures, load frequency, and age condition of the material are studied. This chapter presents, in detail, the experimental program carried out, including studied parameters, test set-up, and procedures. Results on the variability of mechanical properties of rubber are lacking in the literature and constitute a main contribution of this research. They are aimed to aliment reliability and probabilistic models for the seismic analysis and performance of isolated bridges in cold regions, notably in Canada and the northern United States of America.

2.2 Studied experimental parameters

The primary objective of this experimental study is to measure the variation and the variability of mechanical properties of natural rubbers under low temperatures and various conditioning times ranging from 1 hour to 28 days. To attain this objective, the following parameters were

taken into account and integrated into the experimental program, and each is detailed in the following sections.

1. Test temperature.
2. Exposure time to low temperature.
3. Source of natural rubber (samples manufacturer).
4. Age condition.
5. Strain level.
6. Load frequency.

2.3 Test temperature

To test the effect of low temperatures, the Canadian Highway Bridge Design Code (CSA, 2019) prescribes low-temperature tests to evaluate the hysteretic characteristics of elastomeric isolation systems at low temperatures for design purposes. The CSAS6:19 code specifies different levels of seismic intensity (probability of exceedance in 50 years), each associated with a concomitant temperature. Two low temperatures are to be used in the design, in addition to ambient room temperature, and define the test temperatures used in this test program: 1- Minimum service temperature that is equal to the minimum daily average temperature of the site used to determine the seismic demand in presence of a relatively moderate earthquake with a return period of 975 years and; 2- the concomitant temperature used with a very rare earthquake, having a return period of 2475 years (CSA, 2019). the concomitant temperature is taken equal to the average between 15°C and the minimum service temperature. This temperature is more likely to occur when seismic displacement demand corresponding to a probability of exceedance of 2% in 50 years (return period of 2475years) is imposed on the structure (CSA, 2019).

According to the CSA code and considering the locality of Montreal, the test temperatures are -8 ° C and -30 ° which is deemed for this research. Therefore, -8°C and -30°C as the major test temperature, and temperature of 23°C as the reference temperature are selected for this test

program. Figure 2.1 shows the average daily minimum temperatures in Canada provided by CSA (2019).

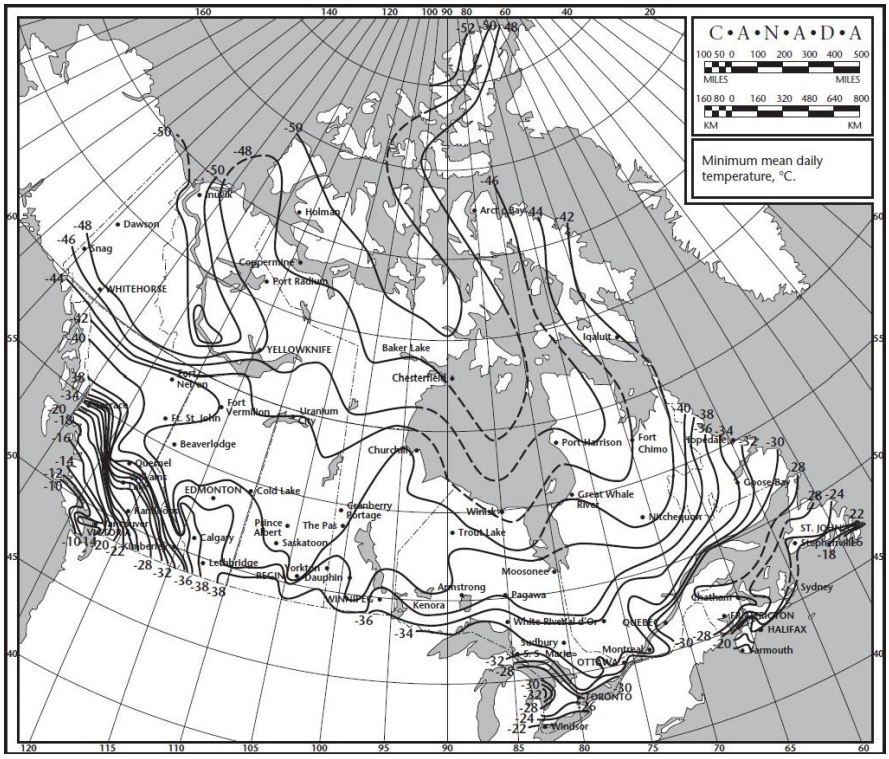

Figure 2.1 Average daily minimum temperatures in Canada
Taken from CSA (2019)

2.4 Exposure time to low temperature

It is important to establish the effect of the duration of exposure to the low temperature on the natural rubber. In this study, the duration of exposure to the low temperature is divided into two main categories, short-term exposure, and long-term exposure. Short conditioning times, 1 hour and 24 hours, are considered to be suitable for studying instantaneous thermal stiffening. This time is calculated according to the ASTM standard (D832, 2007) related to the procedure for conditioning elastomers at low temperatures in order to carry out mechanical tests. In order to evaluate the effects of stiffening corresponding to elastomer crystallization, long periods of time are considered, including 1 day, 3 days, 7 days, 14 days, and 28 days. Cold conditioning is applied by a freezer or thermal chamber.

2.5 Sources of natural rubbers (samples)

Four distinct sources of natural rubber used in seismic bridge isolation are employed to assess variations in their mechanical properties. These samples originate from different production batches and bridge-bearing suppliers located in Canada and the United States. The sources include: room-aged samples manufactured by Hevea Inc, obtained through Goodco Z-Tech, which were previously tested by Ankik in 2018; samples taken from two different types of aged bearings from the Champlain Bridge; and samples supplied by Scougal Rubber, USA. Figure 2.2. shows a typical new sample. Additionally, samples made from the aged bearings taken from the original Champlain Bridge are included and exhibit slight differences, as explained later.

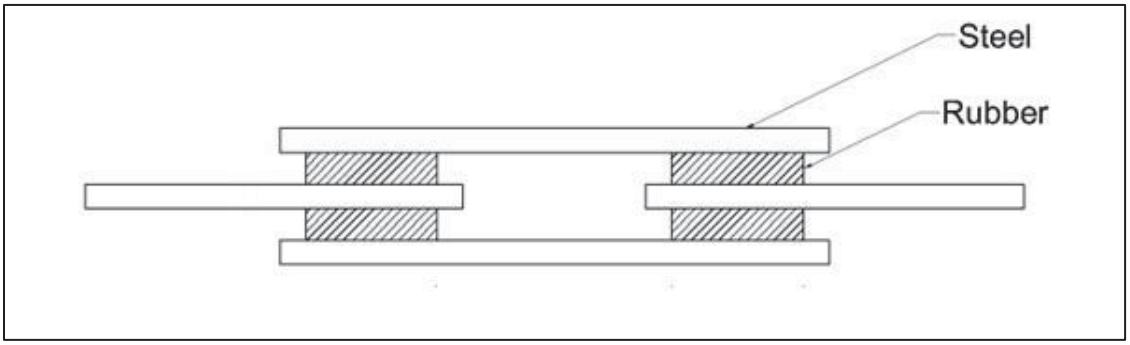

Figure 2.2 Typical quadruple sample

2.5.1 Hevea elastomeric natural rubber (Series 1)

Standard scaled-down quad-shear natural rubber specimens fabricated in 2018 are considered the first type of samples in this study. These specimens were fabricated by Hevea company, located in Richmond, Quebec, and supplied by the Canadian company Goodco Z-Tech, of the Canam-Bridges group, located in Laval, Quebec. Each sample consists of four blocks of rubbers, with dimensions of 25.4 x 25.4 x 6 mm, bonded to the steel bars. The shape and dimensions of the specimens, shown in Figure 2.3, have been recommended by the standard (ASTM D4014, 2007). Hevea's samples were utilized for prior research in 2019. These samples

have undergone testing at low temperatures with cyclic loads. Throughout the following three years, they were kept in the structural laboratory at room temperature. Therefore, samples from Hevea (Series 1) are considered room-aged samples.

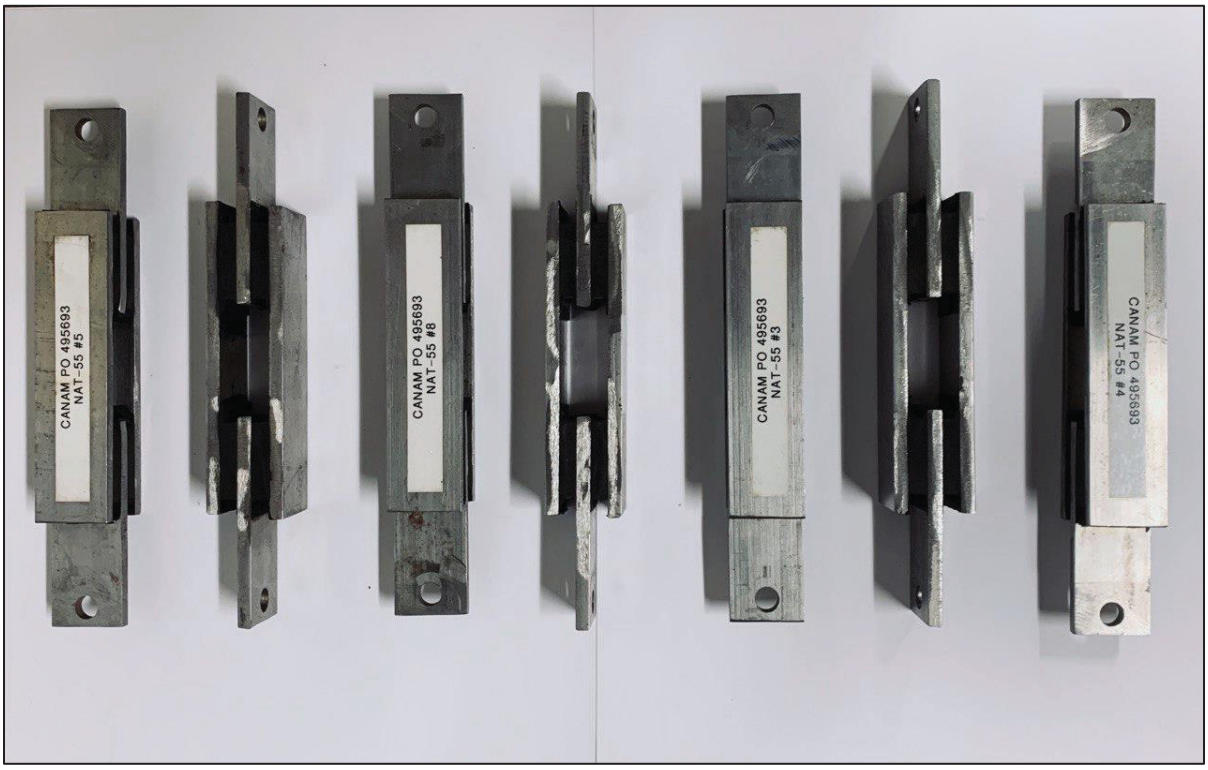

Figure 2.3 Hevea specimens (Series 1) used in the shear test

2.5.2 Original Champlain bridge (CHB) bearings (Series 2 & 3)

The original Champlain Bridge was a steel truss cantilever bridge in Montreal, QC connecting the island of Montreal to the south shore across the St. Lawrence River. It was opened in 1962, had a total length of 3.4 km, and carried six lanes of vehicle traffic. The original Champlain Bridge was closed to traffic in July 2019 after 57 years and deconstruction began a year later in August 2020, https://jacquescartierchamplain.ca/en/major-projects/deconstruction-of-the-original-champlain-bridge/about/. In this study, original Champlain bridge bearings, shown in Figure 2.4, were used as a source of aged natural rubbers to study the mechanical behaviour of aged natural rubbers. Two models of bearings used in the Champlain Bridge have been

recuperated and used in this study: D4.27 and D4.28. The description of these bearings is further detailed according to the as-built drawing provided by JCCBI (the Jacques Cartier and Champlain Bridges Incorporated) as follows:

Figure 2.4 Champlain Bridge bearings D4.27 & D4.28

2.5.2.1 Bearing D4.27 (Series 2)

Bearings D4.27 were constructed in late 2014 and installed in abutment 44W (west) of the original Champlain Bridge, plan and section view of abutment 44 west are shown in Figures 2.5 & 2.6. These bearings were received at the ETS laboratory in October 2020 and kept at room temperature. They aged for approximately 6.5 years under traffic loads and harsh environmental conditions before being stored at room temperature for an additional 3 years, making them about 10 years old at the time of testing.

Bearings D4.27 measure 653 x 553 mm in size with a thickness of 98 mm. They consist of four steel plates and three layers of natural rubber, each 25 mm thick. Additionally, a thin layer of elastomer covers the perimeter of the entire bearing. The design loads and displacement considered for these bearings include: Dead Load =1475 kN, Live Load, including impact factor (dynamic load allowance)= 550 kN, asphalt paving= 125 kN, and maximum longitudinal

movement =26 mm. In this study, bearings D4.27 are identified as the second source (Series 2), and the dimensions and transverse section of one bearing are shown in Figure 2.7.

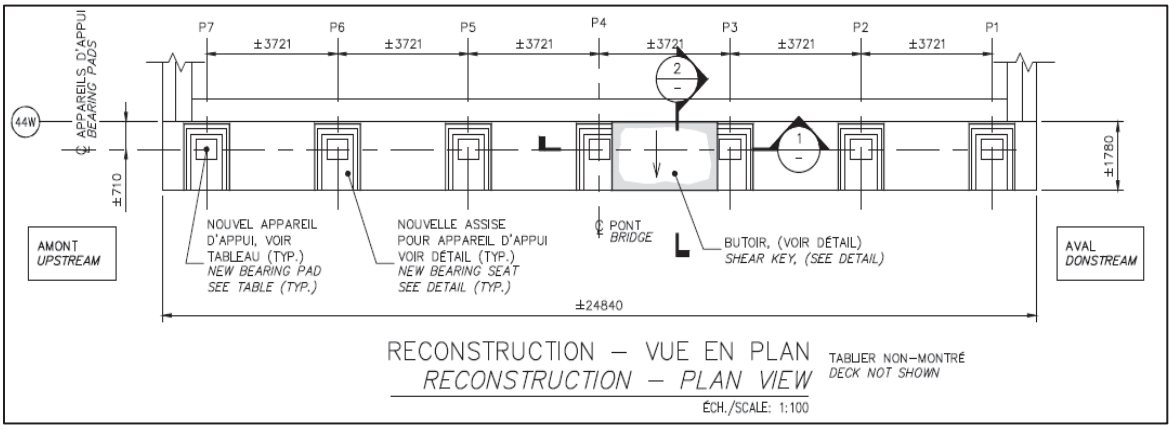

Figure 2.5 Plan view of abutment 44 west of original CHB provided by JCCBI

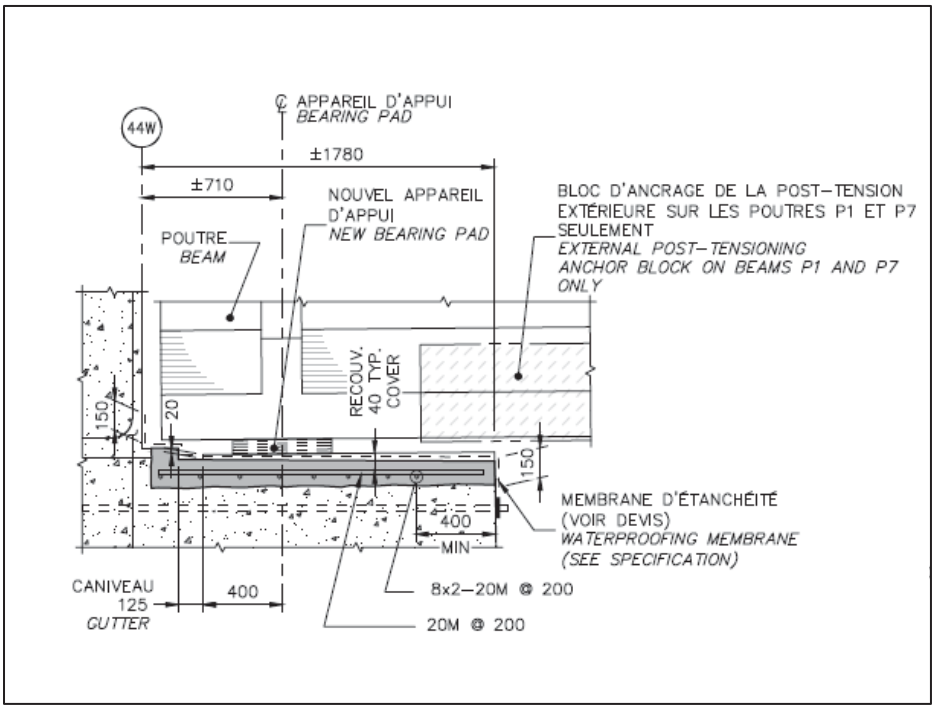

Figure 2.6 Section view of abutment 44 west of the original CHB from the bearing seat reconstruction drawing provided by JCCBI

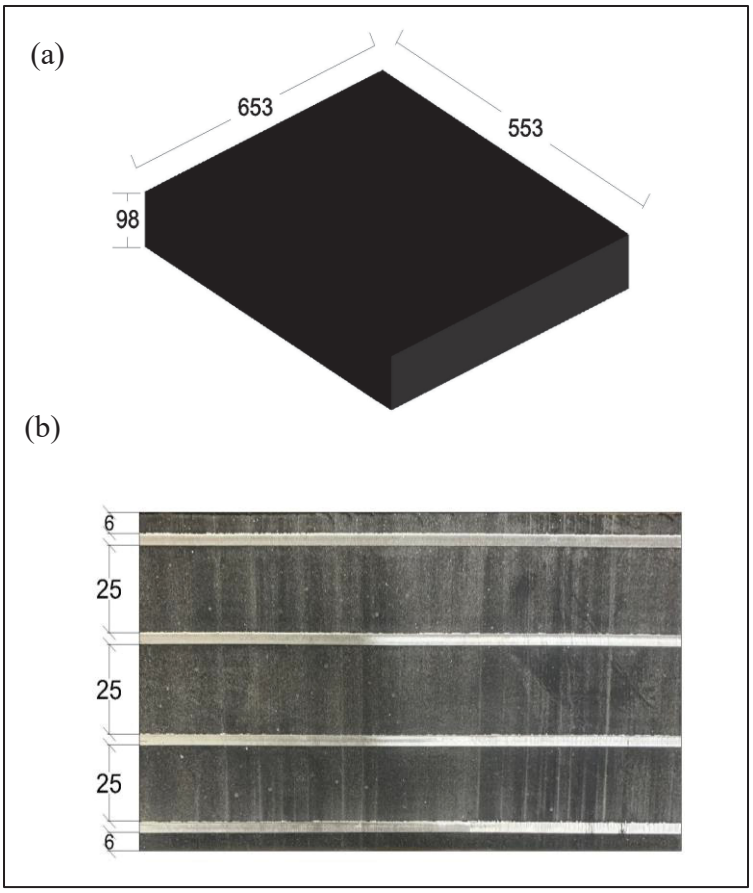

Figure 2.7 (a) Dimensions of original CHB bearing D4.27 (Series 2), (b)transverse section

2.5.2.2 Bearing D4.28

Bearings D4.28 had been installed in pier 42w (west) of the original Champlain Bridge, the top view of pier cap 42 west is shown in Figure 2.8. They were applied on the bridge in the summer of 2005 and sent to the ETS laboratory on January 2021 meaning that bearings D4.28 were 16 years old at the receiving time at ETS. These bearings were also kept at room temperature and in the same condition as D4.27 at the ETS laboratory for approximately 2 years, making them about 18 years old at the time of testing. They have dimensions of 603 x 503 mm and a 72 mm thickness and consist of 3 steel plates with 3 mm thickness, 2 layers of natural rubber each with a thickness of 25 mm, as well as a cover layer. These bearings had been designed to resist the dead loads of the structure =1200 kN, and live load including impact

=745 kN, and the asphalt = 150 kN. In this study, bearings D4.28 are considered as third source (Series 3), and the dimensions and transverse section of one bearing are shown in Figure 2.9

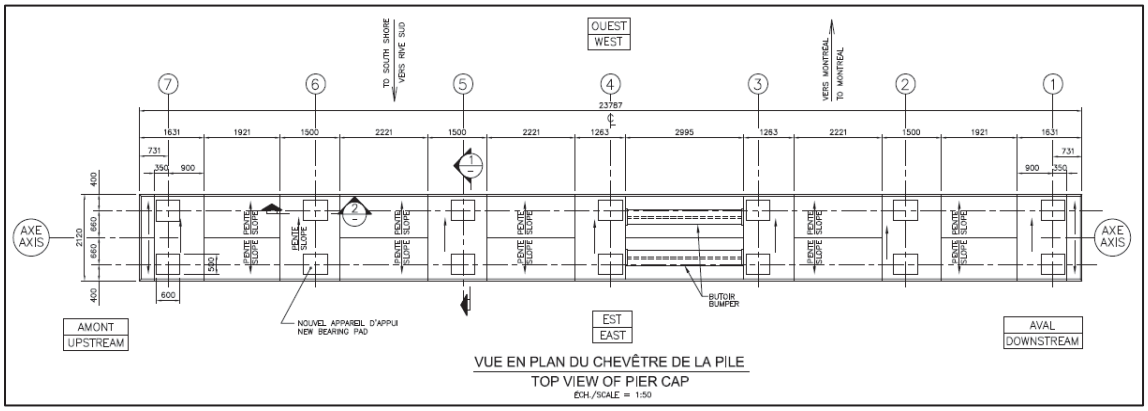

Figure 2.8 Top view of pier cap 42 west of original CHB provided by JCCBI

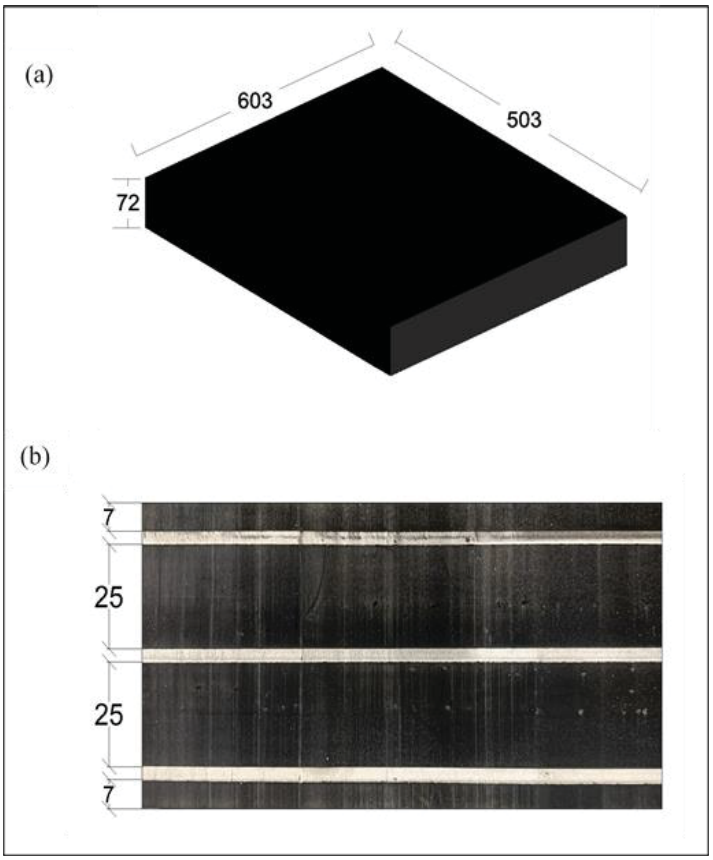

Figure 2.9 (a) Dimensions of original CHB bearing D4.28 (Series 3), (b)transverse section

2.5.2.3 Quadruple shear specimen made from the original CHB bearings

To test the scaled-size original CHB bearings, a total of 10 quadruple shear specimens were prepared, with five specimens obtained from each batch. Two distinct methodologies were considered for making quadruple samples: one involving the separation of rubber from the bearing layers, followed by the adhesive attachment of rubber to metal to form a quadruple shear sample; and the other consists of cutting and shaping the specimens directly form the bearings to create the desired samples. The advantage of the second method is that it avoids the requirement for glue and its adverse effects on sample behaviour by maintaining the initial vulcanized bonding between rubber and metal (shim). However, it has the disadvantage of using the existing thickness of rubber layers which results in lower shape factors, and using the steel shims of the elastomeric bearing, which are more prone to buckling under compression.

In this research, the adopted approach involved cutting and transforming the entire bearing into quad-shear samples, since it was not possible to find a reliable glue working at low temperatures of -30ºC and less. Initial blocks were extracted from bearings D.27 and D.28 according to the layout presented in Figures 2.10 & 2.11. Subsequently, each block was transformed into quadruple samples, following the design for quad-shear samples, which includes a designated space in the middle of samples for movement. This allocated space was carefully designed to accommodate a 150% amplitude of movement. A precise high-pressure water jet was employed to shape the original CHB samples. This process was carried out in Hevea facilities. The obtained samples have nominal dimensions of 318 x 59 mm, consisting of two layers of natural rubber, each 25 mm thick (50 mm in total), and three layers of steel (shim) with a thickness of 3 mm each. The nominal dimensions of specimens cut from a bearing of the original Champlain Bridge are shown in Figure 2.12.

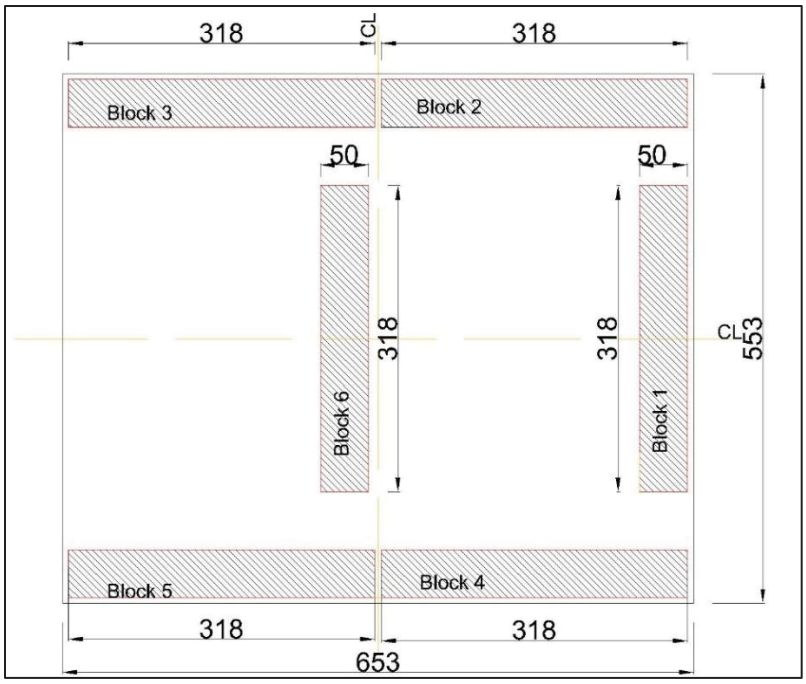

Figure 2.10 Positions of samples in bearing D4.27

As shown in Figures 2.7 & 2.9, the original CHB bearings are reinforced with thin layers of steel (shims). The selection of the number of shims and their respective thickness is determined by the design specifications to ensure optimal performance in seismic isolators. However, in order to test quadrable samples, it is required to test the sample with a thicker plate to avoid buckling. This is necessary because, during the shear test, force is initially applied to the steel, and then transferred from the steel to the rubber meaning that steel plates serve only as shear load transmitters while the main design purpose of the steel plates is to reinforce the rubber, enabling it to withstand vertical loads. At the primary tests, it is found that the original thickness of the steel plates of the prepared samples is insufficient for effective functioning, and they are susceptible to bending. ASTM D4014 recommends that, for shear tests, the steel plate should be a rigid rectangular plate. Also, the standard suggests a plate thickness of 5 mm for use with 6 mm thick blocks (ASTM D4014-03, 2018).

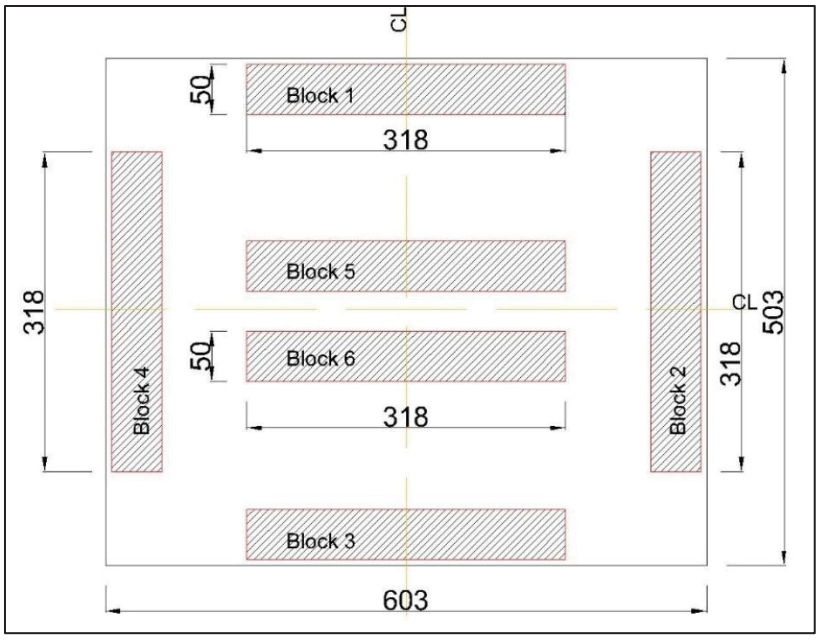

Figure 2.11 Positions of samples in bearing D4.28

To prevent the outer and inner plate buckling of steel plates, two methodologies were explored. The initial approach involved using the metal boxes functioning as stiffeners, secured by screws on both sides to mitigate outer plate buckling, and using a screw in the center of the gap between the blocks to prevent inner buckling. This system is shown in Figure 2.13.

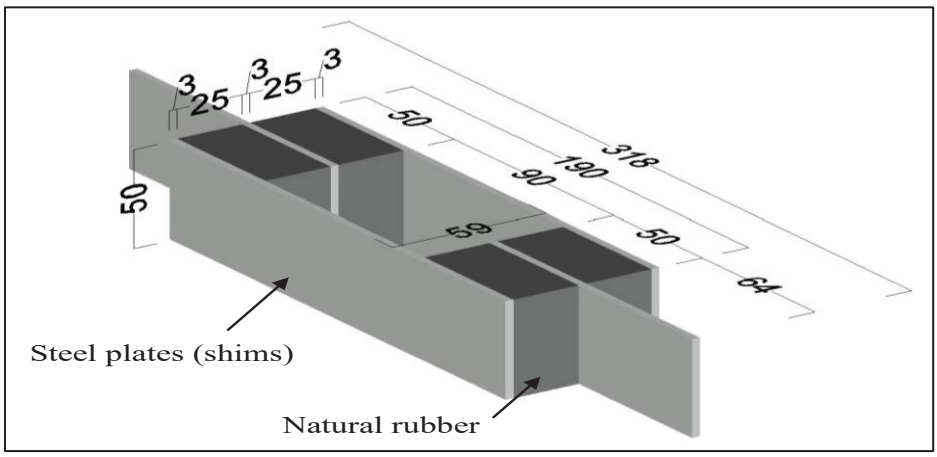

Figure 2.12 Nominal dimensions of specimens cut from
the original Champlain Bridge bearing

Figure 2.13 The Champlain Bridge sample
with metal-box bracing system

The second method was enhancing the steel plate's rigidity by attaching the rigid T-shaped plate to both sides of the samples. The attachment of the metal plate to the samples can be achieved through either welding or adhesive bonding methods. However, the welding process presents a potential drawback as the generated heat might induce rubber alteration. On the other hand, since samples are required to be tested at low temperatures, it is necessary that the adhesive material retains its functionality at low temperatures as well. Therefore, several tests were conducted not only to establish the workability of each system but also to seek a suitable glue. Finally, the decision was made to opt for attaching T-shaped plates by using Sika 300 glue. To glue the T-shaped plates to the samples, first, the outer rubbery cover of the samples was removed to expose the steel surface. Then, using the sandblasting technique, the cleanliness and roughness of the bonding surface were ensured before applying the glue. For

the curing time, samples were kept at room temperature for 7 days. Figures 2.14 to 2.17 feature the process from cutting the bearing to the final samples.

Figure 2.14 Cutting the Champlain Bridge bearings by water jet to make the quadruple samples

Figure 2.15 The surface condition of the original CHB sample before and after the preparation

Figure 2.16 Gluing T-shaped plates to both sides of the original CHB samples by using Sika300 glue

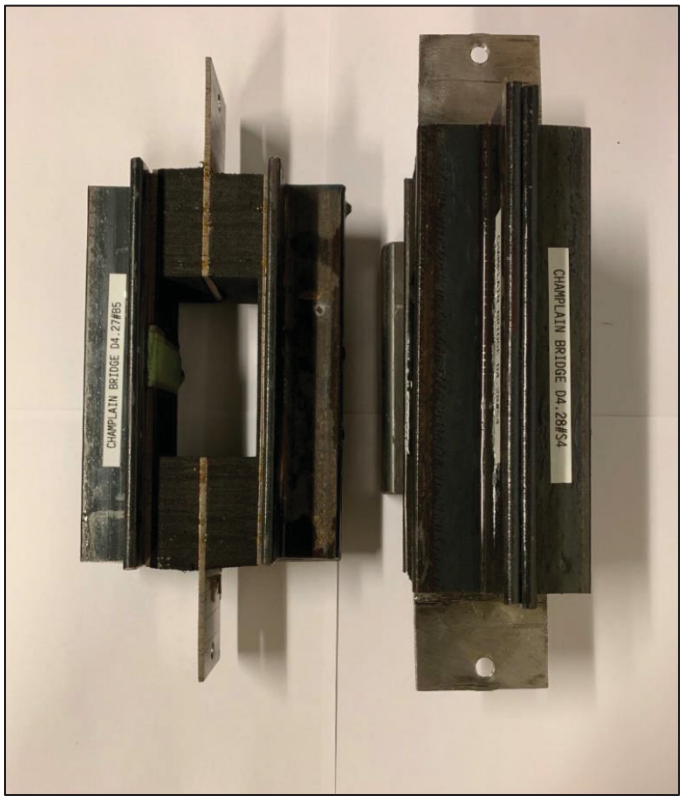

Figure 2.17 Specimens of CHB D4.27(left) and CHB D4.28 (right) with T-shape plate

2.5.3 Scougal specimens (Series 4)

Another and last source of samples used in this study are Scougal specimens (Series 4) fabricated by Scougal Rubber Corporation, located in the United States of America. Scougal Rubber is one of the American companies that supply bridge bearings to the USA and Canada. A total of 6 quadrable natural rubber samples for the cold region with Duro 55 +/- 5, according to the Standard CSA S6-19 was ordered in the summer of 2023 and samples were received in August 2023. The Scougal specimens, shown in Figure 2.18, have 38.1 x 38.1 mm dimensions, with a thickness of 9.52 mm. Also, steel plates have a 4.7 mm thickness which is bonded to the rubber by the vulcanizing process.

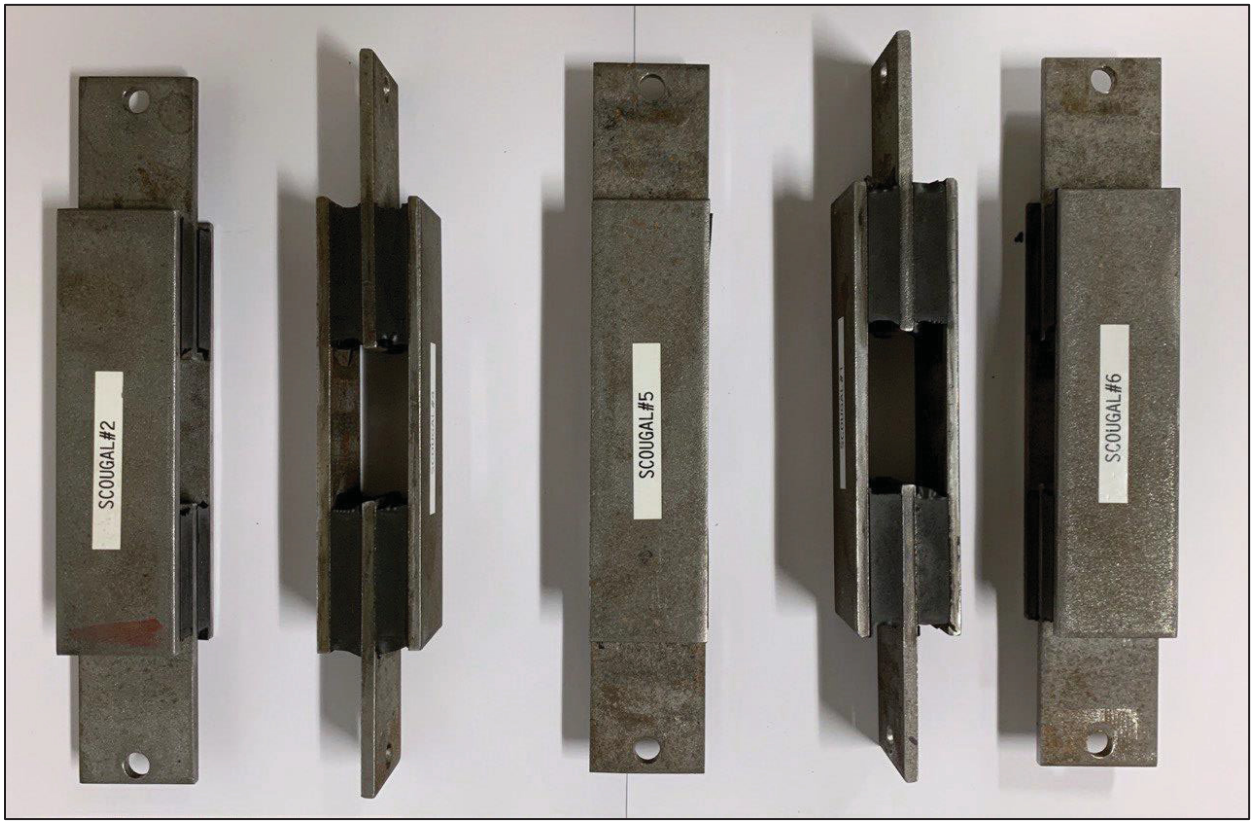

Figure 2.18 Scougal specimens (Series 4) used in the shear test

2.5.4 Summary of the specimens

Table 2.1 Variety of specimens used in the experiment, based on suppliers

Samples Supplier	Identification Code	Condition
Hevea	Series 1	Aged at room temperature for 5 years
Champlain bearing-D4.27	Series 2	Aged in harsh environment for 6.5 years & Aged at room temperature for 3 years
Champlain bearing-D4.28	Series 3	Aged in harsh environment for 16 years & Aged at room temperature for 2 years
Scougal	Series 4	New

2.6 Strain levels

In this study, strain levels were increased from zero to 150% in 25% increments by applying controlled displacement cycles at the selected frequency. This strain range is considered to reflect the actual strain that bearings could experience during low to strong earthquake events. The cycling sequence and strain levels are shown in Figure 2.19.

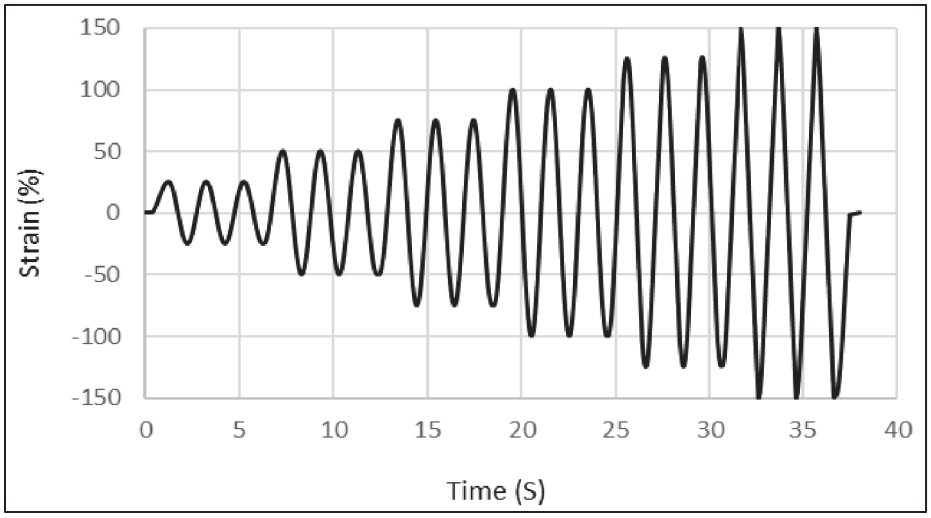

Figure 2.19 Strain amplitude of specimens under cyclic load up to150% strain

Moreover, The same sequence was used in earlier work conducted by Ankik (2019). Since hysteresis curves stabilize after three cycles of loading(Thompson et al., 2000), shear cycles were repeated three times at each amplitude.

2.7 Load frequency

In this study, three different frequency amplitudes (0.5Hz, 0.25Hz, and 0.1Hz) were considered. Both Hevea and Scougal specimens were subjected to all three frequencies. However, due to the substantial height and thickness of the original Champlain Bridge samples (both D.27 & D.28 batches), testing with the frequency of 0.5Hz was unfeasible. This limitation arose from constraints related to the dimensions of the cold chamber and the necessity for a significant displacement (100% strain) with high frequencies, which also was beyond the capacity of the available MTS press. Consequently, the CHB samples were subjected to lower frequencies, specifically 0.25Hz and 0.1Hz.

2.8 Description of the equipment

MTS Landmark 810, as shown in Figure 2.20, and MTS 370 are the hydraulic press utilized in this study for conducting shear tests, comprising two main arms arranged in a vertical configuration. One arm remains stationary, serving as the base for samples, while the other arm moves in response to the actuator, allowing for the imposition of static or dynamic movements on the specimens. The prepared specimen is then mounted onto the arms and secured in place by screws, ensuring proper alignment and contact during testing. Additionally, the press is equipped with a thermal enclosure featuring a cooling and heating system capable of operating within a temperature range of -35 °C to +100 °C with an accuracy of +/- 1 °C. Full computer control over movements and temperature enables advanced programming in accordance with required thermal conditioning and loading sequences. Temperature sensors, also, can be placed closer to the specimen to enable monitoring of the temperature during the testing and improve accuracy. In addition to the thermal enclosure, two freezers have been used to provide cold conditioning for the specimens during the long period. Freezer, shown in Figure 2.21, works between temperatures of -80°C to + 200°C.

Figure 2.20 MTS Landmark 810 used in the shear tests

Figure 2.21 Freezer used to preserve specimens at -8°C
and -30°C for long cold conditioning

2.9 Test procedure

Cold conditioning, especially for long periods, is one of the key parameters that requires preparation before running the test. In this regard, specimens were exposed to cold conditions in the thermal chamber of the press or in the Freezer. For those tests requiring short exposure duration (1 hour and 24 hours), samples were exposed to low temperatures by using the thermal chamber of the press while for long periods of cold conditioning, samples were preserved in the freezer for the desired duration of conditioning. The test procedure used in this study follows the same test procedure established by Ankik (2019) and is explained in the subsequent sections.

Short conditioning time and preparation

Upon reaching the desired temperature within the thermal chamber, the specimen is quickly positioned within the press and allowed to undergo a cooling phase for the designated conditioning period before proceeding to testing procedures. It is evident that when the chamber door is opened to mount the samples, the temperature of the chamber changes. However, upon closure of the chamber door after the installation process, the chamber temperature promptly stabilizes, returning to the predetermined target temperature. Consequently, the start of the conditioning duration precisely coincides with the moment at which the chamber temperature reaches the predetermined target.

Long conditioning time and preparation

For long cold conditioning, the specimens were conditioned in the freezer then transferred and installed in the press. To do so, the temperature of the chamber is first set to a target value. Then, the long-term-conditioned specimen is transferred from the freezer to the chamber of the press. Transferring the specimen from the freezer to the controlled temperature chamber (enclosure) of the MTS landmark, which was very closely located, and the installation of the specimen for testing was carried out in an overall time of less than 3 min. During the

installation of the specimen, the temperature of the enclosure changed slightly following the opening of the door. To remediate this, the testing began once the temperature was back to the target, usually within 5 to 15 minutes.

After the test

In order to ensure that the temperature at the center of the elastomer has reached the ambient temperature and the effects of the previous conditioning at low temperature are eliminated, a conditioning interval at room temperature of 24 °C for a minimum of 12 hours is undertaken systematically between tests at different temperatures and conditioning time. This period of conditioning between tests is supported by the finding of Yakut (2000).

2.10 Test program

In this study, as detailed in Table 2.2 to Table 2.5, Series 1 (Hevea) and Series 4 (Scougal) were exposed to low temperatures for conditioning times ranging from 1 hour to 28 days. They were tested under frequencies of 0.1Hz, 0.25Hz, and 0.5Hz. Meanwhile, Series 2 (CHB D4.27) and Series 3 (CHB D4.28) underwent conditioning for 1 hour to 14 days and were tested under frequencies of 0.1Hz and 0.25Hz. Moreover, Series 1 & 4 experienced 150% strain while Series 2 & 3 (Champlain Bridge samples) tested up to 100%.

Table 2.2 Test parameters and applied conditions for Series 1 (Hevea)

Specimens	Test temperatures	Exposure time	Strain amplitude (%)	Load frequency	Date of tests
2,3,4,7	23ºC	1 Hour	25-50-75-100-125-150	0.1Hz 0.25Hz 0.5Hz	From April to August 2023
2,5,6	-8ºC, -30ºC	1 Hour			
4,5,6		1 Day			
4,5,6		3 Day			
5,6,8		7 Day			
5,9,11		14 Day			
9,11		28 Day			

Table 2.3 Test parameters and applied conditions for Series 2 (Champlain Bridge D4.27)

Specimens	Test temperatures	Exposure time	Strain amplitude (%)	Load frequency	Date of tests
2,4	23ºC	1 Hour	25-50-75-100	0.1Hz, 0.25Hz,	From July to October 2023
3,5	-8ºC, -30ºC	1 Hour			
2,5		1 Day			
3,5		3 Day			
2,5		7 Day			
5,6		14 Day			

Table 2.4 Test parameters and applied conditions for Series 3 (Champlain Bridge D4.28)

Specimens	Test temperatures	Exposure time	Strain amplitude (%)	Load frequency	Date of tests
6,7	23ºC	1 Hour	25-50-75-100	0.1Hz 0.25Hz	From July to October 2023
3,4	-8ºC, -30ºC	1 Hour			
3,4		1 Day			
3,4		3 Day			
3,4		7 Day			
3,4		14 Day			

Table 2.5 Test parameters and applied conditions for Series 4 (Scougal)

Specimens	Test temperatures	Exposure time	Strain amplitude (%)	Load frequency	Date of tests
1,2,3,5	23ºC	1 Hour	25-50-75-100-125-150	0.1Hz, 0.25Hz, 0.5Hz	From August to November 2023
1,4	-8ºC, -30ºC	1 Hour			
1,4		1 Day			
3,4		3 Day			
3,4,5		7 Day			
2,3,6		14 Day			
6		28 Day			

CHAPITRE 3

EFFECTS OF LOW TEMPERATURES AND CONDITIONING TIME ON THE MECHANICAL PROPERTIES OF NEW AND AGED NATURAL RUBBER

3.1 Introduction

In this chapter, the results of the experiments outlined in Chapter 2 are described, focusing on the variation of mechanical properties of natural rubber affected by different cold conditioning times (ranging from 1 hour to 28 days at -8°C and -30°C) for different strain amplitudes (ranging from 25% to 150%). Force (F) and shear displacement (D) during shear tests are recorded for each test for further analysis. Figure 3.1 shows the displacement of a specimen under compressive and tensile force. The forces (F) are divided by the respective areas (A) and the displacements (D) by the thicknesses of a single block of rubber (t_r), using equations (3.1) and (3.2), to obtain the stress and the strain as preliminary parameters in order to determine the stress-strain relationship (hysteresis curves).

$$\tau = F/2A \tag{3.1}$$

$$\gamma = \frac{D/2}{t_r} \tag{3.2}$$

Mechanical characteristics of elastomers including the effective shear modulus (G_{eff}), the equivalent viscous damping (ξ_{eq}), and the stress at zero strain (τ_0) were calculated from the obtained stress-strain curves. These characteristics are determined for each exposure temperature and conditioning time defined in Chapter 2, and they are also established by referring to the third load cycle for each strain amplitude applied. The value of G_{eff} is determined from the following equation (3.3), provided by (Constantinou et al., 2007), in which τ_{max} and τ_{min} are the maximum and minimum shear stress values, respectively, and γ_{max} and γ_{min} are the maximum and minimum strain values, respectively. According to

Constantinou et al (2007), maximum (τ_{max}) and minimum (τ_{min}) shear stresses occur practically at the maximum and minimum shear strains, respectively.

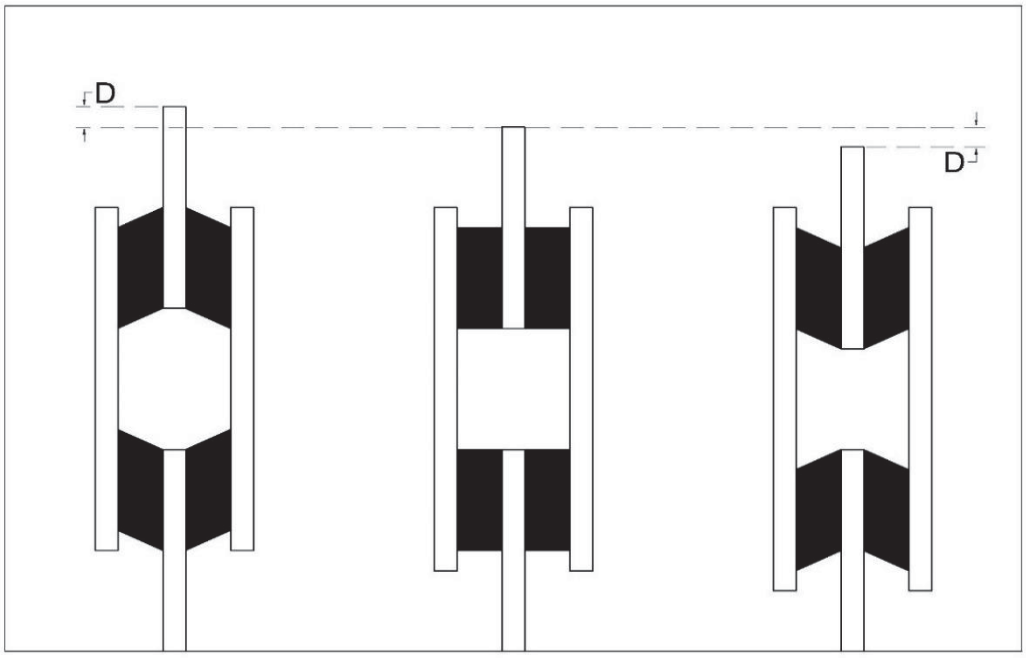

Figure 3.1 Deformation of the specimen under cyclic load

$$G_{\text{eff}} = \frac{\tau_{max} - \tau_{min}}{\gamma_{max} - \gamma_{min}} \tag{3.3}$$

The equivalent damping ratio (ξ_{eq}) is calculated by equation (3.4) described by (Cardone & Gesualdi, 2012). where A_r and t_r are the area and the thickness of a block of rubber, respectively. The energy dissipated per cycle (E_{DC}) is defined as the area bounded by the force-

$$\xi_{eq} = \frac{E_{DC}}{4\,\pi \mathrm{G}_{\text{eff}} A_r t_r \gamma^2} \tag{3.4}$$

displacement relationship for the given cycle (Constantinou et al., 2007). In this study, energy dissipated area ($\mathrm{E_{DC}}$) is calculated numerically. The stress (τ_0) is the stress value corresponding to zero cyclic strain. According to Cardone & Gesualdi (2012), (τ_0) and τ_{max}

play a critical role in the hysteretic model calibration to conduct nonlinear analysis for structures using rubber-based seismic isolators (Cardone & Gesualdi, 2012).

3.2 Mechanical characteristics of natural rubber, Series1 (Hevea)

3.2.1 Influence of cold conditioning time on stress-strain relationship

Natural rubber Series 1 is tested at room temperature 23°C, -8°C, and -30°C for the different conditioning durations ranging from 1 hour to 28 days to establish the effect of low temperatures and cold conditioning duration. By comparing hysteresis curves at room temperature 23°C, shown in Figure 3.2, and at -8C, shown in Figure 3.3, It is found that the max of stress and the hysteresis area increased when the temperature fell from 23°C to -8°C.

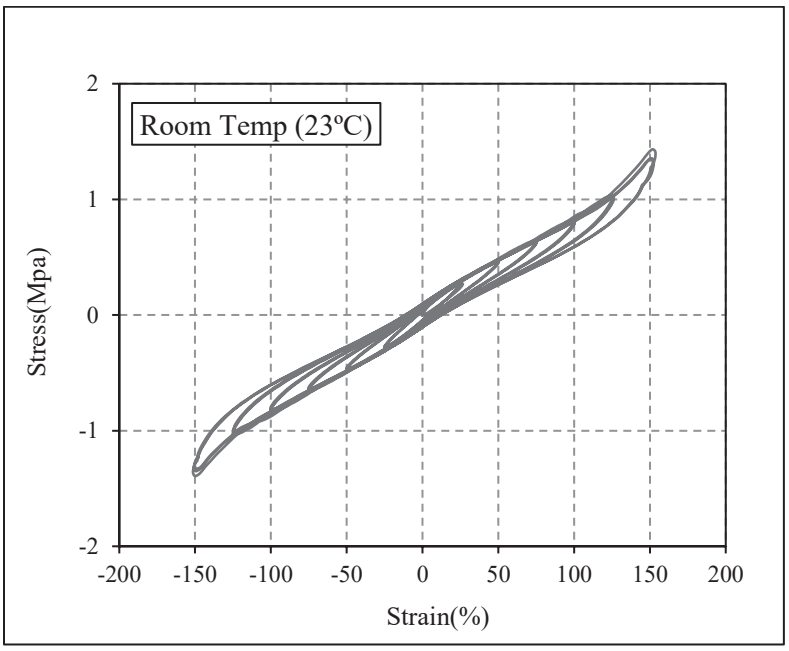

Figure 3.2 Stress-strain relationship of natural rubber, Series1, at room temperature (23ºC)

For example, compared to 23°C the maximum stress at 100% strain increases by approximately 10% after 1 hour of conditioning at -8°C. Regarding the effect of conditioning duration on the

mechanical properties of natural rubber Series 1, maximum stress at 100% deformation increases by approximately 7% when cold condition time is extended from 1 hour to 28 days. This suggests that increasing the conditioning duration at -8ºC does not significantly affect the stress level experienced by elastomer Series 1.

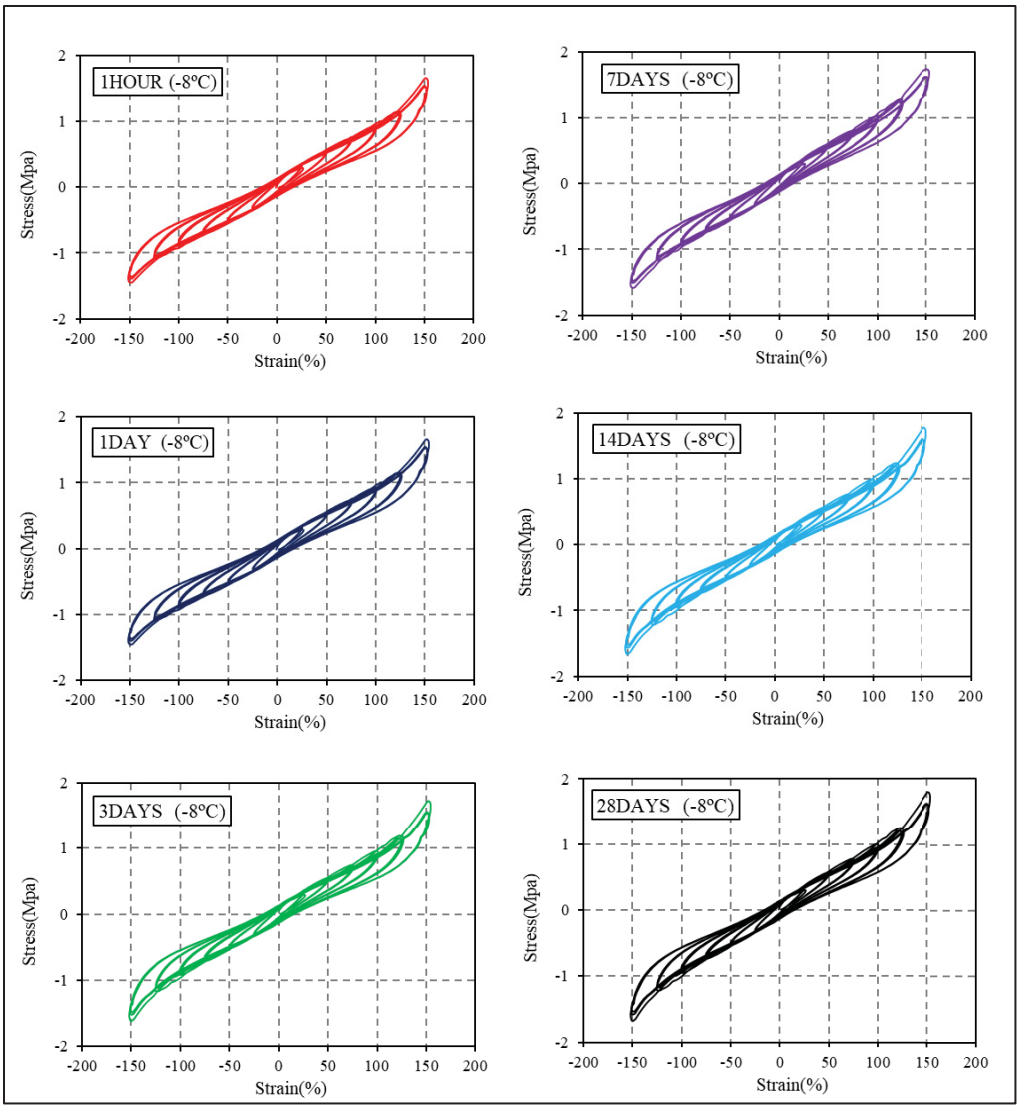

Figure 3.3 Stress-strain relationship of natural rubber, Series1,
at -8ºC for different conditioning times ranging from 1 hour to 28 days

Test result at -30°C shows an increase in the hysteresis area and the maximum stress in comparison with not only room temperature 23°C but also -8°C. As an example, at 100% strain

and after conditioning time of 1 hour at -30°C, the maximum stress level increases by approximately 31% compared to a temperature of 23°C.

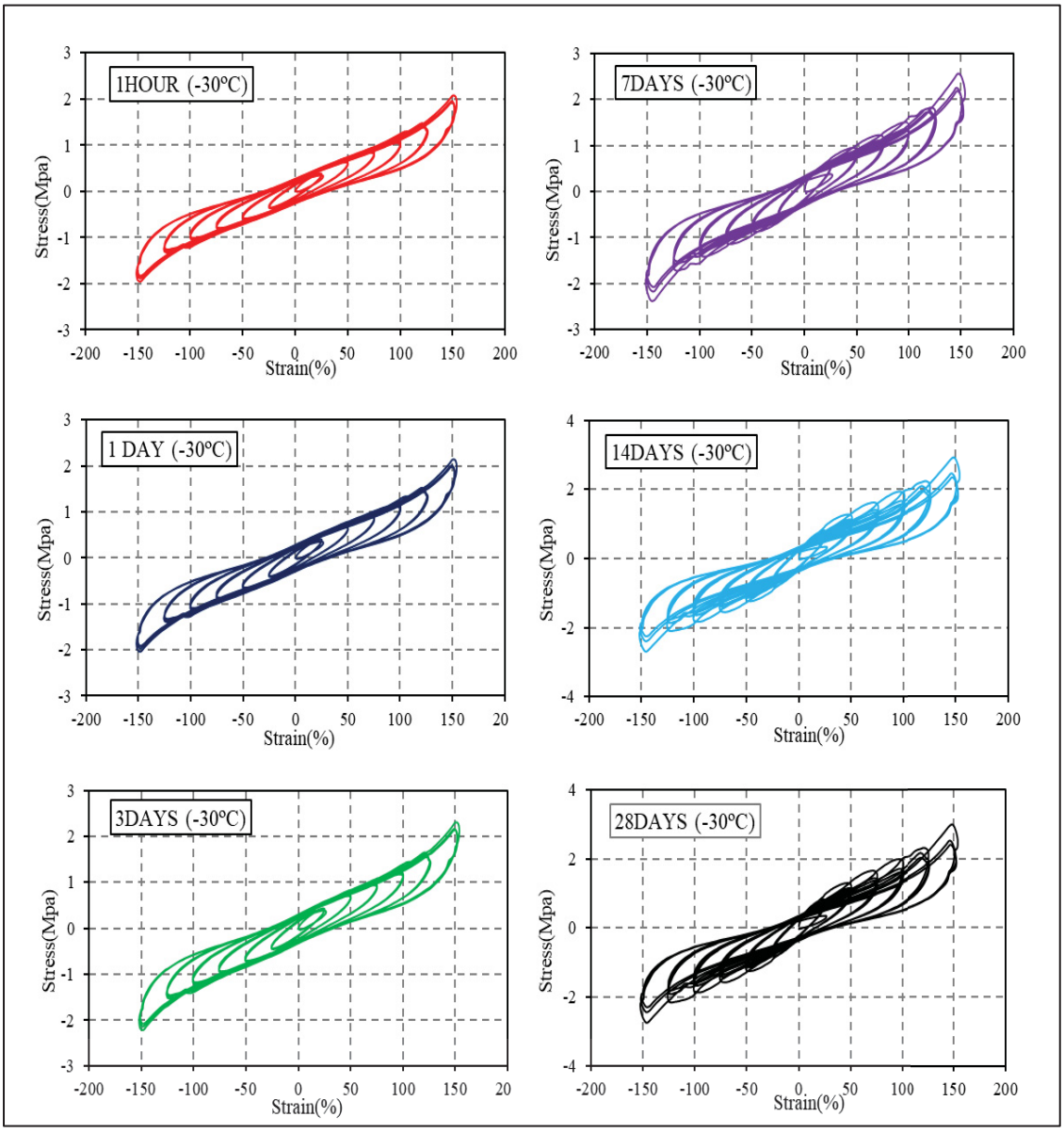

Figure 3.4 Stress-strain relationship of natural rubber, Series1, at -30ºC for different conditioning times ranging from 1 hour to 28 days

The superposition of the hysteresis curves for 1 hour as well as 14 days of cold conditioning obtained at 23°C and -8°C are shown in Figure 3.5, and at -30ºC are shown in Figure 3.6. These

figures are plotted to show the differences between hysteresis curves of different conditioning times at different temperatures (23°C, -8°C, and -30ºC).

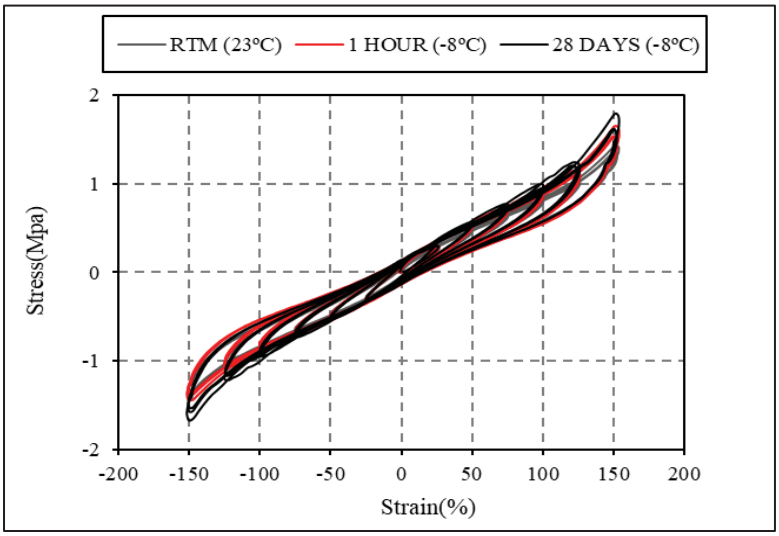

Figure 3.5 Superposition of hysteresis curves of Series 1, obtained at 23ºC, -8ºC for different conditioning time

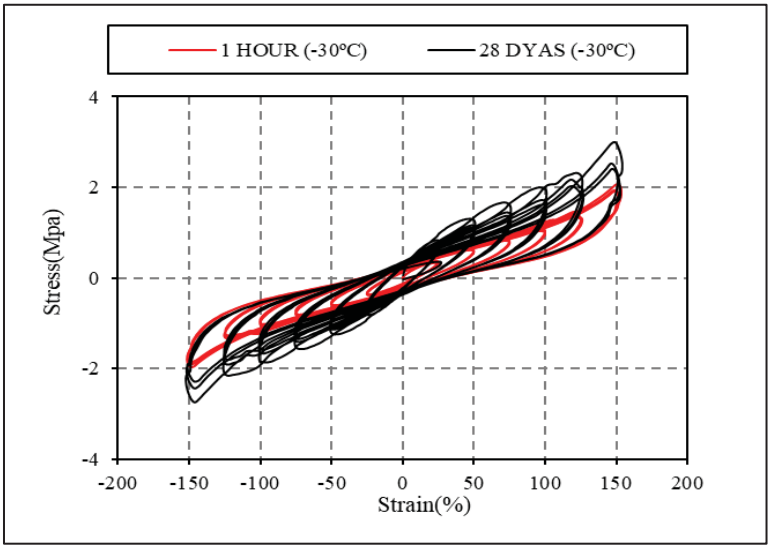

Figure 3.6 Superposition of hysteresis curves of Series 1, obtained at -30ºC for different conditioning time

3.2.2 Effect of cold conditioning time on shear modulus, damping, and τ_0

The variation of G_{eff} due to could conditioning duration ranging from 1 hour to 28 days as a function of strain amplitude at temperatures of -8°C and -30°C is shown in Figures 3.7(a) and 3.8(a), respectively. During the experiments conducted at a temperature of -8°C, it was observed that from 1 hour to 24 hours, the effective shear modulus (G_{eff}) at desired strain level remains nearly constant, regardless of the conditioning period. While throughout conditioning from 24 hours to 3 days, it is observed a minor rise in G_{eff}, approximately 4% increase. During extended periods, G_{eff} at 100% strain, from 3 to 28 days, increases approximately by 4%. It is also evident from the results that G_{eff} decreases with increasing strain levels. This is more pronounced for small deformation amplitudes between 25 and 75% (approximately 10 to 20%) than for large deformations between 100 and 125% (less than 1%), and then a slight stiffening of the material is observed at 150% strain. This stiffening, which led to an increase in G_{eff}, occurred due to the stiffening of the elastomer at large deformation, as reported in previous studies (Ankik, 2019; Clark, 1996). Additionally, at -30°C, between 1 hour and 24 hours of conditioning, approximately 6% increase in G_{eff} at 100 % strain is observed. With longer conditioning durations ranging from 24 hours to 28 days, there is also a gradual increase in G_{eff}. For instance, at 100% deformation, G_{eff} rises by approximately 7% between 24 hours and 3 days, and by 36% between 3 and 28 days. Similar to the findings at -8°C, it is observed that G_{eff} decreases as strain level increases, with a more pronounced effect at lower strains compared to higher strains.

Figures 3.7(b) & 3.8(b), present the variation of ξ_{eq} with strain levels at temperatures of -8°C and -30°C for different conditioning durations, respectively. At -8°C, the equivalent viscous damping shows low sensitivity to conditioning duration. Moreover, ξ_{eq} decreases almost linearly as the strain level increases from 25% to 150%. Similarly, at -30°C, ξ_{eq} exhibits minimal variation with conditioning duration. Figures 3.7(c) & 3.8(c) illustrate the variation of stress τ_0 at temperatures of -8°C and -30°C, respectively, concerning the level of deformation for different conditioning durations. At -8°C, results show minor changes in τ_0

with conditioning duration. τ_0 increases with rising overall shear strain levels, peaking at 125%. This increase is more pronounced at strains below 75% (approximately 11% to 40%) compared to levels of 100% to 125% (approximate average of 3%).

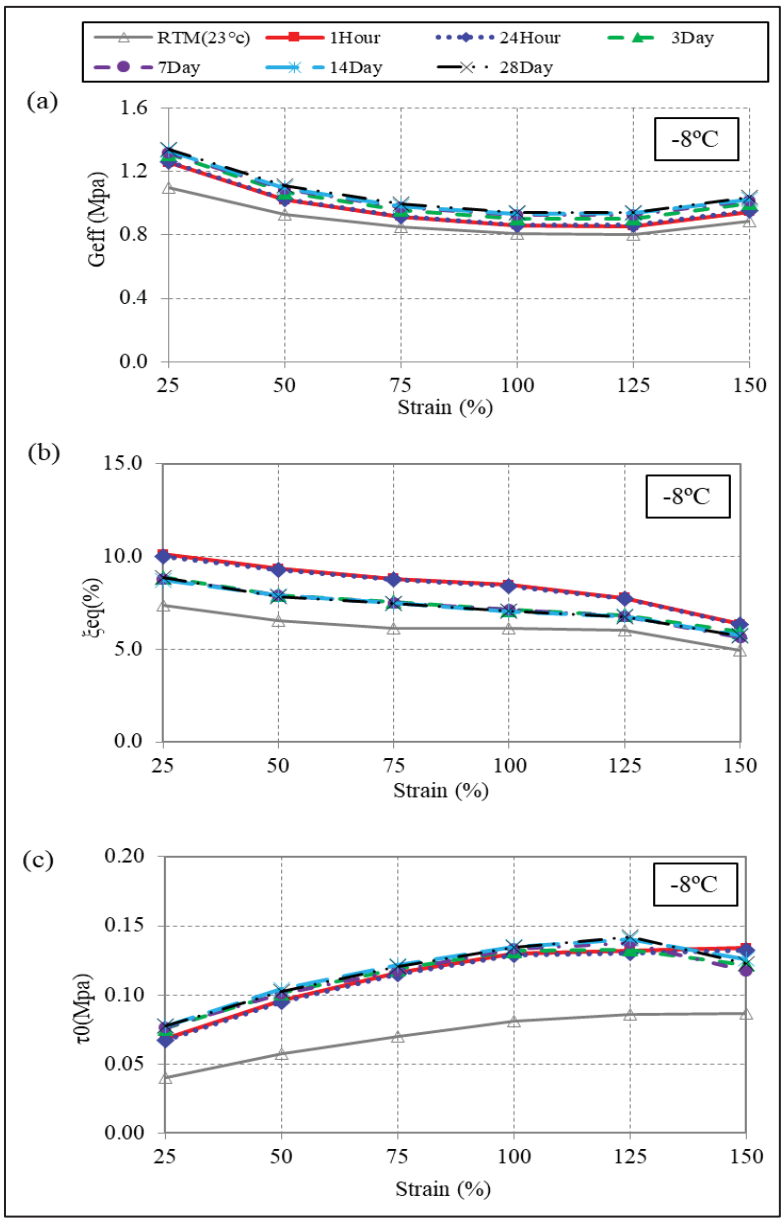

Figure 3.7 Cold conditioning time effect on (a) shear modulus, (b) damping ratio, and (c) stress at zero strain of natural rubber, Series 1(Hevea), at -8ºC

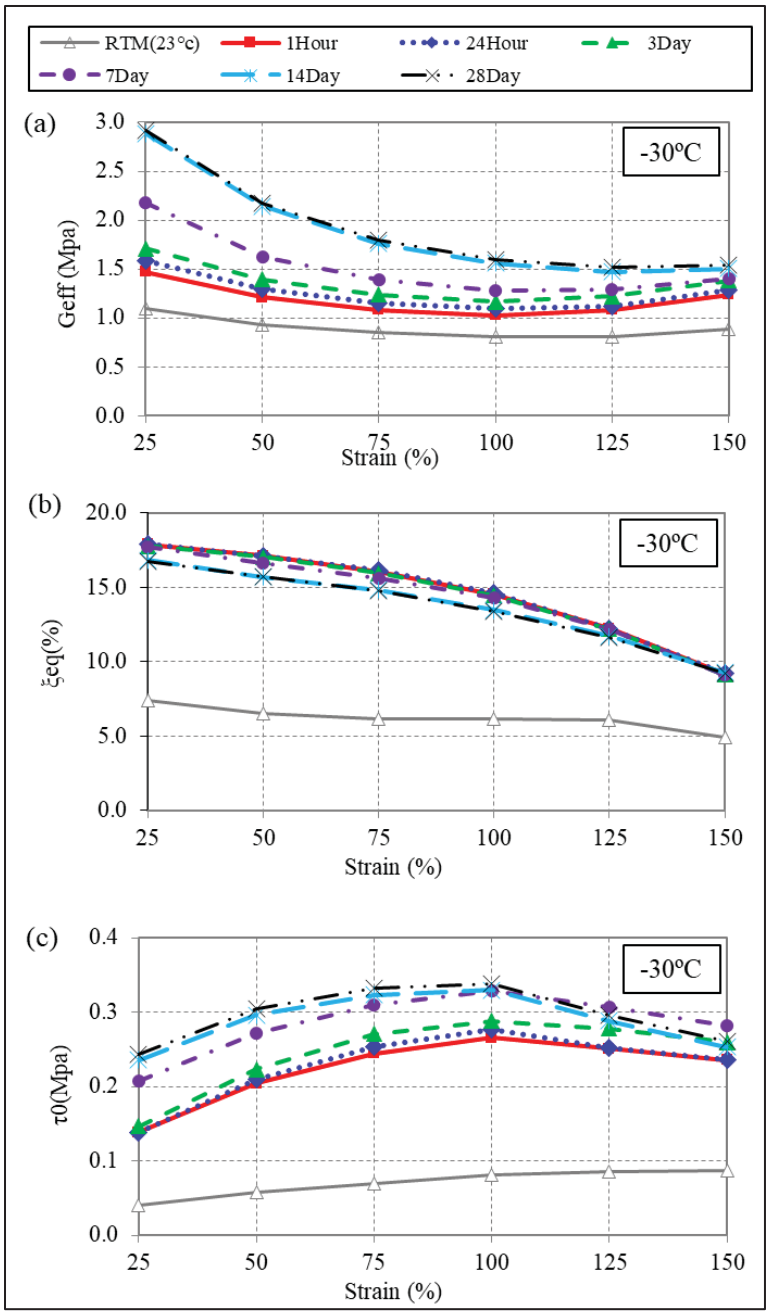

Figure 3.8 Cold conditioning time effect on (a) shear modulus, (b) damping ratio, and (c) stress at zero strain of natural rubber, Series 1(Hevea), at -30ºC

Regarding tests conducted at -30°C, minimal variation in τ_0 is observed for conditioning durations between 1 hour and 24 hours. However, for the overall shear strain of 100%, with increasing conditioning duration, τ_0 rises by 4% between 24 hours and 3 days, by 14% between

3 and 7 days, and by approximately 3% between 7 and 28 days. Moreover, τ_0 increases with overall strain up to 100%, then decreases at strains of 125% and 150%. This reduction can be attributed to the internal heating of the elastomer during incremental cyclic loading and the rupture of crystals formed in the elastomer during the initial load amplitudes, leading to a decrease in lateral stiffness and, consequently, a decrease in the stress level required to deform it at larger amplitudes.

3.3 Room temperature Aging effect on shear modulus

Figure 3.9 illustrates the effect of room temperature aging on the effective shear modulus of natural rubber (G_{eff}) by comparing G_{eff} obtained in 2018 and 2023 as a function of strain level at 20ºC as well as -8°C and -30°C for different cold conditioning times, including 1 hour, 1 day, and 7 days. The shear modulus data for 2018 were acquired through experimental tests conducted by Ankik (2019) during the summer of that year. It is worth noting that the same samples tested in 2018 underwent further testing in 2023, using the same test procedure employed in the experiments in 2018.

The comparison of results indicates that the shear modulus increases at both room temperature and low temperatures, for various strain levels ranging from 25% to 150%. This increase is more pronounced at low temperatures compared to room temperature as well as large deformations compared to smaller ones. For example, at room temperature, G_{eff} increases by approximately 6% at the 25% strain level and then reaches 12% at the 150% strain level, compared to the results of 2018. Similarly, at -8ºC after 1 hour of conditioning, G_{eff} shows an increase of around 12% at the 25% strain level and reaches 13% at the 150% strain level, compared to 2018. Additionally, at -30ºC, G_{eff} shows an increase of up to around 15%. This increase in shear modulus is likely due to stiffening and the progress of vulcanization over time.

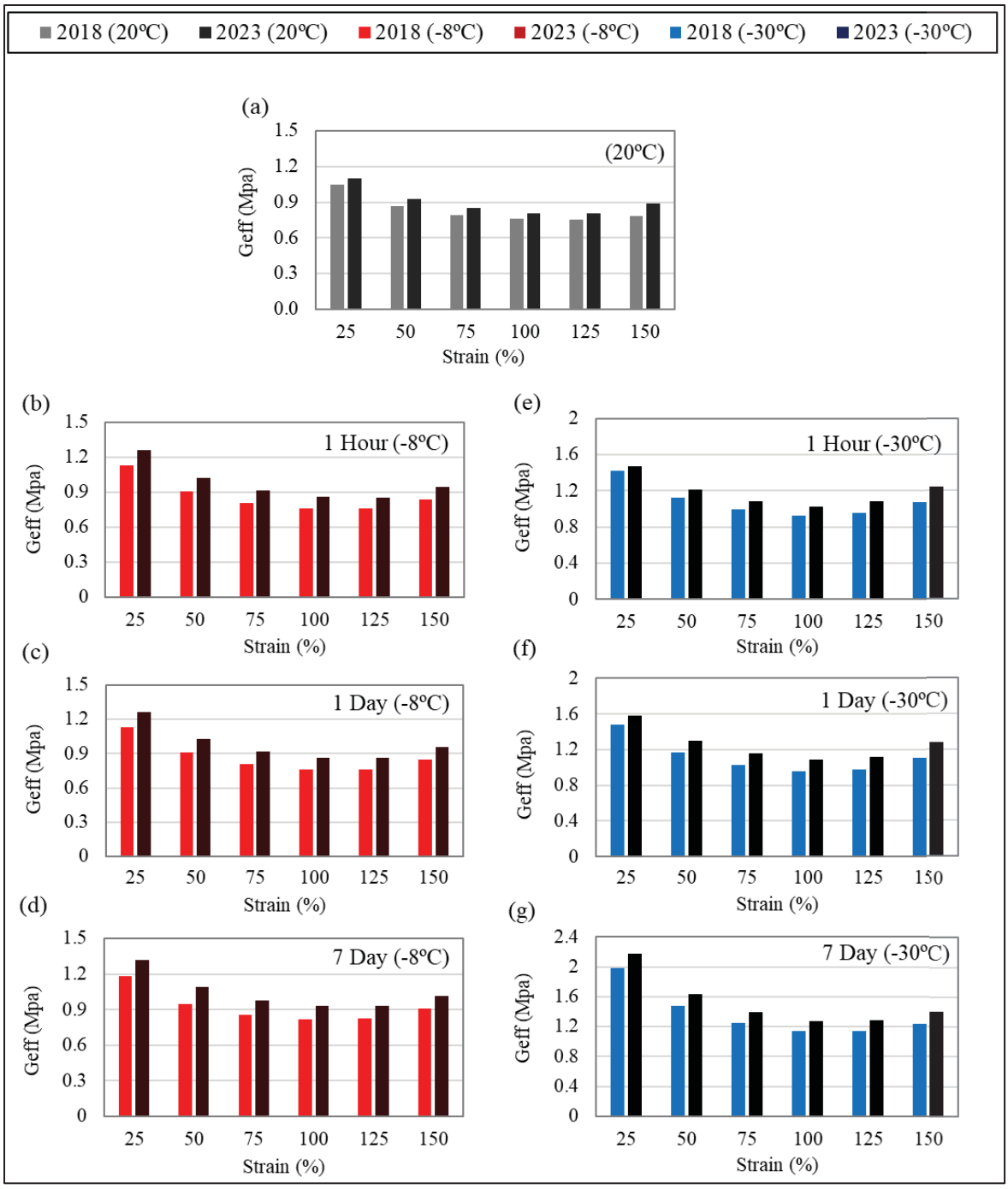

Figure 3.9 Variations in the shear modulus of natural rubber under different time conditioning, at 20ºC (a), for conditioning time from 1 hour (b) to 7 days (d) at -8ºC, and for conditioning time from 1 hour (e) to 7 days (g) at -30ºC, influenced by aging effects

3.4 Mechanical characteristics of natural rubber, Series2 (CHB D4.27)

3.4.1 Influence of cold conditioning time on stress-strain relationship

Effects of cold temperature on the stress-strain relationship of natural rubber Series 2 at -8ºC and -30ºC, for different conditioning time are shown in Figures 3.103.11, respectively. For the purpose of comparison, the shear behaviour of Series2 at room temperature is provided in Figure 3.10, as well. Compared to room temperature, the hysteresis curve after 1 hour of cold conditioning at -8°C indicates that both the enclosed area of the hysteresis curve and the maximum stress increase. However, extending the cold conditioning time from 1 hour to 14 days shows an insignificant increase in maximum stress and the enclosed area of the hysteresis curve. For instance, after 1 hour of conditioning at -8°C, the maximum stress for the third cycle at 100% strain increased by approximately 8%, while increasing the duration of cold conditioning from 1 hour to 14 days resulted in a maximum stress increase of around 3%. In Figure 3.12, a superposition of the hysteresis curves obtained at 23°C and -8°C after 1 hour and 14 days of cold conditioning is illustrated to provide a better understanding of the impact of low temperatures(-8ºC).

The results of tests conducted at -30°C indicate that the rubber Series 2 experienced higher stress values compared to those observed at 23°C and -8°C. As an example, the maximum stress at the 100% strain level increased by approximately 20% when samples were exposed to cold temperatures of -30°C for 1 hour, compared to the stress observed at 23°C. Additionally, the enclosed area of the hysteresis curves at -30°C is greater than those obtained at 23°C and -8°C. It is also observed that by increasing the conditioning time from 1 hour to 14 days, the maximum stress and the enclosed area of the hysteresis curve increase. For example, maximum stress at 100% strain increases by approximately 12% when the conditioning time increases from 1 day to 3 days conditioning, by approximately 14% when it increases from 3 days to 7 days, and by approximately 26% when it increases from 7 days to 14 days. In total, maximum stress increased by 68% when the conditioning time increased from 1 hour to 14 days, which indicates that the phenomenon of crystallization occurred.

Figure 3.13 shows the superposition of hysteresis curves after 1 hour, 7 days, and 14 days of cold conditioning at -30ºC, illustrating the differences between hysteresis curves of different conditioning times.

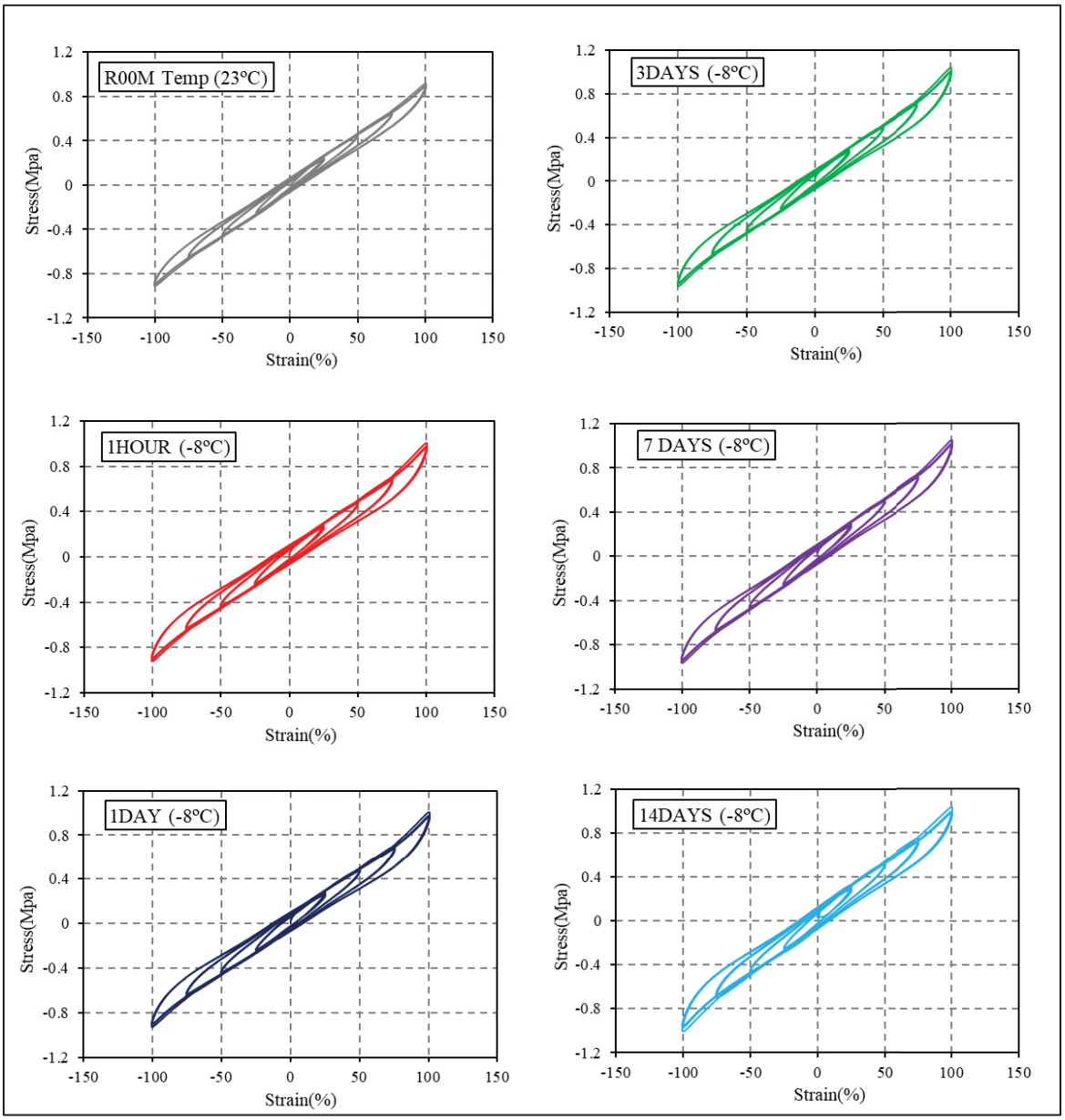

Figure 3.10 Stress-strain relationship of natural rubber, Series2 (Champlain bridge batch D.27), at room temperature (23ºC) and -8ºC for different conditioning times ranging from 1 hour to 14 days

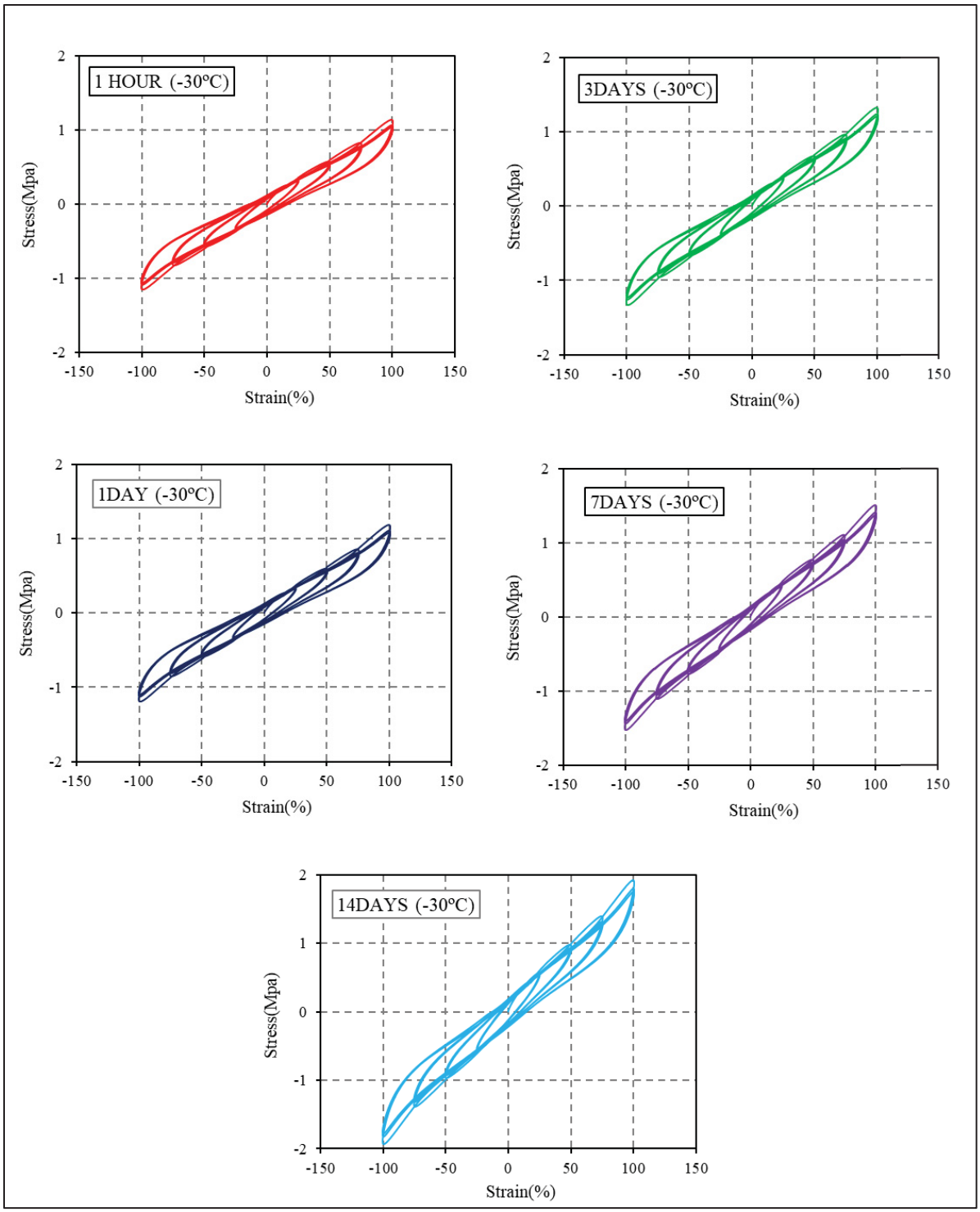

Figure 3.11 Stress-strain relationship of natural rubber, Series 2 (Champlain bridge batch D4.27), at -30ºC for different conditioning times ranging from 1 hour to 14 days

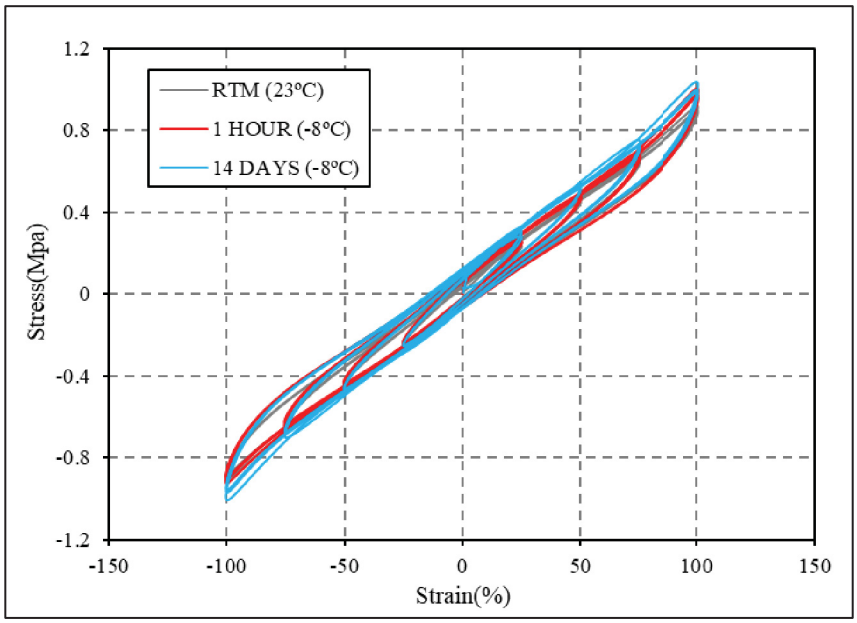

Figure 3.12 Superposition of hysteresis curves of Series 2, obtained at 23ºC, -8ºC for different conditioning time

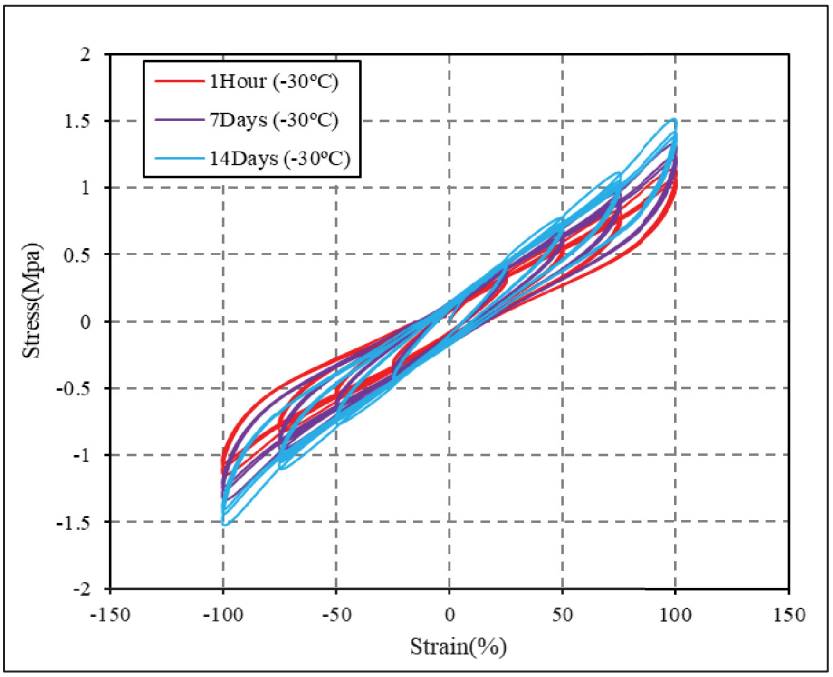

Figure 3.13 Superposition of hysteresis curves of Series 2, obtained at -30ºC for different conditioning time

3.4.2 Effect of cold conditioning time on shear modulus, damping, and τ_0

Figure 3.14(a) illustrates the variation of the effective shear modulus (G_{eff}) of natural rubber Series 2 (CHB D.27) concerning the strain level at temperatures of -8°C for different conditioning durations. It is observed that for conditioning durations ranging from 1 hour to 1 day, G_{eff} remains practically unchanged for the various deformation levels. However, with an increase in conditioning time from 1 day to 3 days, G_{eff} experiences an increment of 3% at 100% strain level. Subsequently, from 3 days to 14 days, G_{eff} exhibits a slight increase. This increase is more pronounced in small deformations (ranging from 25% to 50%) than in large deformations (ranging from 75 to 100% strain). For example, from 3 days to 14 days, at 25% strain, G_{eff} increases by approximately 4% while at 100% strain, it increases by approximately 1%. Overall, G_{eff} for long conditioning (3 days to 14 days) remains almost unchanged, specifically for large deformation which is likely the most pertinent for seismic isolation applications.

Figure 3.15(a) depicts the variation of G_{eff} of natural rubber Series 2 with respect to the strain levels for various conditioning durations at -30°C. The findings reveal negligible changes in G_{eff} between 1 hour and 24 hours (1 day) of conditioning. However, as the conditioning duration extends from 1 day to 14 days, there is a gradual increase in G_{eff}. For instance, at 100% deformation, G_{eff} rises by approximately 12% between 1 day and 3 days, and further increases by 45% between 3 days and 14 days. Overall, G_{eff} at 100% strain increases by 68% when conditioning time is prolonged from 1 hour to 14 days.

Additionally, the results at both temperatures of -8°C and -30°C indicate that G_{eff} decreases with increasing strain levels up to 75%, whereas a slight increase is observed at 100% strain. For example, among different conditioning times, when the strain increases from 25 to 75%, G_{eff} decreases by approximately 15% at -8°C and by approximately 20% at -30°C. However, G_{eff} slightly increases by 6% at -8°C and by 2% at -30°C when the strain level increases from 75% to 100%.

Figure 3.14 (b) illustrates the variation of the equivalent damping ratio (ξ_{eq}) as a function of strain level at temperatures of -8°C for different conditioning times. It is observed that there is no significant difference in the ξ_{eq} of natural rubber Series 2 when the cold conditioning duration is extended from 1 hour to 14 days, indicating that the equivalent damping ratio has low sensitivity to conditioning duration changes. This insensitivity can be attributed to the fact that, despite an increase in both shear modulus (G_{eff}) and energy dissipated per cycle (E_{DC}), the ratio of E_{DC} to G_{eff}, which is the main factor in damping calculation, remains almost constant. As a result, there is no significant change in damping when conditioning time increases. However, the results suggest that by increasing the strain level from 25 to 100%, ξ_{eq} significantly decreases. For example, when the strain level rises from 25 to 100%, ξ_{eq} decreases by approximately 35%. That ξ_{eq} decreases when the strain level increases is consistent with previous research, particularly the experiments conducted by Ankik in 2019. In Figure 3.15(b), the variation of the ξ_{eq} as a function of strain level at temperatures of -30°C for different conditioning times is shown. The results demonstrate a similar trend to that observed at -8°C, indicating that ξ_{eq} varies only slightly with the conditioning duration. However, for the conditioning duration of 14 days, a decrease in ξ_{eq} is observed. This is because the increase in the energy dissipated per cycle is less than the increase in the effective shear modulus. This performance of the damping ratio after 14 days of conditioning at -30ºC was also observed in previous experiments conducted by Ankik in 2019.

Figure 3.14(c) presents the variation of the stress at zero strain (τ_0) as a function of strain level for the different conditioning durations at -8°C. The results indicate a slight increase in τ_0 when conditioning duration increases. For example, τ_0 at 100% strain increases around 4% from 1 hour to 3 days, 3% from 3 days to 7 days, and 12% from 7 days to 14 days. Regarding the variation of τ_0 with respect to the overall shear strain level, it is observed that τ_0 increases when the overall shear strain level increases. For example, τ_0 increases by 37% when the overall strain level increases from 25 to 50%, by 17% when it increases from 50 to 75%, and by 10% when it increases from 75 to 100%. Figure 3.15 (c) shows the variation of τ_0 at -30ºC. This figure indicates that between conditioning times of 1 hour and 24 hours, the variation in

τ_0 is negligible. However, for longer conditioning duration, τ_0 increases. For example, τ_0 at 100 % strain increases by 14% between 24 hours and 3 days and by 27% between 7 days and 14 days.

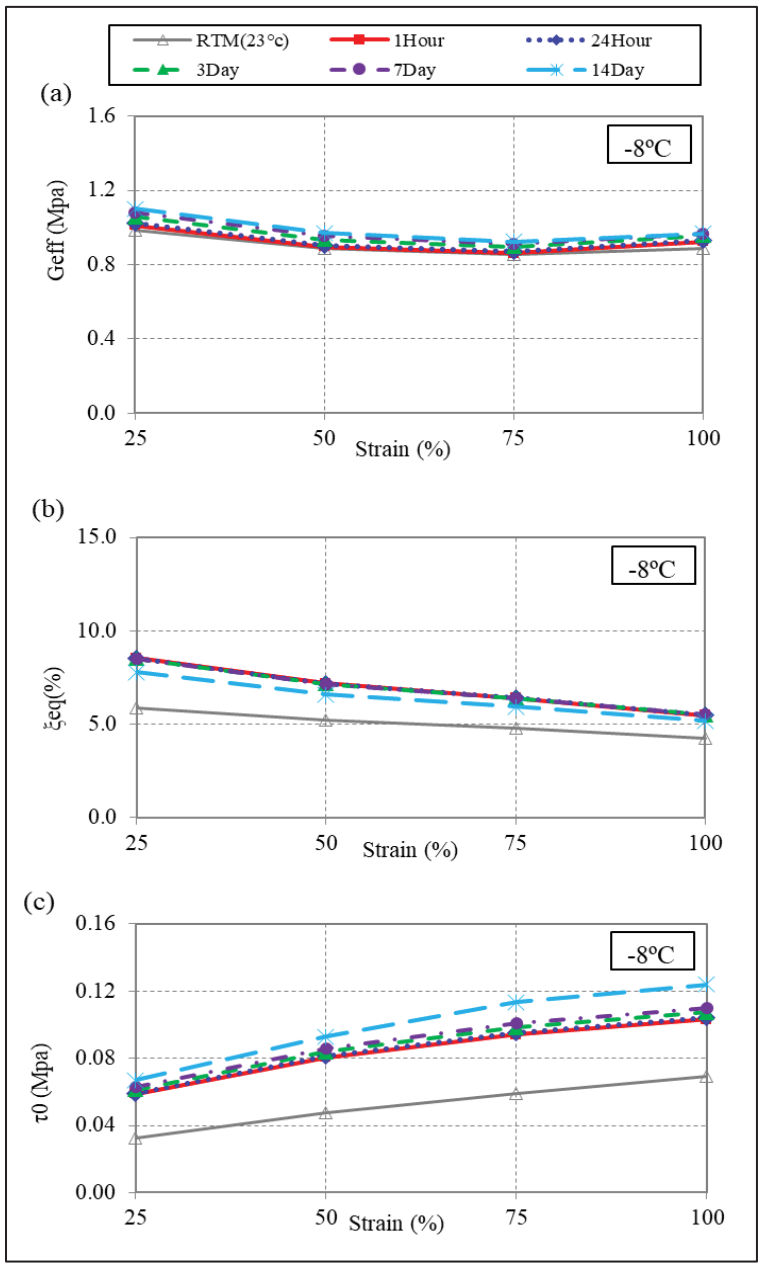

Figure 3.14 Cold conditioning time effect on (a) shear modulus, (b) damping ratio, and (c) stress at zero strain of natural rubber, Series2 (CHB D4.27), at -8ºC

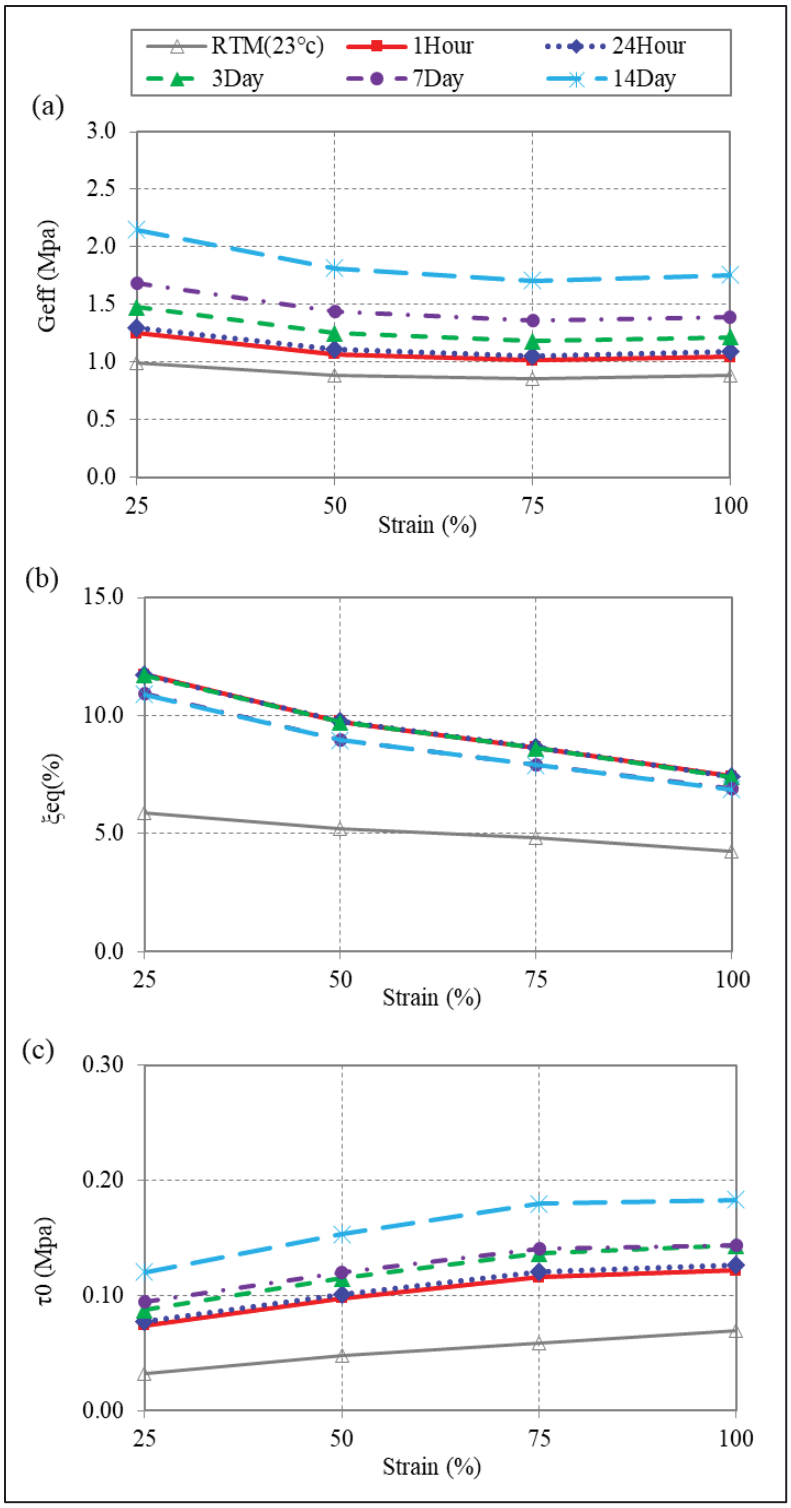

Figure 3.15 Cold conditioning time effect on (a) shear modulus, (b) damping ratio, and (c) stress at zero strain of natural rubber, Series2 (CHB D4.27), at -30ºC

3.5 Mechanical characteristics of natural rubber, Series3 (CHB D4.28)

3.5.1 Influence of cold conditioning time on stress-strain relationship

Figures 3.16 and 3.17 show the effects of cold temperatures at -8ºC and -30ºC on the stress-strain relationship of natural rubber Series 3, respectively, illustrating various conditioning times and strain levels. Additionally, for comparison purposes, the shear behaviour of Series 3 at room temperature is provided in Figure 3.16. After 1 hour of cold conditioning at -8°C, the hysteresis curve reveals notable increases in the enclosed area of hysteresis curve and maximum stress compared to room temperature. For example, after 1 hour of cold conditioning at -8ºC, the maximum stress at 100% strain elevates by approximately 15%. This increase in stress is due to the instantaneous stiffening of rubber. Prolonging the conditioning period from 1 hour to 1 day, also, yields an insignificant increase in these parameters. However, by increasing the conditioning time from 1 day to 3 days, maximum stress during the third cycle at 100% strain increases by approximately 5%. Similarly, from 3 days to 14 days of conditioning, the maximum stress increases by approximately 3%.

At -30°C, test results reveal that rubber Series 3 exhibits significant increases in the stress levels and the enclosed area of the hysteresis curve compared to those observed at 23°C and -8°C. For instance, exposure to -30°C for 1 hour resulted in a roughly 36% increase in maximum stress at the 100% strain level compared to the stress observed at 23°C. Additionally, extending the conditioning time from 1 hour to 14 days leads to gradual increases in maximum stress and enclosed area of the hysteresis curve. For example, maximum stress at 100% strain increases by approximately 3% when the conditioning time increases from 1 hour to 1 day conditioning, by approximately 3% when it increases from 1 day to 3 days, by approximately 10% when it increases from 3 days to 7 days, and by approximately 4% when it increases from 7 days to 14 days. Overall, maximum stress increases by 22% when the conditioning time extends from 1 hour to 14 days, indicating the occurrence of the crystallization phenomenon.

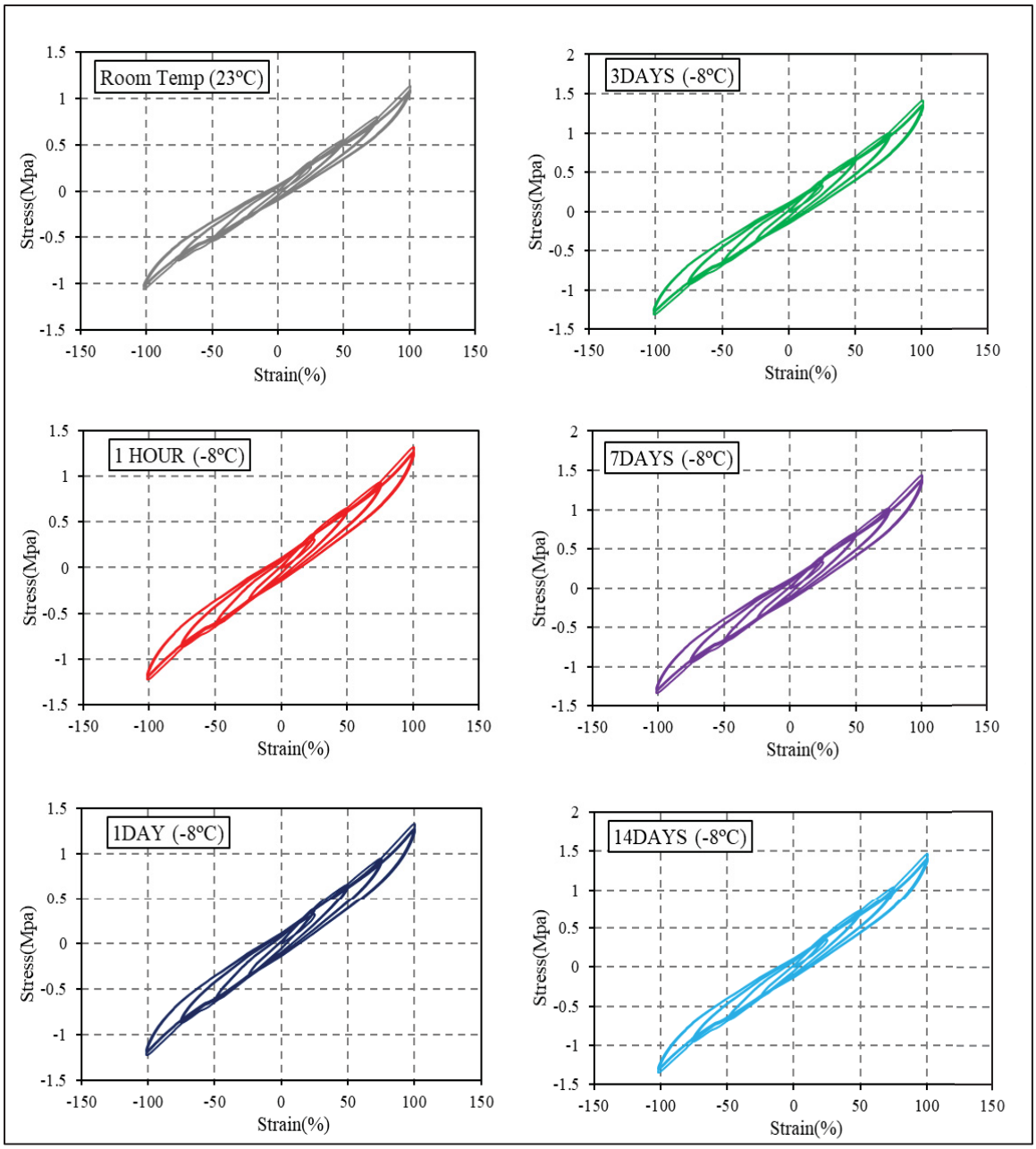

Figure 3.16 Stress-strain relationship of natural rubber Series 3 (CHB D.28), at room temperature (23ºC) and -8ºC for different conditioning times ranging from 1 hour to 14 days

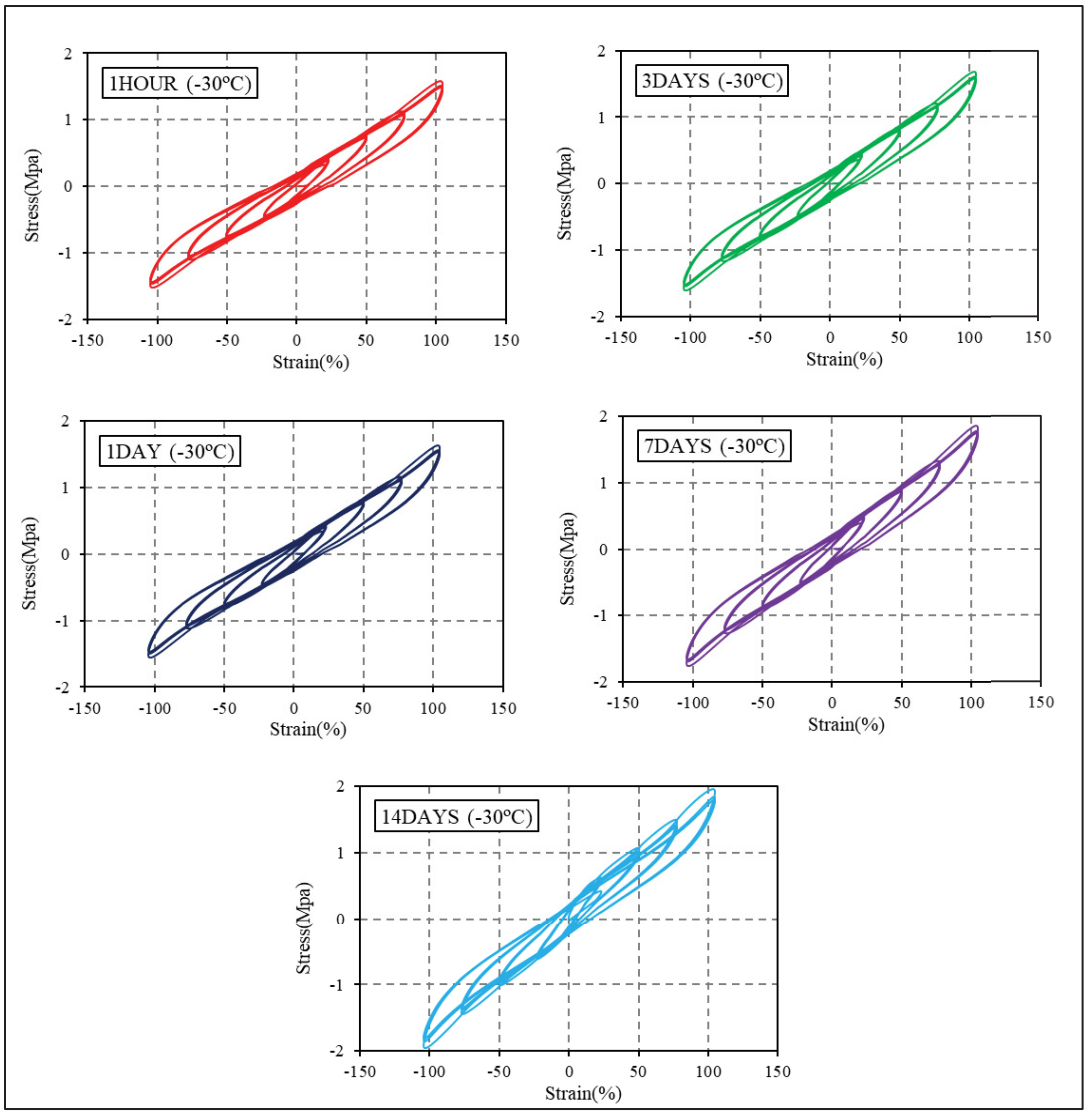

Figure 3.17 Stress-strain relationship of natural rubber Series 3 (CHB D.28), at -30ºC for different conditioning times ranging from 1 hour to 14 days

3.5.2 Effect of cold conditioning time on shear modulus, damping, and τ_0

In Figure 3.18(a), the variation of the effective shear modulus (G_{eff}) of natural rubber Series 3, with respect to the strain level, at -8°C is depicted for various conditioning durations. Notably, G_{eff} remains practically unchanged for conditioning periods from 1 hour to 1 day, for the considered deformation levels. However, a noticeable increase of 5% in G_{eff} is observed when the conditioning time extends from 1 day to 3 days across different strain levels.

Subsequently, from 3 days to 14 days, G_{eff} exhibits a slight increase. For example, from 3 days to 14 days, at 25% strain, G_{eff} increases by approximately 4% and at 100% strain, it increases by approximately 3%. In Figure 3.19(a), the variation of G_{eff} of natural rubber Series 3 with respect to the strain levels for different conditioning durations at -30°C is depicted. The results indicate minimal changes in G_{eff} between 1 hour and 1 day of conditioning. However, as the conditioning duration progresses from 1 day to 14 days, there is a gradual increase in G_{eff}. For example, at 100% deformation, G_{eff} increases by approximately 20% between 1 day and 14 days. The findings at both -8°C and -30°C reveal that, regardless of conditioning times, there is a consistent trend wherein G_{eff} decreases with rising strain levels up to 75%. For instance, as the strain escalates from 25 to 75%, G_{eff} experiences a reduction of approximately 18% at -8°C and approximately 25% at -30°C. However, when the strain level progresses from 75% to 100%, it is observed that G_{eff} at both -8°C and -30°C remains nearly unchanged.

Figure 3.18 (b) illustrates the variation of the equivalent damping ratio (ξ_{eq}) as a function of strain level at temperatures of -8°C for different conditioning times. It is observed that there is no significant difference in the ξ_{eq} of natural rubber Series 3 when the cold conditioning duration is extended from 1 hour to 7 days. However, a decrease of less than 1% (approximately 0.5%) in the damping ratio is found when conditioning time increases from 7 days to 14 days. Similar to Series 1 and 2, the equivalent damping ratio exhibits low sensitivity to conditioning duration. Regarding the variation due to the strain amplitude, the results suggest that despite an increase between 25 and 50% strain, equivalent damping decreases by approximately 20% between 50 and 100% strain levels. It is worth noting that, a small increase between 25 to 50% strain levels at -10ºC was observed in previous studies conducted by Cardone in 2012, which is consistent with the result of Series 3. In Figure 3.19 (b), the variation of the ξ_{eq} at temperatures of -30°C is shown. The results indicate that ξ_{eq} varies slightly with the conditioning duration. However, for the conditioning duration of 14 days, a decrease (approximately 1.5%) in ξ_{eq} is observed. Figure 3.18 (c) presents the variation of the stress at zero deformation (τ_0) as a function of the overall shear strain level for the different conditioning durations at -8°C. The results indicate slight changes in τ_0 when conditioning

duration increases. For example, τ_0 at 100% strain increases around 5% from 1 hour to 3 days, 3% from 3 days to 7 days, and it decrease by 3% from 7 days to 14 days. Similar to the other Series, it is observed that the τ_0 increases when the overall shear strain level increases.

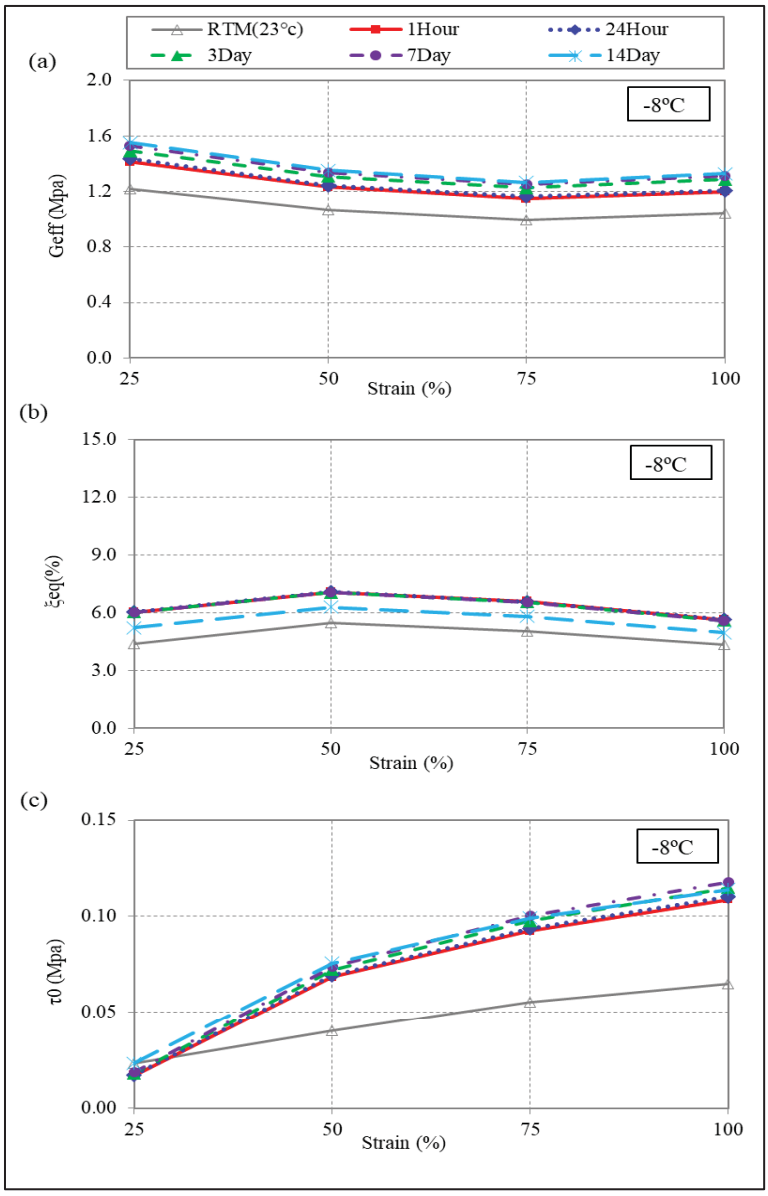

Figure 3.18 Cold conditioning time effect on (a) shear modulus, (b) damping ratio, and (c) stress at zero strain of natural rubber Series 3 (CHB D.28), at -8ºC

Figure 3.19(c) shows the variation of τ_0 at -30ºC. This figure indicates that between conditioning times of 1 hour and 24 hours, the variation in τ_0 is negligible. However, for longer conditioning duration, τ_0 increases. For example, τ_0 at 100 % strain increases by 5% between 24 hours and 3 days and by 8% between 3 days and 7 days, and it decreases by 5% from 7 days to 14 days.

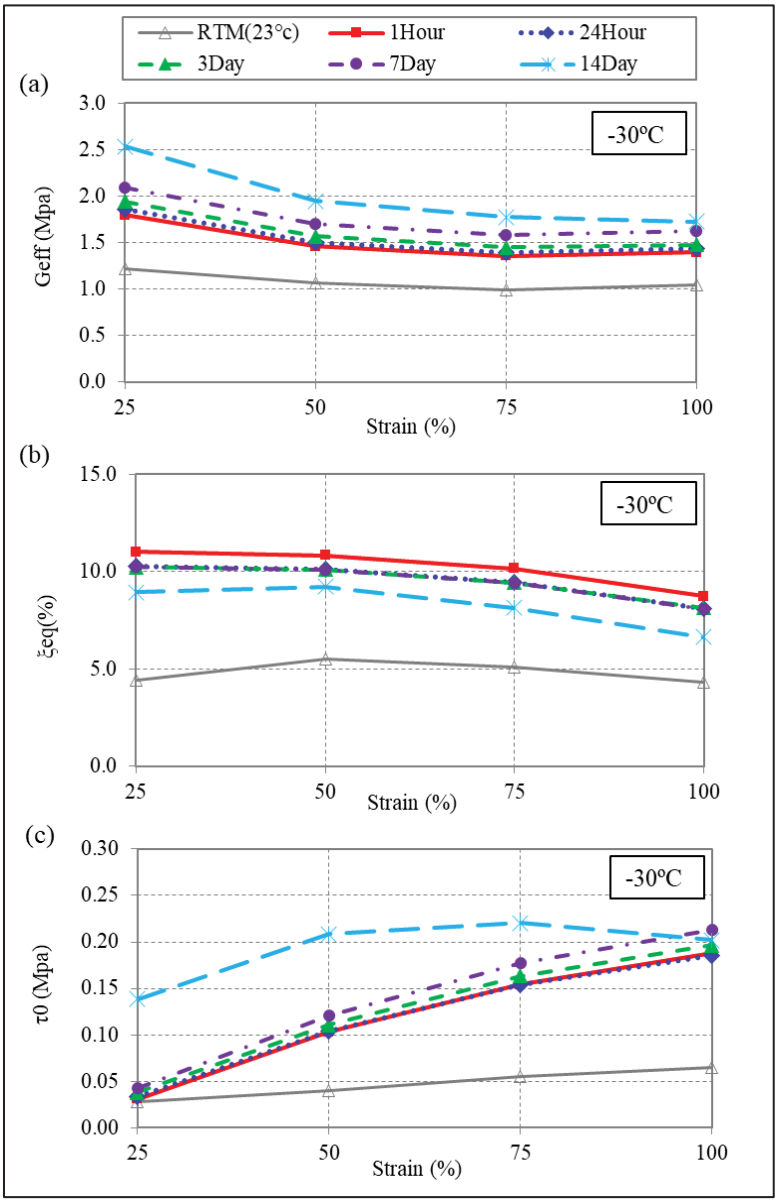

Figure 3.19 Cold conditioning time effect on (a) shear modulus, (b) damping ratio, and (c) stress at zero strain of natural rubber Series 3 (CHB D.28) at -30ºC

3.6 Mechanical characteristics of natural rubber, Series4 (Scougal)

3.6.1 Influence of cold conditioning time on stress-strain relationship

Stress-strain relationship of natural rubber Series 4 at room temperature 23ºC as well as low temperature -8ºC for different conditioning time, ranging from 1 hour to 28 days, and various strain levels is shown in Figure 3.20. The hysteresis curve associated with 1 hour of conditioning time at -8ºC indicates an increase in the enclosed area of hysteresis curve and maximum stress compared to room temperature. For example, natural rubber Series 4 at 100% strain experienced approximately a 7% increase in the maximum stress after 1 hour of cold conditioning at -8ºC, compared to room temperature. Increasing the maximum stress and enclosed area of the hysteresis curve after 1 hour of cold conditioning at -8°C is observed in other Series tested in this study. This phenomenon is attributed to the instantaneous stiffening of natural rubber, and the results are consistent with findings from previous experimental studies, particularly those conducted by Ankik in 2019. Extending the conditioning period from 1 hour to 1 day results in an insignificant increase in maximum stress. Additionally, with a further increase in conditioning time, the maximum stress during the third cycle at 100% strain rises by approximately 3% when the conditioning time increases from 1 day to 3 days, similarly, by approximately 3% when it increases from 3 days to 14 days, and by approximately 1% when it increases from 14 days to 28 days. Likewise, approximately similar behaviour in the stress level of new samples during the cold conditioning period at -8°C was noted in previous experiments conducted by Ankik in 2019.

Figure 3.21 shows hysteresis responses of natural rubber Series 4 at -30°C. Findings indicate that rubber Series 4 demonstrates significant elevations in stress levels and the enclosed area of the hysteresis curve compared to those observed at 23°C and -8°C. For instance, exposure to -30°C for 1 hour led to an approximately 32% increase in maximum stress at the 100% strain level compared to stress levels observed at 23°C. Moreover, extending the conditioning time from 1 hour to 14 days results in notable increases in both maximum stress and the enclosed area of the hysteresis curve. As an example, maximum stress at 100% strain increases by

approximately 3% when the conditioning time extends from 1 hour to 1 day, by approximately 7% from 1 day to 3 days, by approximately 12% from 3 days to 7 days, and by approximately 23% from 7 days to 14 days. Additionally, rubber Series 4 experiences about 2% increase when the conditioning time extends from 14 days to 28 days, indicating that the most significant increase in stress occurred between 7 days and 14 days of cold conditioning at -30°C.

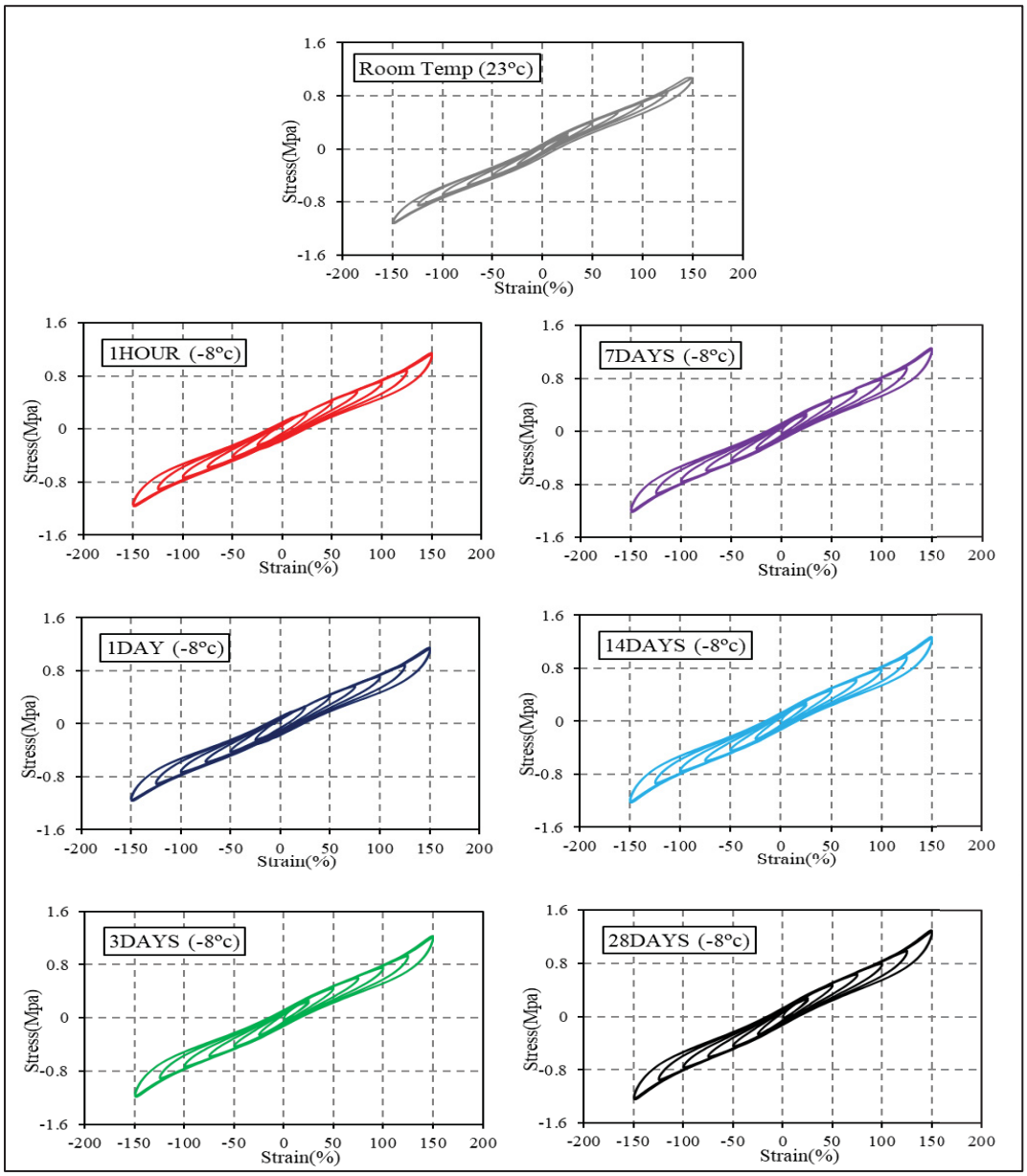

Figure 3.20 Stress-strain relationship of natural rubber Series 4, at room temp and -8ºC for different conditioning times ranging from 1 hour to 28 day

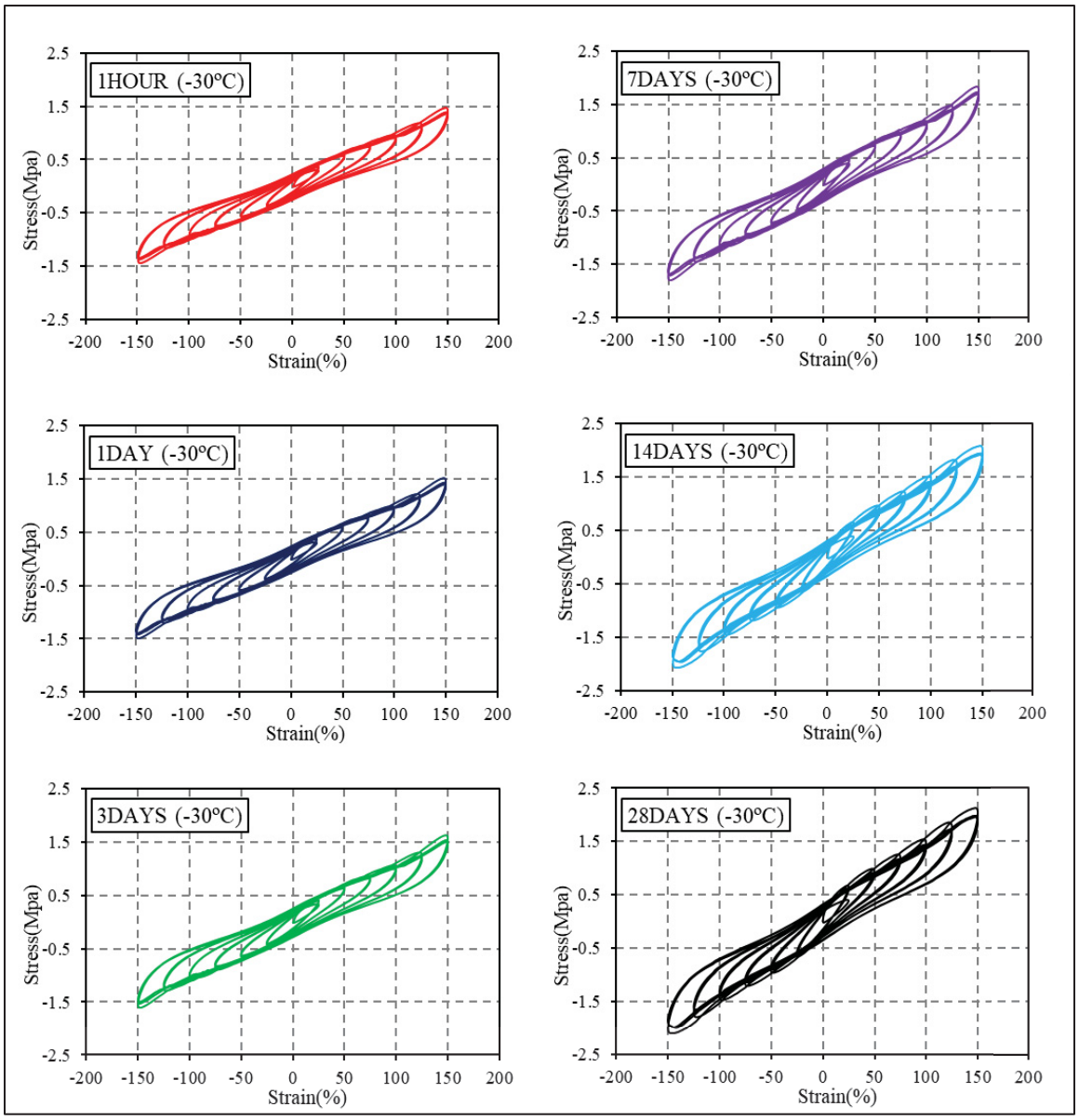

Figure 3.21 Stress-strain relationship of natural rubber Series 4, at -30ºC for different conditioning times ranging from 1 hour to 28 days

Overall, maximum stress increases by 54% when the conditioning time extends from 1 hour to 28 days, implying the occurrence of the crystallization phenomenon. These results are consistent with previous experiments, notably those conducted by Ankik in 2019, wherein new samples exposed to -30°C exhibited a similar percentage increase in stress levels across various cold conditioning periods ranging from 1 hour to 14 days.

3.6.2 Effect of cold conditioning time on shear modulus, damping, and τ_0

Figure 3.22(a) shows how the effective shear modulus (G_{eff}) of natural rubber Series 4 varies with strain levels at -8°C under different conditioning durations. It is observed that for conditioning durations ranging from 1 hour to 1 day, G_{eff} remains practically unchanged for the various deformation levels considered. However, extending the conditioning time from 1 day to 3 days results in an average increase of 4% in G_{eff} for different strain levels. Subsequently, between 3 days and 14 days of conditioning, G_{eff} increases by approximately 3% on average.

Figure 3.23(a) presents the variation of G_{eff} for natural rubber Series 4 in relation to strain levels for various conditioning durations at -30°C. The results indicate a 3% increase in G_{eff} between 1 hour and 1 day of conditioning. However, extending the conditioning period from 1 day to 28 days shows a progressive rise in G_{eff}. Specifically, at 100% deformation, G_{eff} increases by about 7% between 1 day and 3 days, followed by a 35% increase between 3 days and 14 days. Additionally, for longer conditioning periods, there is an approximately 3% increase in G_{eff} as the conditioning time extends from 14 days to 28 days.

The findings at both -8°C and -30°C temperatures indicate that G_{eff} exhibits a decrease with increasing strain levels up to 100%, followed by a slight increase between 125% to 150% strain. For instance, when the strain rises from 25% to 100%, G_{eff} decreases by approximately 28% at -8°C and approximately 40% at -30°C. However, there is an increase in G_{eff}, by approximately 8% at -8°C and 2% at -30°C, when the strain level increases from 125% to 150%. This observed increase in G_{eff}, as discussed in earlier sections, is likely attributable to the stiffening of the elastomer at larger deformations, as reported in previous studies (Ankik, 2019; Clark, 1996).

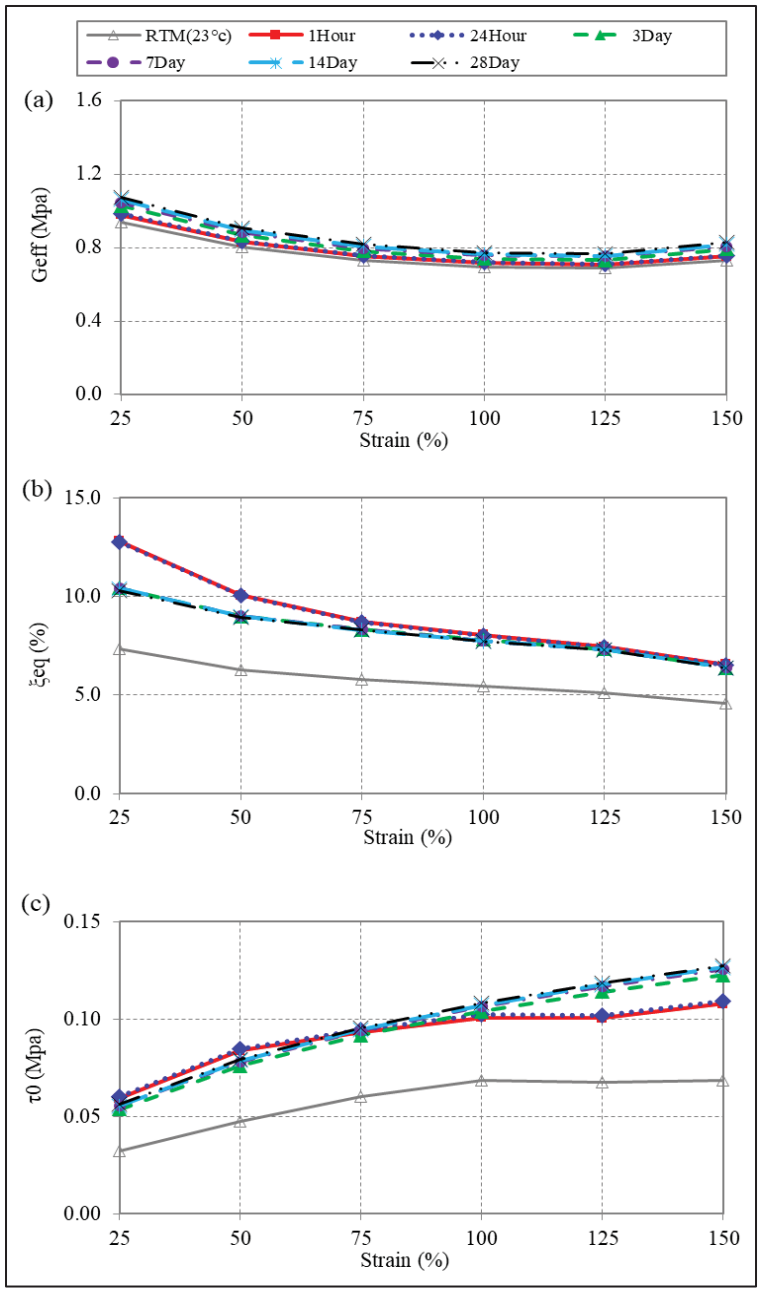

Figure 3.22 Cold conditioning time effect on (a) shear modulus, (b) damping ratio, and (c) stress at zero strain of natural rubber Series 4 (Scougal), at -8ºC

Figure 3.22(b) illustrates the variation of the equivalent damping ratio (ξ_{eq}) of natural rubber Series 4 as a function of strain level at temperatures of -8°C for different conditioning times. It is observed that regardless of small deformation ranging from 25 to 50%, there is no

significant difference in the ξ_{eq} when the cold conditioning duration is extended from 1 hour to 14 days, indicating that the equivalent damping ratio has low sensitivity to conditioning duration. The results suggest that by increasing the strain level from 25 to 150%, ξ_{eq} significantly decreases for all conditioning time ranging from 1 hour to 28 days. For example, when strain level rises from 25 to 75%, ξ_{eq} decreases by approximately 32% for conditioning time between 1 hour to 24 hours and by 20% for conditioning time between 3 days to 28 days. Also, when the strain level rises from 75 to 150%, ξ_{eq} decreases by approximately 24% for all conditioning time ranging from 1 hour to 28 days. In Figure 3.23(b), the variation of the ξ_{eq} as a function of strain level at temperatures of -30°C for different conditioning times is shown. The results indicate that ξ_{eq} varies only slightly with the conditioning duration. However, for the conditioning duration of 14 days and 28 days, a decrease in ξ_{eq} is observed. This is because the increase in the energy dissipated per cycle is less than the increase in the effective shear modulus. Reduction in damping ratio for the 14 days conditioning at -30ºC was also observed in previous experiments conducted by Ankik in 2019. Additionally, when the strain level increases from 25 to 150%, ξ_{eq} decreases by approximately between 30% to 25%.

In Figure 3.22 (c), the variation of the stress at zero strain (τ_0) is presented as a function of overall shear strain level for different conditioning durations at -8°C. The results show a slight increase in τ_0 with longer conditioning durations. For instance, at 100% strain, τ_0 increases by approximately 3% from 1 hour to 3 days, another 3% from 3 days to 7 days, and then by 2% from 7 days to 28 days. When examining the variation of τ_0 with respect to changes in overall shear strain levels, it is observed that τ_0 gradually increases as the overall strain level increases. For instance, when the deformation level increases from 25 to 150%, τ_0 increases by 82% to 127% for short conditioning times (ranging from 1 hour to 24 hours) and long conditioning times (from 1 day to 28 days), respectively. Figure 3.23 (c) depicts the variation of τ_0 at -30ºC. It is evident that between conditioning times of 1 hour and 24 hours, the variation in τ_0 is negligible. However, for longer conditioning durations, τ_0 gradually increases. For example, at 100% strain, τ_0 increases by 7% between 24 hours and 3 days, by 16% between 3 days and 7 days, by 8% between 7 days and 14 days, and finally by 3% between 14 days and 28 days.

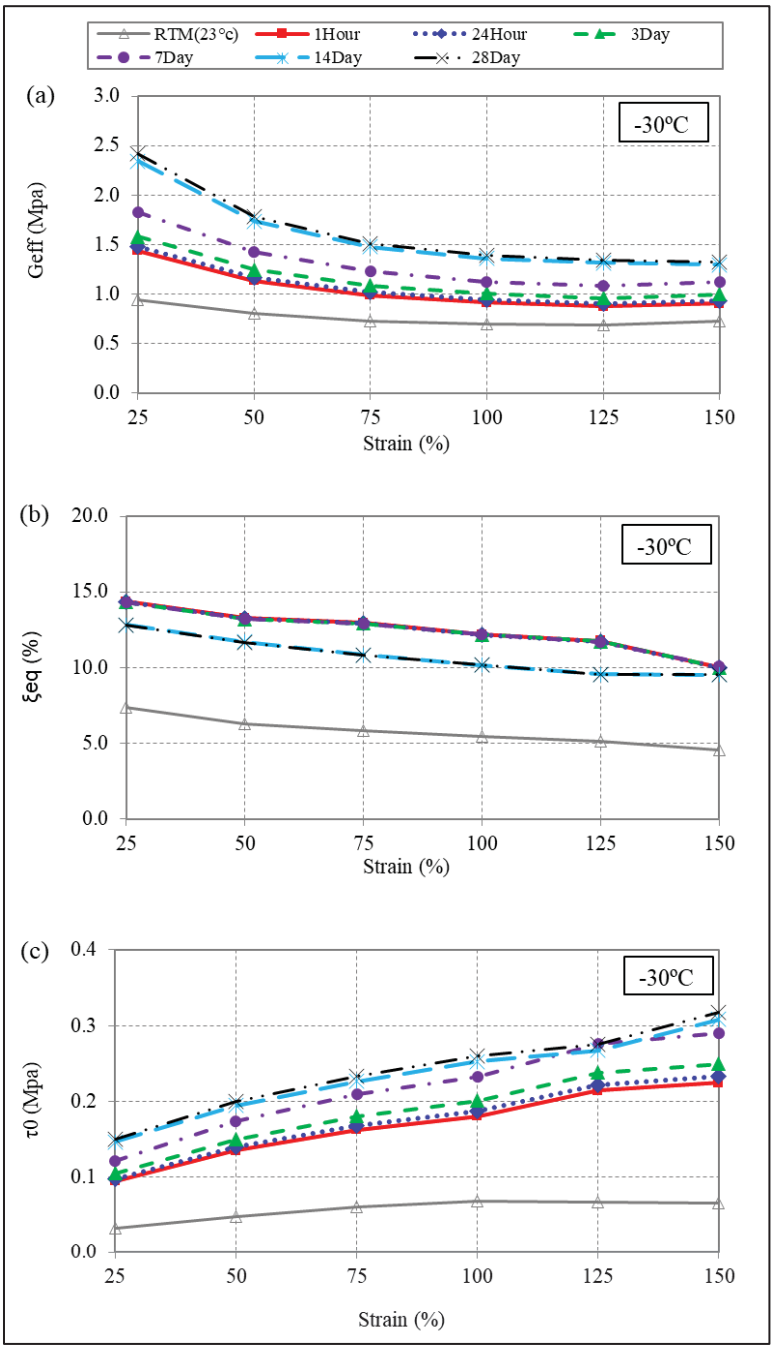

Figure 3.23 Cold conditioning time effect on (a) shear modulus, (b) damping ratio, and (c) stress at zero strain of natural rubber Series 4 (Scougal), at -30ºC

3.7 Crystallization

Figure 3.24 shows the normalized shear modulus curves of Series 1 to Series 4 at temperatures of -30°C as a function of conditioning duration for 100% strain amplitudes. In this figure, the conditioning time is provided in hours and plotted on a logarithmic scale to better visualize the progress of the crystallization over time. The normalized shear modulus at -30°C shows that for all Series, natural rubber stiffens instantly, at approximately 1 hour of cold conditioning. Between 1 hour and 24 hours of conditioning, the normalized shear modulus remains practically unchanged. However, as the conditioning duration increases from 24 hours to 14 days (336 hours), the normalized shear modulus gradually increases, indicating that the crystallization occurred. Table 3.1 presents the values of the normalized shear modulus at different conditioning times for Series 1 to Series 4. These results are consistent with the results reported by previous studies (Fuller et al., 2004; Ankik, 2019), indicating that the maximum speed of crystallization for natural rubber occurs around -25°C, a temperature close to the -30°C used in this study.

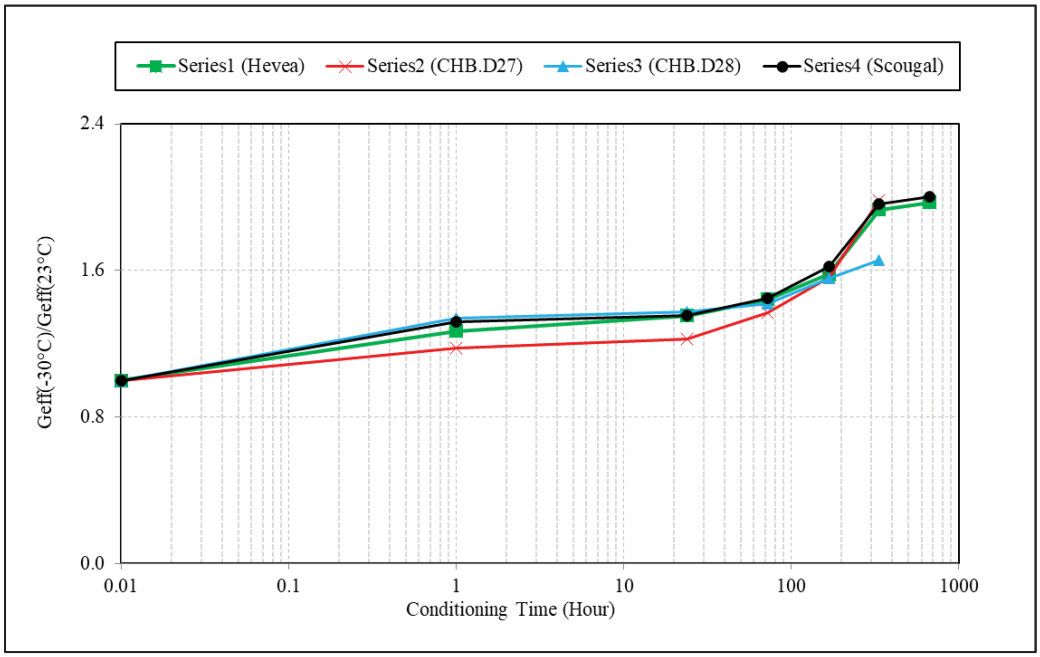

Figure 3.24 Crystallization curves for Series 1 to Series 4 at 100% strain amplitude, at -30°C

Table 3.1 Normalized shear modulus of Series1 to Series4, for 100%strain, at -30°C

Series	$G_{eff}(-30°C)/G_{eff}(23°C)$, 100%					
	1 Hour	24 Hours	72 Hours (3 days)	168 Hours (7 days)	336 Hours (14 days)	672 Hours (28 days)
Series1 (Hevea)	1.269	1.352	1.443	1.579	1.931	1.973
Series2 (CHB.D27)	1.178	1.227	1.371	1.565	1.984	-
Series3 (CHB.D28)	1.337	1.375	1.417	1.559	1.656	-
Series4 (Scougal)	1.319	1.357	1.448	1.622	1.961	2.001
Average	1.276	1.328	1.420	1.581	1.883	1.987

CHAPITRE 4

VARIABILITY IN THE MECHANICAL PROPERTIES OF NATURAL RUBBER AT LOW TEMPERATURES, AFFECTED BY LOAD FREQUENCY AND SUPPLIERS IN QUEBEC

4.1 Introduction

In this chapter, statistical analysis is employed to evaluate the variation in the mechanical properties of natural rubber as a function of strain amplitude for different temperatures and cold conditioning times affected by different suppliers in Quebec. The probability distribution functions are also used to characterize the distribution of the shear modulus of natural rubber for different suppliers at room temperature (23ºC) and low temperatures (-8ºC & -30ºC). Subsequently, statistical tests are utilized to validate the probability distribution functions. Additionally, the effect of loading frequency on mechanical properties at different strain amplitudes considering cold-time conditioning is investigated.

4.2 Variation in mechanical properties of natural rubber affected by load frequency at low temperatures

Figure 4.1 presents the effect of different load frequencies on the variation of shear modulus (G_{eff}) as a function of strain levels for two sources of natural rubber, Series 2 (Champlain Bridge D.27) represents aged rubber and Series 4 (Scougal) represent new rubber, at low temperatures (-8ºC & -30ºC). Test results reveal that by increasing frequency from 0.01 Hz to 0.25Hz at -8ºC, shear modulus at 100% strain increases by approximately 1% for Series 2 and by approximately 2% for Series 4, and it increases by approximately 2% for Series 4 when load frequency increase from 0.25 Hz to 0.5 Hz. Moreover, at -30ºC, by increasing frequency from 0.01 Hz to 0.25Hz, shear modulus at 100% strain increases by approximately 1% for Series 2 and by approximately 1% for Series 4, and it increases by approximately 3% for Series 4 when load frequency increases from 0.25 Hz to 0.5 Hz. These results indicate that changing the load frequency from 0.1Hz to 0.25Hz and 0.5Hz has an insignificant impact on the shear

modulus of rubber at temperatures of -8ºC and -30ºC. This finding is consistent with the other studies conducted by Constantinou et al. (2007) and Nobari Azar et al. (2022), which conclude that load frequency or testing velocity has an insignificant impact on shear modulus.

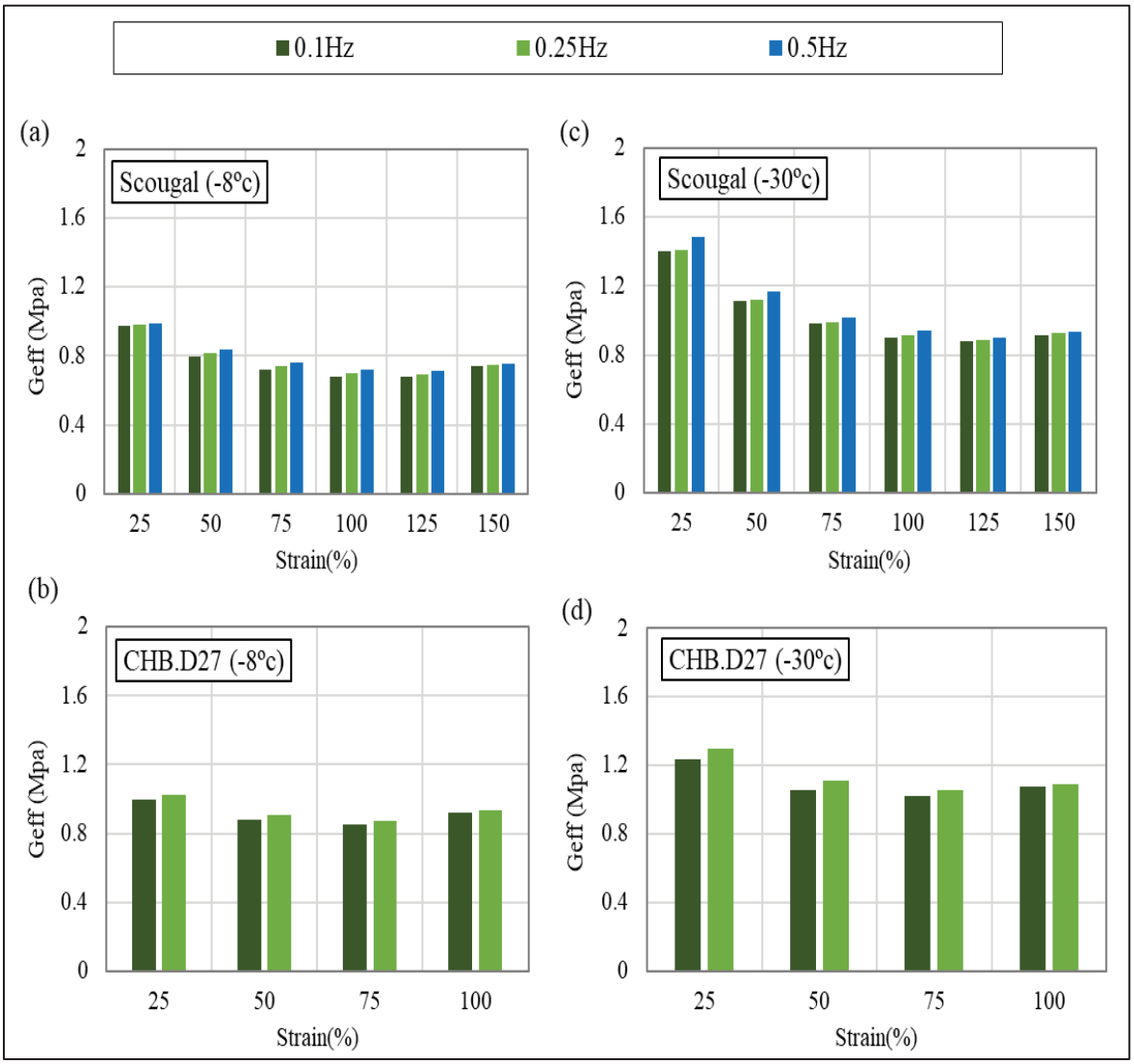

Figure 4.1 Variation in shear modulus of Series4 (Scougal) & Series2 (CHB D.27) at -8ºC & -30ºC, impacted by different frequencies

4.3 Variation in mechanical properties of natural rubber affected by different suppliers

4.3.1 Statistical analysis of the variation of the shear modulus

Figure 4.2 (a) presents the variation of shear modulus among four different bridge-bearing suppliers in Quebec: Series 1 (Hevea), Series 2 (Champlain Bridge batch D4.27), Series 3 (Champlain Bridge batch D4.28), and Series 4 (Scougal), These results are obtained at room temperature (23°C) for strain amplitudes ranging from 25% to 150%. Notably, Series 3 exhibits the highest shear modulus, indicating its stiffness relative to the others. This aligns with the fact that Series 3 represents the oldest rubber among the specified Series, resulting in the highest level of shear modulus, as anticipated. Conversely, Series 4 (Scougal), characterized by new rubber, displays the lowest shear modulus among the specified Series. This observation corresponds to the stiffness difference between aged and new rubber, with new rubber typically demonstrating a lower shear modulus. Figures 4.2(b) and (c) present the variation of the equivalent damping ratio (ξ_{eq}) and the stress at zero strain (τ_0) among Series 1 to Series 4 at 23ºC, respectively. It is evident that Series 1 and Series 4 (Scougal and Hevea) exhibit the highest level of damping. Concerning τ_0, the results are nearly close however, Series 1 demonstrates the highest, while Series 3 shows the lowest stress at zero strain. Moreover, in order to assess the variation in mechanical properties within each Series, we compared the shear modulus of samples of each Series at 23ºC. For instance, the shear modulus at 100% strain for Series 1 (Hevea) varies by approximately 3% among the samples, while for Series 4 (Scougal), it varies by less than 4%. Our findings indicate that there is no significant difference in the shear modulus among the samples at 23ºC.

Table 4.1 presents the mechanical properties of Series 1 to 4 for 100% strain at room temperature, including equivalent damping ratio (ξ_{eq}) which varies between 4.25< (ξ_{eq}) <6.14 among Series 1 to 4, stress at zero strain (τ_0) which varies between 0.064< (τ_0) <0.081, and most importantly shear modulus (G_{eff}). To delve into the variation of G_{eff},

Table 4.2 is provided. This table presents the variation of shear modulus among Series 1 to 4 for different strain levels at room temperature (23ºC). As indicated, shear modulus (G_{eff}) for 100% strain varies between 0.69<G_{eff}<1.04. Additionally, Table 4.2 presents statistical analysis, including the ANOVA (analysis of variance) test, to assess whether there are statistical differences among Series1 (Hevea), Series2 (CHB D.27), Series3 (CHB.D28), and Series4 (Scougal).

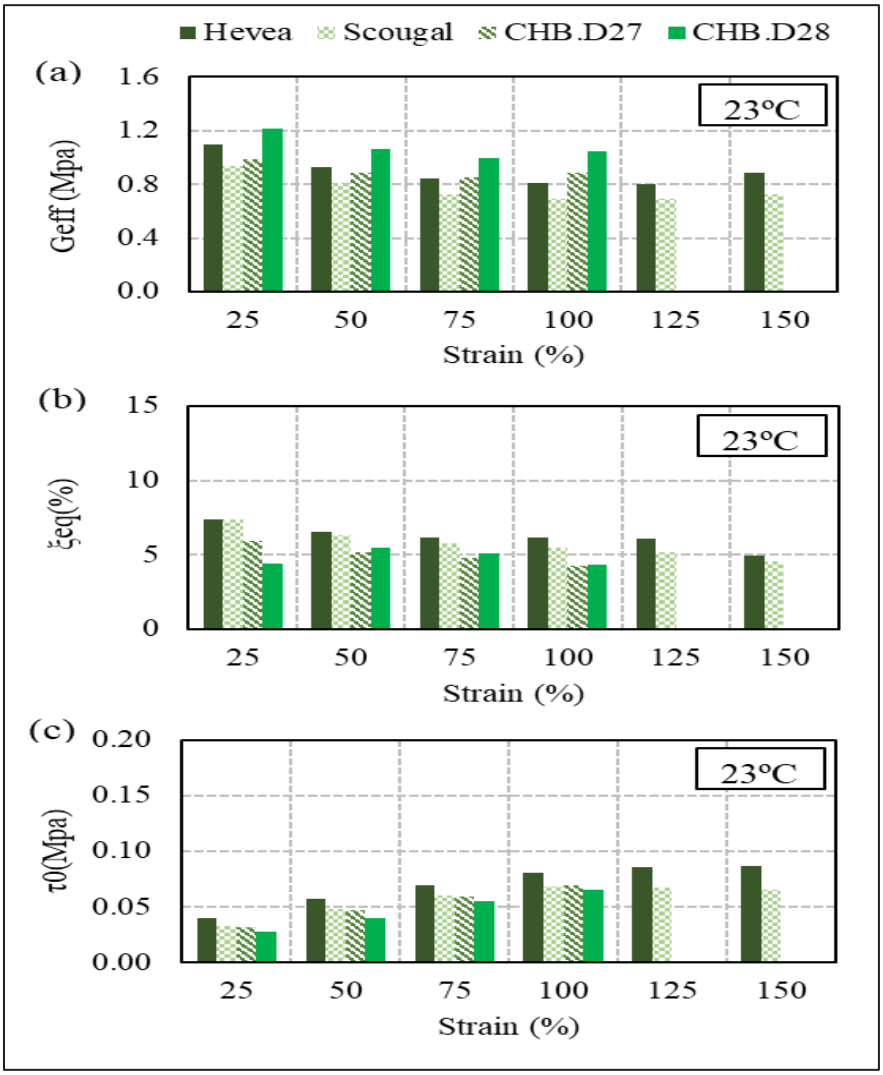

Figure 4.2 Variation in (a) effective shear modulus, (b) equivalent damping ratio, and (c) stress at zero strain of natural rubber manufactured by different suppliers at (23ºC)

Table 4.1 Mechanical Properties of Series 1 to 4 at 23ºC, 100% Strain

Room Temp (23ºC)	Mechanical Properties at *100%* Strain						
	Series 1 (Hevea)	Series 2 (CHB.D27)	Series 3 (CHB.D28)	Series 4 (Scougal)	Mean	SD	CV
G_{eff} (MPa)	0.808	0.885	1.0422	0.694	0.857	0.127	0.148
ξ_{eq} (%)	6.138 %	4.260 %	4.334 %	5.458 %	5.05 %	0.788%	0.156
τ_0 (MPa)	0.081	0.069	0.0650	0.069	0.071	0.006	0.086

Table 4.2 Statistical analysis of G_{eff} at room temperature (23ºC) among Series 1 to 4

Strain level %	G_{eff} (MPa)				ANOVA Test		
	Range (MPa)	Mean	SD	CV	F-critical	F-statistic	P-value
25	$0.937 \leq G_{eff} \leq 1.217$	1.061	0.108	0.102	≈ 3.24	≈ 8.93	≈ 0.00
50	$0.801 \leq G_{eff} \leq 1.065$	0.921	0.095	0.103			
75	$0.729 \leq G_{eff} \leq 0.994$	0.856	0.094	0.110			
100	$0.694 \leq G_{eff} \leq 1.042$	0.857	0.127	0.148			
125	$0.690 \leq G_{eff} \leq 0.805$	0.747	0.058	0.077			
150	$0.728 \leq G_{eff} \leq 0.886$	0.807	0.079	0.098			
Average			0.093	0.106			

ANOVA compares the means of the Series and classifies the total observed variance into variation between groups and variation within groups. It evaluates the null hypothesis against the alternative hypothesis, yielding the P-value and the F-statistic as results. The null hypothesis typically states that there is no effect, no difference, or no relationship between variables, suggesting that any observed differences or effects in the data are due to random variation or chance. If the p-value is less than the chosen significance level, typically 0.05, it indicates that the observed result is statistically significant. In other words, there is strong evidence against the null hypothesis, leading to its rejection in favor of the alternative

hypothesis. Extremely small p-values, also, indicate very strong evidence against the null hypothesis, suggesting that the observed effect, difference, or relationship in the data is unlikely to have arisen by chance alone. Conversely, larger p-values ($p > 0.05$) indicate weaker evidence against the null hypothesis and fail to provide strong support for rejecting the null hypothesis. As for the F-statistic, also known as the F-ratio, If the obtained F-statistic is greater than the critical value (F-statistic > F-critical), the null hypothesis is rejected. This indicates that at least one group's mean significantly differs from the others. On the other hand, if the obtained F-statistic is not greater than the critical value (F-statistic ≤ F-critical), the rejection of the null hypothesis fails, suggesting insufficient evidence to conclude significant differences among the group means (Rutherford, 2012). As indicated in Table 4.2, the P-value is less than the significance level of 0.05 (extremely small ≈0). The F-statistic is higher than F-critical values (F-statistic 175 > 3.24 F-critical), suggesting that the observed differences in the means of the groups (G_{eff} for Series 1 to 4 at room temperature) are statistically significant, and they are unlikely to have arisen due to random variation.

In Figures 4.3 & 4.4, the variation of shear modulus for each supplier and different conditioning time as a function of strain amplitude at -8ºC and -30ºC is shown, respectively. At -8ºC, similar to 23ºC, Series 3 (CHB D.28) exhibits the highest level of G_{eff}, while Series 4 (Scougal) shows the lowest G_{eff}. Moreover, the highest value of G_{eff} for each Series is observed after the longest conditioning time. Regarding comparison at -30ºC, Series 2 and Series 3, representing aged rubber subjected to harsh environments, exhibit lower G_{eff} values at small strain amplitudes (ranging from 25% to 50%) compared to Series1 (Hevea; aged at room temperature) and Series4 (Scougal; new), respectively. Interestingly, despite Series 2 and Series 3 showing higher G_{eff} values for all strain amplitudes at -8ºC, they exhibit lower values for small strain amplitudes (ranging from 25% to 50%) at -30ºC compared to the other Series. This observation suggests that aged rubber may have reduced sensitivity to temperatures of -30ºC for small strain amplitudes (ranging from 25% to 50%) compared to new materials. However, Series 3 (CHB D.28) and Series 2 (CHB D.27) exhibit higher G_{eff} values at 100%

strain amplitude for all conditioning times ranging from 1 hour to 14 days, compared to the other Series.

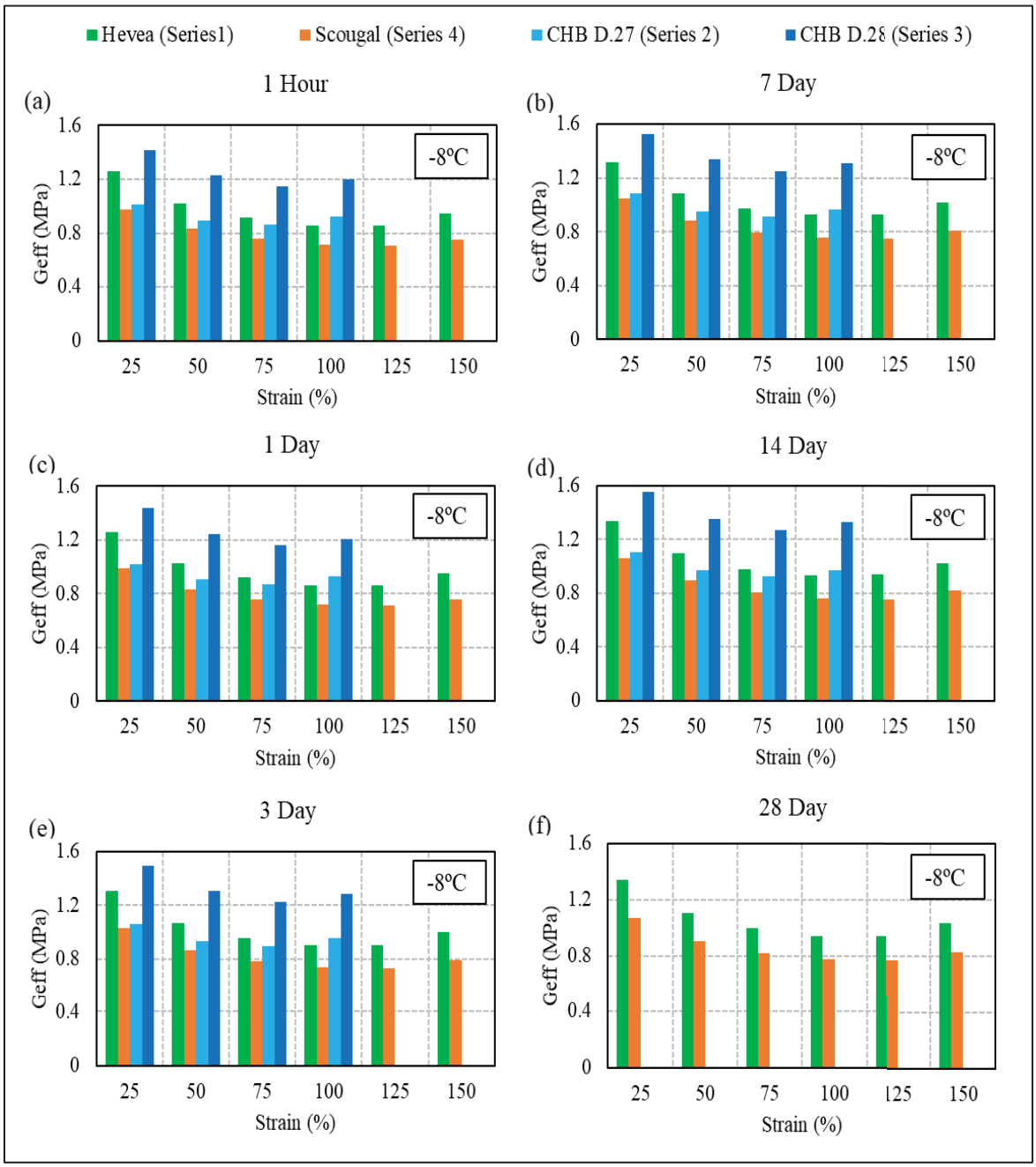

Figure 4.3 Variation in effective shear modulus of natural rubber manufactured by different suppliers under time conditioning, ranging from (a) 1 hour to (f) 28 days, at -8ºC

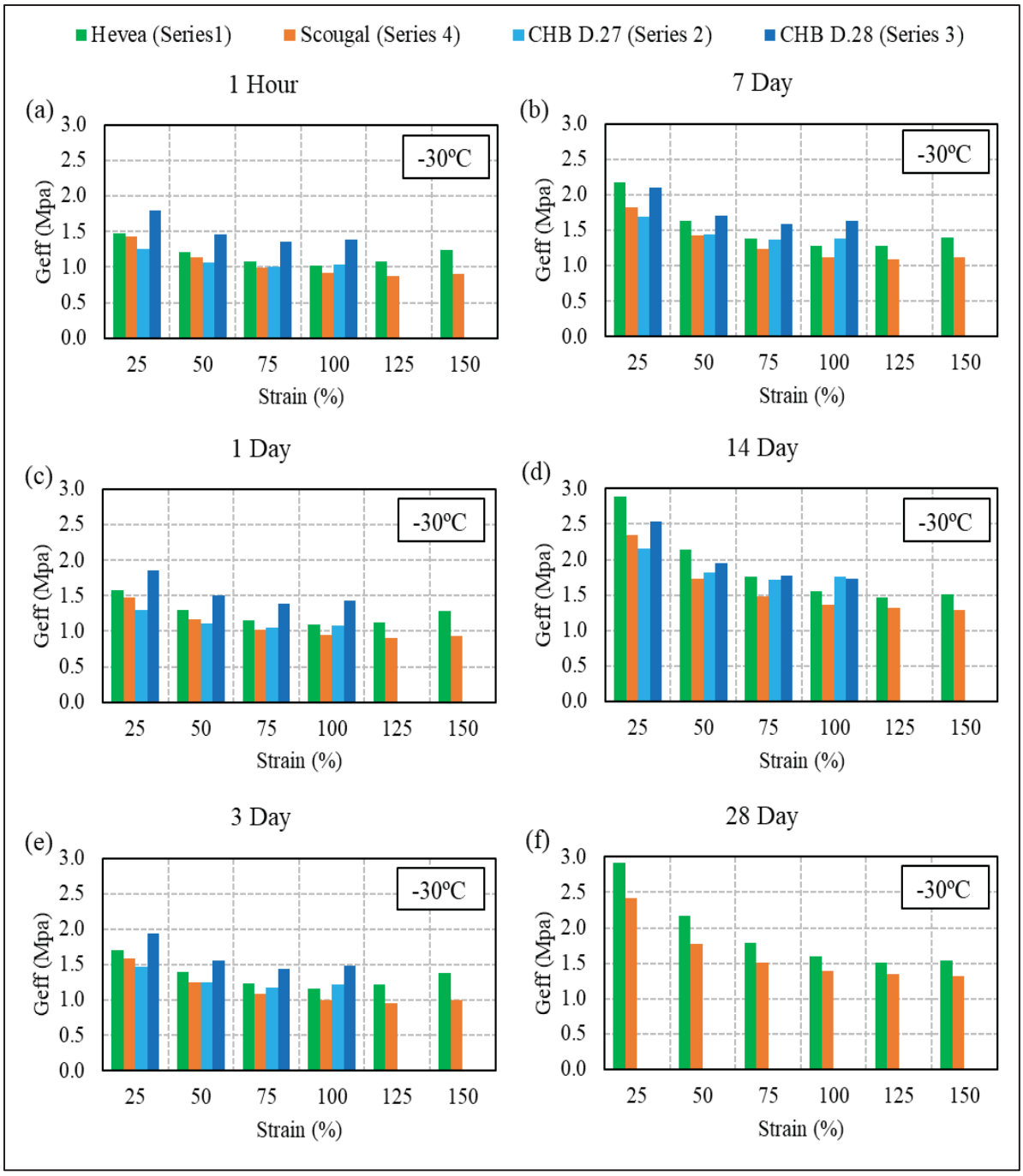

Figure 4.4 Variation in effective shear modulus of natural rubber manufactured by different suppliers under time conditioning ranging from (a) 1 hour to (f) 28 days, at -30ºC

Tables 4.3 & 4.4 present the statistical analysis of G_{eff} at 100% strain among Series 1 to 4 at -8ºC and -30ºC, respectively. As indicated, the P-value is less than the significance level 0.05

(extremely small (≈0) and small (≈0.025) for -8ºC and -30ºC, respectively), and the F-statistic is higher than F-critical values at both -8ºC (F-statistic 175 > 3.24 F-critical) and -30ºC (F-statistic 4 > 3.24 F-critical). This suggests that the observed differences in the means of Series 1 to 4, considering the different cold conditioning periods, are statistically significant and unlikely to have arisen due to random variation.

Table 4.3 Statistical analysis of G_{eff} at 100% strain at -8ºC among Series 1 to 4

Duration at -8ºC	G_{eff} (MPa), *100%*				ANOVA Test		
	Range (MPa)	Mean	SD	CV	F-critical	F-statistic	P-value
1 Hour	$0.716 \leq G_{eff}^{100\%} \leq 1.200$	0.925	0.175	0.190	≈ 3.24	≈ 175	≈ 0.00
24 Hour	$0.717 \leq G_{eff}^{100\%} \leq 1.208$	0.930	0.177	0.191			
3 Days	$0.738 \leq G_{eff}^{100\%} \leq 1.285$	0.970	0.198	0.204			
7 Days	$0.759 \leq G_{eff}^{100\%} \leq 1.310$	0.991	0.200	0.202			
14 Days	$0.762 \leq G_{eff}^{100\%} \leq 1.327$	0.997	0.205	0.206			
Average			0.192	0.199			

Table 4.4 Statistical analysis of G_{eff} at 100% strain at -30ºC among Series 1 to 4

Duration at -30ºC	G_{eff} (MPa), *100%*				ANOVA Test		
	Range (MPa)	Mean	SD	CV	F-critical	F-statistic	P-value
1 Hour	$0.916 \leq G_{eff}^{100\%} \leq 1.394$	1.094	0.179	0.164	≈3.2	≈ 4.01	≈ 0.02
24 Hour	$0.942 \leq G_{eff}^{100\%} \leq 1.433$	1.138	0.180	0.158			
3 Days	$1.006 \leq G_{eff}^{100\%} \leq 1.477$	1.215	0.169	0.139			
7 Days	$1.126 \leq G_{eff}^{100\%} \leq 1.625$	1.352	0.181	0.134			
14 Days	$1.361 \leq G_{eff}^{100\%} \leq 1.726$	1.600	0.157	0.098			
Average			0.174	0.139			

4.3.2 Statistical analysis of the variation of the equivalent damping

In Figures 4.5 & 4.6, variations of equivalent damping ratio for different suppliers and different conditioning time as a function of strain amplitude at temperatures of -8ºC and -30ºC are shown, respectively. At -8ºC, Series 4 (Scougal) exhibits the highest equivalent damping values among all Series, except during short conditioning times (1 hour and 24 hours) in which Series1 (Hevea) shows the higher damping for large displacement (100 to 125% strain). Specifically, the damping ratio for Series4 at 100% strain varies between 7.71% $< \xi_{eq} <$ 8% among different conditioning time. Series1, also, shows a damping ratio between 7.04% $< \xi_{eq} <$ 8.47% at 100% strain. Series 2 & Series 3, show approximately the same ξ_{eq} for all conditioning time and all the strain levels except 25% strain, wherein Series 2 shows the higher damping. The damping ratio of Series 2 & Series 3 at 100% strain, among different conditioning time, vary between 5.48% $< G_{eff} <$ 5.19% & 5.64 % $< G_{eff} <$ 4.97%, respectively.

Despite Series 4 showing the highest ξ_{eq} at -8ºC, it is Series 1 (Hevea) that demonstrates the highest ξ_{eq} among all Series at -30ºC. This suggests that, in terms of damping, different rubbers may exhibit varying sensitivity and performance at low temperatures. Specifically, the damping ratio of Series 1 & Series 4 at -30ºC and at 100% strain, among different conditioning time, vary between 13.38% $< \xi_{eq} <$ 14.6% and 10.15% $< \xi_{eq} <$ 12.16%, respectively. Additionally, ξ_{eq} for Series 2 & Series 3 at -30ºC and at 100% strain, among different conditioning time, vary between 6.86% $< \xi_{eq} <$ 7.42 and 8.08% $< \xi_{eq} <$ 8.71%, respectively. Tables 4.5 & 4.6 present the variation of ξ_{eq} at 100% strain and statistical analysis including standard deviation and coefficient of variation among all Series for different conditioning time.

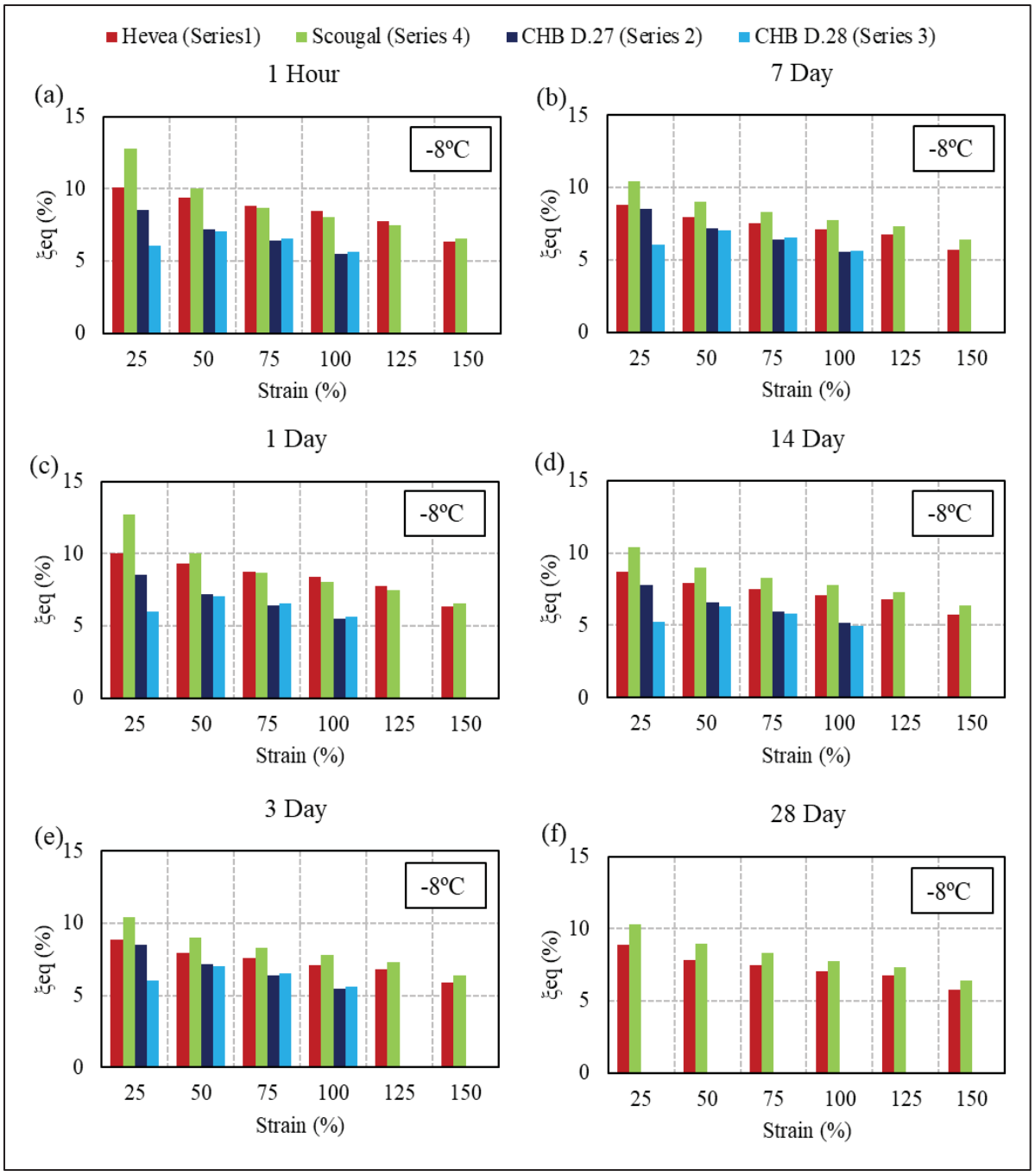

Figure 4.5 Variation in equivalent damping ratio of natural rubber manufactured by different suppliers under time conditioning ranging from (a) 1 hour to (f) 28 days, at -8ºC

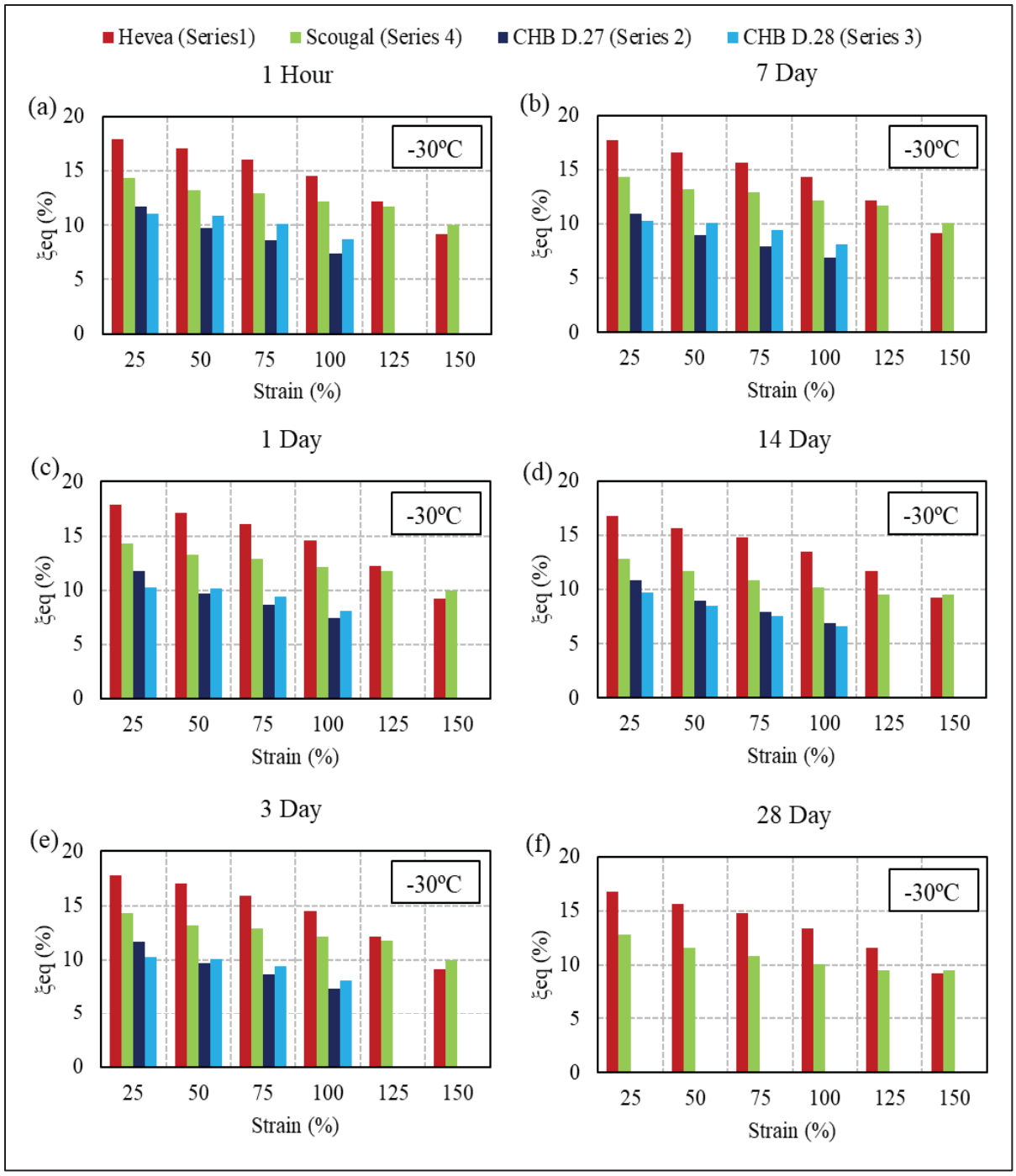

Figure 4.6 Variation in equivalent damping ratio of natural rubber manufactured by different suppliers under time conditioning ranging from (a) 1 hour to (f) 28 days, at -30ºC

Table 4.5 Statistical analysis of ξ_{eq} at 100% strain at -8ºC among Series 1 to 4

Duration at -8ºC	ξ_{eq}, *100%*			
	Range	Mean	SD	CV
1 Hour	5.5 % ≤$\xi_{eq}^{100\%}$≤ 8.5 %	6.9 %	1.357 %	0.196
24 Hour	5.5 % ≤$\xi_{eq}^{100\%}$≤ 8.4 %	6.9 %	1.340 %	0.194
3 Days	5.5 % ≤$\xi_{eq}^{100\%}$≤ 7.8 %	6.5 %	0.993 %	0.152
7 Days	5.5 % ≤$\xi_{eq}^{100\%}$≤ 7.8 %	6.5 %	0.969 %	0.149
14 Days	5.0 % ≤$\xi_{eq}^{100\%}$≤ 7.8 %	6.2 %	1.188 %	0.190
Average			1.169 %	0.176

Table 4.6 Statistical analysis of ξ_{eq} at 100% strain at -30ºC among Series 1 to 4

Duration at -30ºC	ξ_{eq}, 100%			
	Range	Mean	SD	CV
1 Hour	7.4 % ≤$\xi_{eq}^{100\%}$≤ 14.5 %	10.706 %	2.800 %	0.262
24 Hour	7.4 % ≤$\xi_{eq}^{100\%}$≤ 14.6 %	10.565 %	2.968 %	0.281
3 Days	7.4 % ≤$\xi_{eq}^{100\%}$≤ 14.5 %	10.542 %	2.903 %	0.275
7 Days	6.9 % ≤$\xi_{eq}^{100\%}$≤ 14.3 %	10.359 %	3.004 %	0.290
14 Days	6.9 % ≤$\xi_{eq}^{100\%}$≤ 13.4 %	9.280 %	2.784 %	0.300
Average			2.892 %	0.282

4.3.3 Statistical analysis of the variation of the τ_0

Figures 4.7 & 4.8 present the variations of stress at zero strain (τ_0) for different suppliers and conditioning times as a function of strain amplitude at temperatures of -8ºC and -30ºC, respectively. Among all sources, Series 1 consistently exhibits the highest τ_0 values for nearly all conditioning times at both -8ºC and -30ºC temperatures. At -8ºC, τ_0 varies slightly within Series 2 to 4, specifically at 100% strain. At -30ºC, τ_0 for Series 3 and 4 also shows slight

variation, while for Series 2, τ_0 shows lower values than the other Series. Tables 4.7 & 4.8 present the variation of ξ_{eq} at 100% strain and statistical analysis among all Series for different conditioning time.

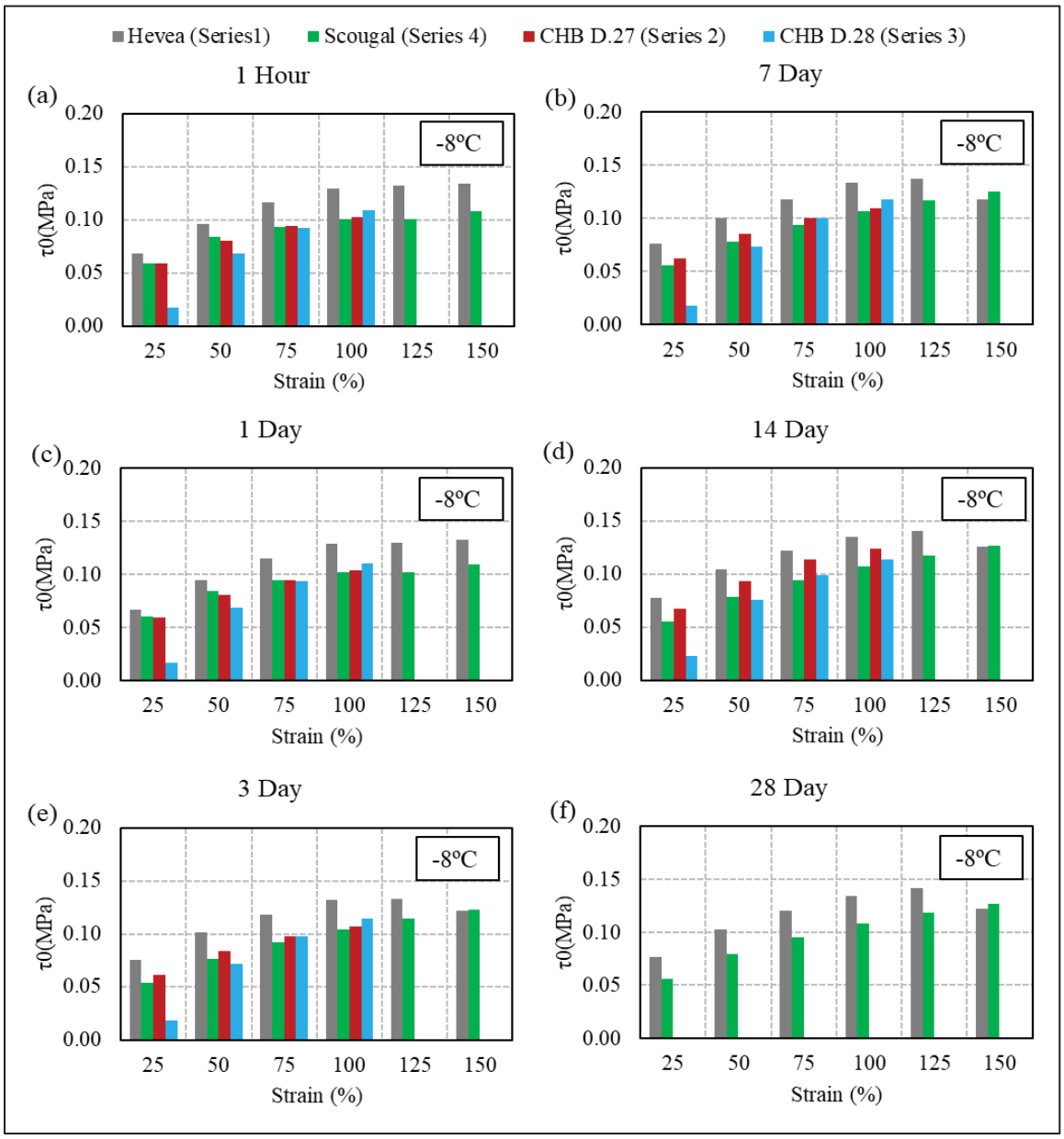

Figure 4.7 Variation in stress at zero strain of natural rubber manufactured by different suppliers under time conditioning ranging from (a) 1 hour to (f) 28 days, at -8ºC

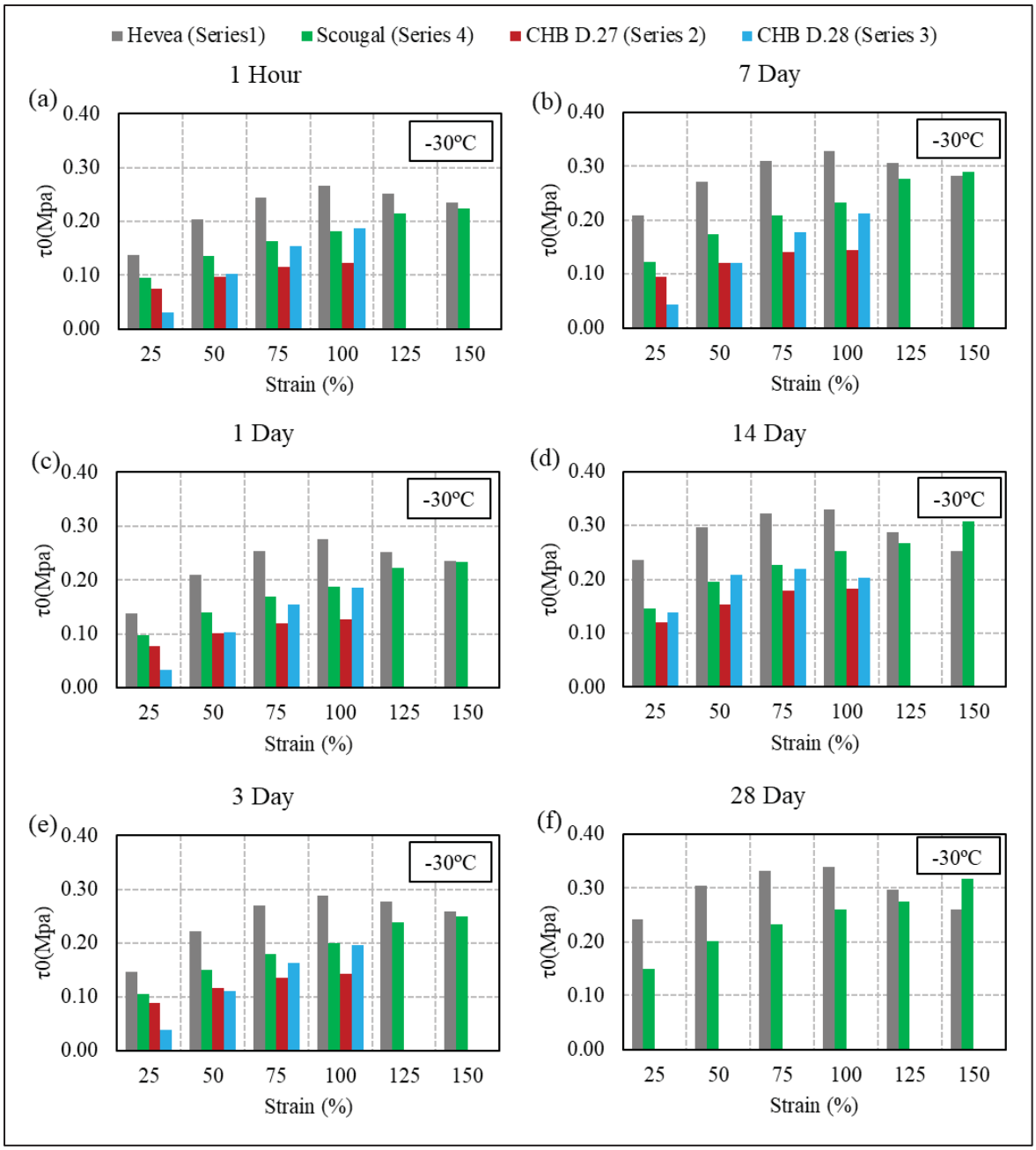

Figure 4.8 Variation in stress at zero strain of natural rubber manufactured by different suppliers under time conditioning, ranging from (a) 1 hour to (f) 28 days, at -30ºC

Table 4.7 Statistical analysis of τ_0 at 100% strain at -8ºC among Series 1 to 4

Duration at -8ºC	τ_0 (MPa), *100%*			
	Range (MPa)	Mean	SD	CV
1 Hour	$0.1009 \leq \tau_0^{100\%} \leq 0.1299$	0.1107	0.0115	0.1037
24 Hour	$0.1024 \leq \tau_0^{100\%} \leq 0.1286$	0.1113	0.0104	0.0937
3 Days	$0.1039 \leq \tau_0^{100\%} \leq 0.1320$	0.1145	0.0108	0.0945
7 Days	$0.1065 \leq \tau_0^{100\%} \leq 0.1334$	0.1170	0.0103	0.0884
14 Days	$0.1072 \leq \tau_0^{100\%} \leq 0.1351$	0.1201	0.0106	0.0879
Average			0.0107	0.0936

Table 4.8 Statistical analysis of τ_0 at 100% strain at -30ºC among Series 1 to 4

Duration at -30ºC	τ_0 (MPa), *100%*			
	Range (MPa)	Mean	SD	CV
1 Hour	$0.1220 \leq \tau_0^{100\%} \leq 0.2655$	0.1890	0.0510	0.2698
24 Hour	$0.1264 \leq \tau_0^{100\%} \leq 0.2763$	0.1938	0.0535	0.2761
3 Days	$0.1435 \leq \tau_0^{100\%} \leq 0.2878$	0.2072	0.0517	0.2497
7 Days	$0.1439 \leq \tau_0^{100\%} \leq 0.3288$	0.2297	0.0661	0.2878
14 Days	$0.1833 \leq \tau_0^{100\%} \leq 0.3299$	0.2420	0.0567	0.2344
Average			0.0558	0.2636

4.3.4 Probability distribution analysis of shear modulus

To determine the actual distribution of mechanical properties of natural rubber used in bridge isolation systems, affected by low-temperature, four types of distribution functions including the generalized extreme value distribution (GEV), the normal distribution (NORM), the lognormal distribution (LOGN), and the extreme value (EV) Type I distribution are employed, as their mathematical functions are provided in Table 4.9. These probability distribution

functions (PDFs) are chosen based on previous studies conducted by Wu et al. (2022) and Zhang and Li (2022) on probability distribution characteristics of mechanical properties of rubber bearings. These four PDFs are employed to fit the probability distribution of obtained results from different sources of rubber (Series 1 to Series 4) at room temperature (23ºC) and low temperatures of -8ºC and -30ºC, by using MATLAB 2023.

Table 4.9 Probabilistic distribution functions.

Distribution	Probabilistic distribution function
GEV	$f(x,\xi,\mu,\sigma)= \sigma^{-1}exp(1+\xi(\frac{x-\mu}{\sigma})^{\xi^{-1}})(1+\xi(\frac{x-\mu}{\sigma}))^{-1-\xi^{-1}}$
NORM	$f(x,\mu,\sigma)= \frac{1}{\sigma\sqrt{2\pi}}\, exp(\frac{-(x-\mu)^2}{2\sigma^2})$
LOGN	$f(x,\mu,\sigma)= \frac{1}{x\sigma\sqrt{2\pi}}\, exp(\frac{-(\ln x-\mu)^2}{2\sigma^2})$
EV Type I	$f(x,\mu,\sigma)= \sigma^{-1}\, exp(\frac{x-\mu}{\sigma})\, exp(-exp\,(\frac{(x-\mu)}{\sigma}))$

Figure 4.9 presents the shear modulus distribution of datasets including Series 1 to 4, obtained at 23ºC with strain amplitude ranging from 25 to 150% for Series 1 (Hevea) & Series 4 (Scougal) and ranging from 25 to 100% for Series 2 (CHB D.27) & Series 3 (CHB D.28). Similarly, Figure 4.10 presents the distribution of shear modulus obtained at -8ºC for datasets including Series 1 and Series 4 (with cold conditioning ranging from 1 hour to 28 days) as well as Series 2 and Series 3 (with cold conditioning ranging from 1 hour to 14 days). The fitting curves of the four chosen probability distributions are also shown in these figures. It is observed that the shear modulus of each Series deviates from the EV and NORM distributions, while the LOGN and the GEV distributions fit the data better.

To assess the goodness of fit of distributions to our data, the Kolmogorov-Smirnov test (KS test) is employed. This test allows us to measure how closely our data matches a given distribution. KS test considers the concepts of null and alternative hypotheses, in which the null hypothesis assumes that the sample data follows the specified distribution, and the alternative hypothesis suggests that the sample data does not follow the specified distribution.

There are two approaches available to analyze the data by KS test. The first is the critical value approach, which involves comparing the test statistic (D) to a critical value. The critical value depends on the significance level (α) chosen for the test and the sample size. If the test statistic (D) exceeds the critical value, the null hypothesis is rejected otherwise rejecting the null hypothesis fails. The latter approach is the P-value, which directly computes the P-value associated with the test statistic (D). The P-value presents the likelihood of observing a test statistic assuming the null hypothesis is true. If the p-value is less than the chosen significance level (typically 0.05), the null hypothesis is rejected otherwise rejecting the null hypothesis fails (Hollander et al., 2013).

In this study, we adopt the P-value approach using MATLAB for analysis. MATLAB provides an additional feature called the h-value, which simplifies the interpretation of the KS test results. The h-value is a binary indicator used to determine whether there is evidence to reject the null hypothesis. A value of 1 indicates rejection of the null hypothesis, implying a significant deviation of the sample data from the specified theoretical distribution. Conversely, a value of 0 indicates failure to reject the null hypothesis, suggesting insufficient evidence to conclude that the sample data deviates from the specified distribution.

Tables 4.10 & 4.11 show the KS test results for the goodness-of-fit of the probability distribution curves fitted to the shear modulus of our natural rubber sources at room temperature (23ºC) and -8ºC. A higher P-value suggests stronger evidence in favor of the null hypothesis. This means the higher the P-value, the better fit to the distribution of data. Thus, As indicated in this table, among all distributions (Lognormal, Generalized EV, Extreme value, and Normal), the Generalized EV shows an excellent match on the probabilistic distribution of shear modulus for all sources (Series 1 to Series 4) at room temperature(23ºC) and -8ºC.

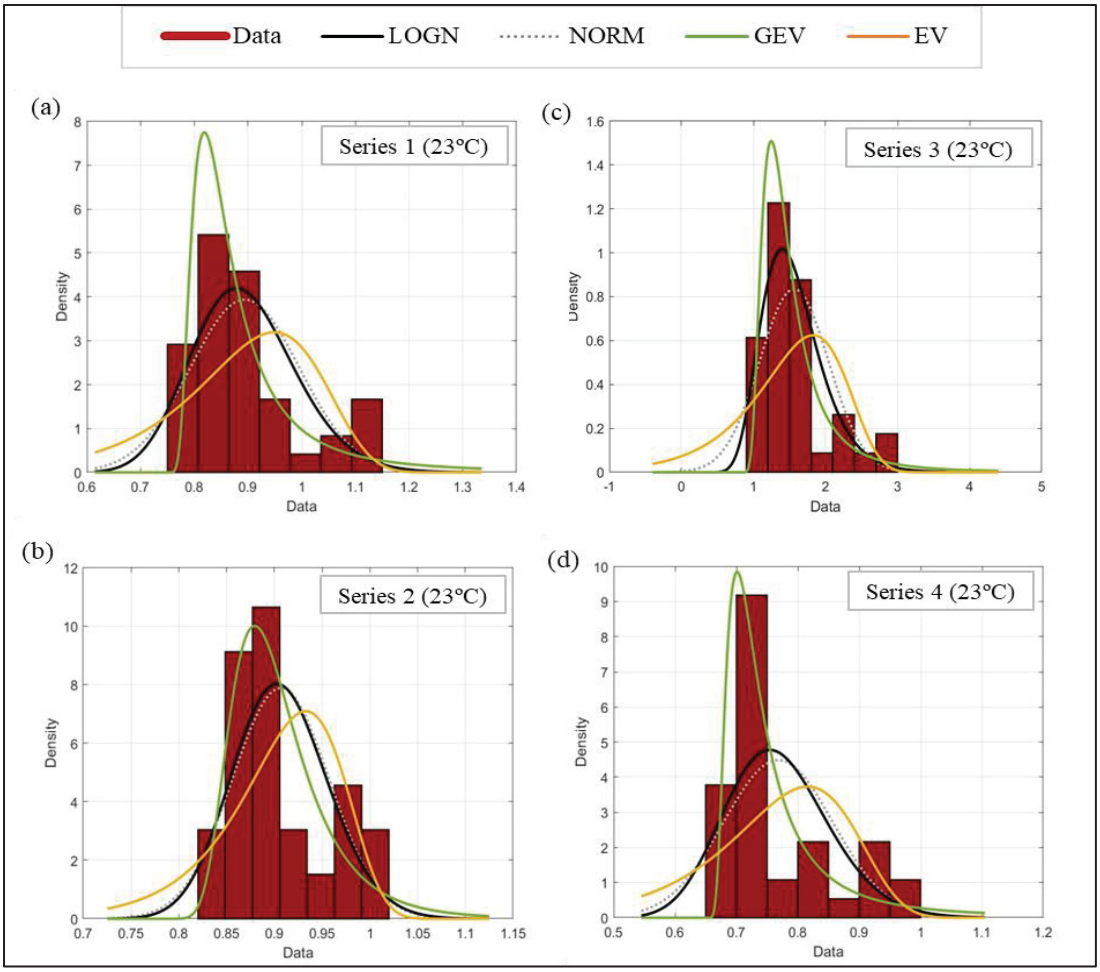

Figure 4.9 Statistical distribution of the effective shear modulus of (a) Series 1, (b) & (c) Series 2 & 3, respectively, and (d) Series 4 at 23ºC

Table 4.10 Results of the Kolmogorov-Smirnov test on PDFs for natural rubber at 23ºC

Probability Distribution	Series1 (Hevea)		Series2 (CHB.D27)		Series 3 (CHB.D28)		Series4 (Scougal)	
	h-value	*p*-value	*h*-value	*p*-value	*h*-value	*p*-value	*h*-value	*p*-value
Lognormal	0	0.446	0	0.613	0	0.618	1	0.021
Generalized EV	0	0.959	0	0.930	0	0.886	0	0.934
Extreme value	1	0.037	0	0.243	0	0.238	1	0.008
Normal	0	0.320	0	0.530	0	0.528	1	0.012

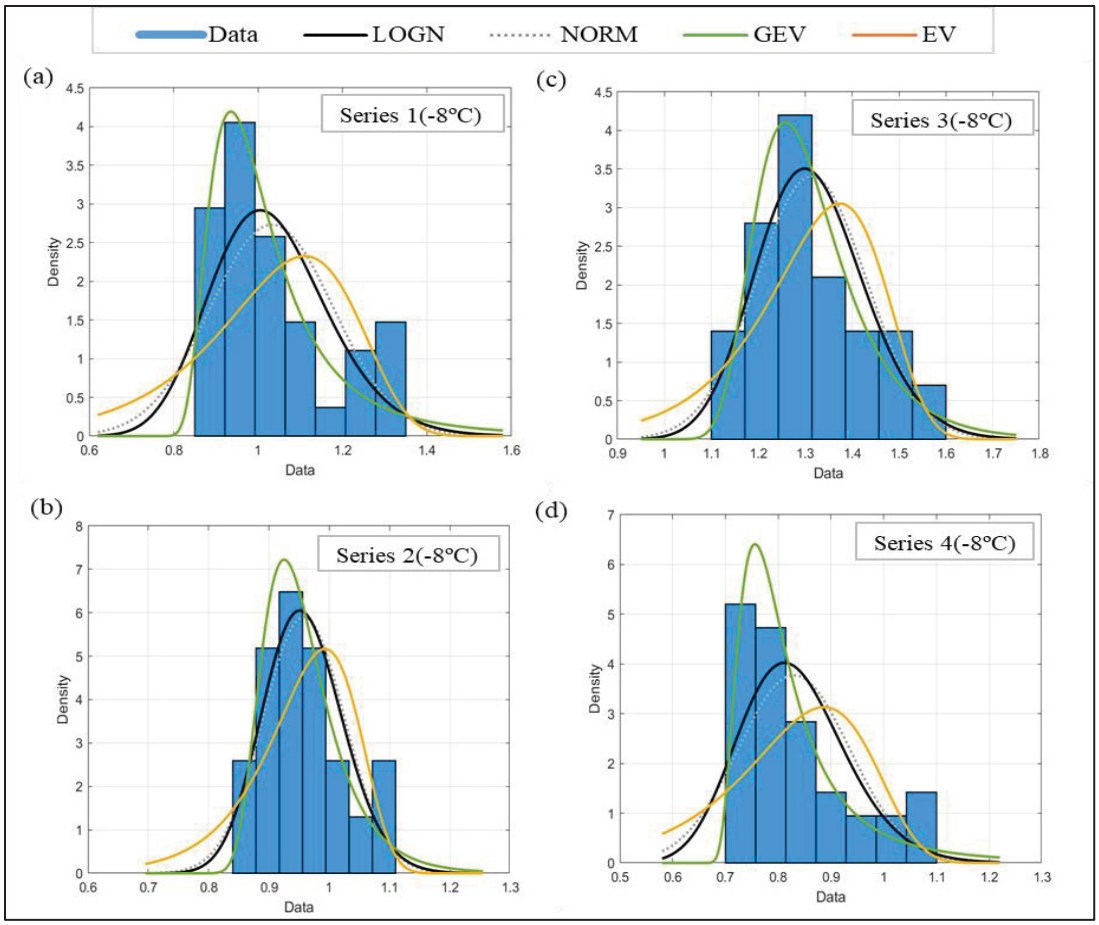

Figure 4.10 Probability distribution of shear modulus of (a) Series 1, (b) & (c) Series 2 & 3, respectively, and (d) Series 4 at -8ºC

Table 4.11 Results of the Kolmogorov-Smirnov test on PDFs for natural rubber at -8ºC

Probability Distribution	Series1 (Hevea)		Series2 (CHB.D27)		Series 3 (CHB.D28)		Series4 (Scougal)	
	h-value	*p*-value	*h*-value	*p*-value	*h*-value	*p*-value	*h*-value	*p*-value
Lognormal	0	0.319	0	0.645	0	0.958	0	0.271
Generalized EV	0	0.839	0	0.986	0	0.997	0	0.957
Extreme value	1	0.047	0	0.212	0	0.464	1	0.035
Normal	0	0.164	0	0.539	0	0.881	0	0.140

Figure 4.11 presents the distribution of shear modulus at -30ºC for our data including Series 1 (Hevea) and Series 4 (Scougal), for strain levels ranging from 25 to 150% and cold conditioning ranging from 1 hour to 28 days, as well as Series 2 (CHB D.27) and Series 3 (CHB D.28), for strain level ranging from 25 to 100% and cold conditioning ranging from 1 hour to 14 days. The fitting curves of the given probability distributions are also shown in this figure. Table 4.12 shows the KS test results for the goodness-of-fit of the probability distribution curves fitted to the shear modulus of our natural rubber sources at -30ºC.

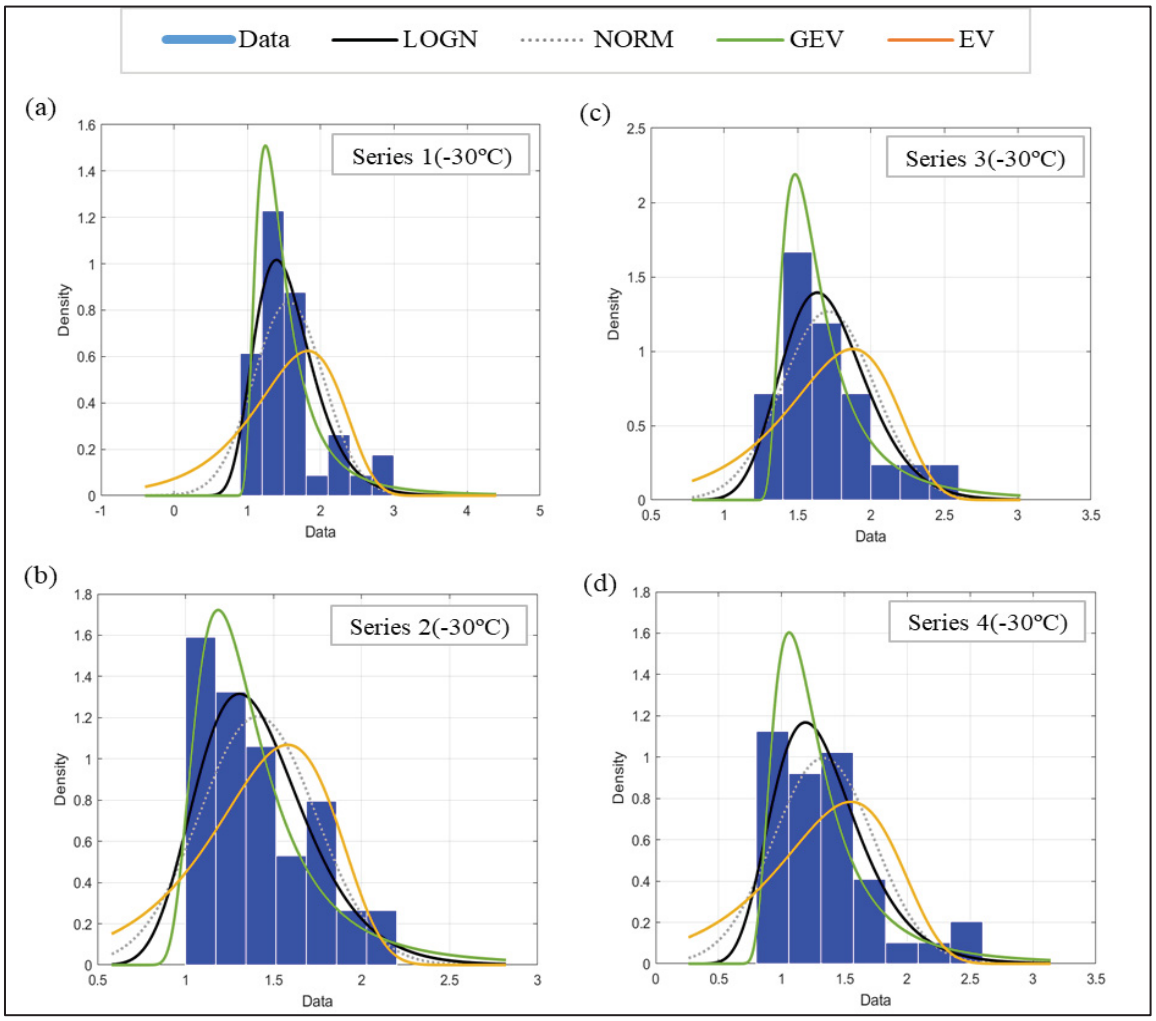

Figure 4.11 Probability distribution of shear modulus of (a) Series 1, (b) & (c) Series 2 & 3, respectively, and (d) Series 4 at -30ºC

Based on the h-value, both Lognormal and Generalized EV match the probabilistic distribution of shear modulus for all Series. However, according to the P-value, Generalized EV shows an excellent match for the probabilistic distribution of shear modulus for Series 1 (Hevea) and Series 3 (CHB D.28), while Lognormal demonstrates a better fit for Series 2 (CHB D.27) and Series 4 (Scougal) at -30ºC.

Table 4.12 Results of the Kolmogorov-Smirnov test on PDFs for natural rubber at -30ºC

Probability Distribution	Series1 (Hevea)		Series2 (CHB.D27)		Series 3 (CHB.D28)		Series4 (Scougal)	
	h-value	*p*-value	*h*-value	*p*-value	*h*-value	*p*-value	*h*-value	*p*-value
Lognormal	0	0.543	0	0.803	0	0.838	0	0.837
Generalized EV	0	0.992	0	0.673	0	0.917	0	0.828
Extreme value	1	0.034	0	0.456	0	0.259	1	0.058
Normal	0	0.131	0	0.747	0	0.810	0	0.543

CONCLUSION

The mechanical properties of natural rubber used in seismic isolation bridges vary among different sources of rubber. This variation is also affected by several factors, including temperature, duration of exposure to that temperature, and strain amplitude. The main objective of this study is to assess the variation in mechanical properties among different sources of natural rubber when exposed to low temperatures and to characterize their shear responses accordingly.

In the first phase of this study, four sources of natural rubber used in seismic isolation bridges, supplied by different suppliers in Quebec, were tested under various conditions including different low temperatures, conditioning times, strain amplitudes, and load frequencies. These sources encompass both aged and new rubber: Series 1, aged about 5 years at room temperature; Series 2 and 3 (CHB D.27 and CHB D.28), which were cut from actual-size Champlain Bridge Bearings batches D4.27 and D4.28 aged for approximately 10 years and 18 years, respectively; and Series 4 (Scougal), which was new rubber supplied by a US supplier. Samples were exposed to low temperatures, specifically -8°C and -30°C, for different conditioning times ranging from 1 hour to 28 days. They were then subjected to cyclic displacement ranging from 25% to 150% strain level to characterize the shear behaviour of rubber at low temperatures. The main conclusions obtained from the experimental tests are listed below:

- Natural rubber experienced instantaneous stiffening at low temperatures, resulting in an increase in shear modulus. Increasing conditioning time escalates this stiffening of natural rubber. However, the effect of long conditioning time, known as crystallization, is minimal at -8ºC while being pronounced at much lower temperatures (-30ºC).

- Extending cold conditioning time from 14 days to 28 days causes no significant differences in the mechanical properties of natural rubber. At the very low temperature (-30°C), increasing the conditioning period from 14 to 28 days resulted in an increase of

approximately 1 to 3% in shear modulus. This indicates that testing after 28 days of cold conditioning is unnecessary, in addition to the fact that such a period of extreme low temperature is highly improbable in all developed regions of Canada.

- Natural rubber at low temperatures is more sensitive to the strain amplitude compared to room temperatures. At low temperatures, natural rubber exhibits greater stiffness in small deformations (up to 75% strain), resulting in higher shear modulus compared to large deformations (100 to 150% strain). This means that shear modulus at low temperatures is dependent on deformation amplitude.

- low temperatures cause an increase in the equivalent viscous damping. However, by increasing the cold conditioning time, equivalent damping remains practically unchanged, and even for very long conditioning periods (14 and 28 days), it slightly decreases.

- The shear modulus of natural rubber remains relatively stable across different frequencies. When increasing the frequency from 0.1Hz to 0.5Hz, the change is marginal, ranging from 1 to 2% at -8°C and 1 to 3% at -30°C. Thus, the impact of load frequency on natural rubber behaviour at low temperatures is negligible.

- The differences in mechanical properties between the new rubber and the same rubber that has experienced the aging effect (approximately 5 years at room temperature) are significant. Aged rubber exhibits greater stiffness, with the shear modulus being approximately 10% to 15% higher than the new rubber at low temperatures. However, at room temperature, the effect of aging is less pronounced, with the shear modulus being only about 6% to 10% higher compared to new rubber. These results are slightly higher, however still consistent with the aging modification factor (=1.1) proposed in the AASHTO and CSA-S6.

- The results show that the equivalent shear modulus of the natural rubber specimens follows both Generalized extreme value and lognormal distribution functions at room temperature

(23ºC) and low temperatures (-8ºC & -30ºC). Even though, the GEV distribution shows an excellent fit at room temperature (23ºC) and -8°C.

- The statistical analysis reveals that the average of the standard deviation and the coefficient of variation among the Series of natural rubber at 100 % strain for shear modulus, in MPa, are 0.093 and 0.106 at room temperature, 0.192 and 0.199 at -8ºC, and 0.174 & 0.139 at -30ºC, respectively. For the equivalent damping ratio, these parameters are 0.788% and 0.156 at room temperature, 1.169 % and 0.176 at -8ºC, and 2.892 % & 0.282 at -30ºC, respectively. For stress at zero strain, in MPa, statistical parameters are 0.0061 and 0.0861 at room temperature, 0.0107 and 0.0936 at -8ºC, and 0.0558 & 0.2636 at -30ºC, respectively.

RECOMMENDATIONS

In light of the results and conclusions achieved in this study, future research is recommended.

- Elastomers have been subjected to the shear tests at low temperatures. However, additional tests are suggested to establish the ultimate tensile strength at low temperatures.

- In the literature and this study, tests are done at constant and specific temperatures. However, in reality, temperature is often variable and fluctuates significantly between days. One recommendation is to characterize crystallization when natural rubber is subjected to variable low temperatures to find the effect of a history of low temperatures. Therefore, cold conditioning with a thermal pattern is also desirable.

- In this study specimens were reinforced with T-shaped plates to only enhance their resistance against buckling. Thus, there is potential to improve other mechanical properties as well. Therefore, it is advisable to assess the behaviour and performance of either scaled-down samples or full-size specimens reinforced with alternative materials such as U-shape plates.

- In this study, specimens were exposed to cold temperatures for extended conditioning periods of 7 days, 14 days, and 28 days, and the crystallization curve was obtained for these durations. However, to delve deeper into the crystallization effect, additional conditioning times between 7 days and 14 days, such as 10 days and 12 days, are recommended.

BIBLIOGRAPHY

AASHTO, 2020. LRFD bridge design specifications., 9th edition. ed. American Association of State Highway and Transportation Officials, Washington, DC.

Ankik, D., 2019. Comportement sous basses températures des composés en élastomère utilisés dans les isolateurs sismiques de ponts. École de technologie supérieure, Montréal.

ASTM D4014-03, 2018. Standard Specification for Plain and Steel Laminated Elastomeric Bearings for Bridges.

ASTMD412-16, 2021. Standard Test Methods for Vulcanized Rubber and Thermoplastic Elastomers—Tension.

Barlow, F.W., 1993. Rubber compounding: principles, materials, and techniques. CRC Press.

Bhuiyan, A.R., Alam, M.S., 2013. Seismic performance assessment of highway bridges equipped with superelastic shape memory alloy-based laminated rubber isolation bearing. Engineering Structures 49, 396–407.https://doi.org/10.1016/j.engstruct.2012.11.022

Billah, A.M., Todorov, B., 2019. Effects of subfreezing temperature on the seismic response of lead rubber bearing isolated bridge. Soil Dynamics and Earthquake Engineering 126, 105814. https://doi.org/10.1016/j.soildyn.2019.105814

Broitman, E., 2016. Indentation Hardness Measurements at Macro-, Micro-, and Nanoscale: A Critical Overview. Tribology Letters 65, 23. https://doi.org/10.1007/s11249-016-0805-5

Buckle, I., Constantinou, M., Dicleli, M., Ghasemi, H., 2006. Seismic isolation of highway bridges. Multidisciplinary Center for Earthquake Engineering Research (MCEER).

Cardone, D., Gesualdi, G., 2012. Experimental evaluation of the mechanical behaviour of elastomeric materials for seismic applications at different air temperatures. International Journal of Mechanical Sciences 64, 127–143. https://doi.org/10.1016/j.ijmecsci.2012.07.008

Chen, R.A., 1995. Elastomeric bridge bearings: ozone protection, leachate analysis and a national survey on movement. University of Texas at Austin.

Ciesielski, A., 1999. An introduction to rubber technology. iSmithers Rapra publishing.

Clark, P.W., 1996. Experimental studies of the ultimate behaviour of seismically-isolated structures. University of California, Berkeley.

Constantinou, M., Whittaker, A., Kalpakidis, I., Fenz, D., Warn, G., 2007. Performance of seismic isolation hardware under service and seismic loading. https://doi.org/10.13140/RG.2.1.4633.8166

CSA, 2019. CSA, Canadian Highway Bridge Design Code, National Standard of Canada, CAN/CSA-S6-19.

CSA, 2014. CSA, Canadian Highway Bridge Design Code, 10th ed. National Standard of Canada, CAN/CSA-S6-14.

Fatemi, H., Conklin, J., 2019. Experimental Behaviour of Friction-Based EradiQuake Seismic Isolation Systems.

Fuller, K.N.G., Gough, J., Pond, T.J., Ahmadi, H.R., 1997. High damping natural rubber seismic isolators. Journal of Structural Control 4, 19–40.

Fuller, K.N.G., Gough, J., Thomas, A.G., 2004. The effect of low-temperature crystallization on the mechanical behaviour of rubber. Journal of Polymer Science Part B: Polymer Physics 42, 2181–2190.

Guizani, L., 2007. Isolation sismique et technologies parasismiques pour les ponts au Québec: Mise au point, in: 14e Colloque Sur La Progression de La Recherche Québécoise Sur Les Ouvrages d'art.

He, Z., Song, Y., Wang, J., Xu, W., Guan, H., Pang, Y., 2023. Experimental study on mechanical property degradation of thermal aging laminated rubber bearing. Case Studies in Construction Materials 18, e02060. https://doi.org/10.1016/j.cscm.2023.e02060

Hedayati .D, F., 2015. Hysteretic behaviour of steel-and fibre-reinforced elastomeric isolators fitted with superelastic shape memory alloy wire. University of British Columbia.

Hollander, M., Wolfe, D.A., Chicken, E., 2013. Nonparametric statistical methods. John Wiley & Sons.

Kelly, J.M., 1999. Analysis of fiber-reinforced elastomeric isolators. Journal of Seismology and Earthquake Engineering 2, 19–34.

Ma, Y., Jia-run, L., Jie, C., Chao-yong, S., Zhou, F., 2016. Performance deterioration tests of rubber isolators for offshore bridges under marine environment. China Journal of Highway and Transport 29, 52.

Ma, Y., Li, Y., Zhao, G., Zhou, F., 2019. Experimental research on the time-varying law of performance for natural rubber laminated bearings subjected to seawater dry-wet

cycles. Engineering Structures 195, 159–171. https://doi.org/10.1016/j.engstruct.2019.05.101

Mishra, S.K., Gur, S., Roy, K., Chakraborty, S., 2016. Response of bridges isolated by shape memory–alloy rubber bearing. Journal of Bridge Engineering 21, 04015071.

Moon, B.-Y., Kang, G.-J., Kang, B.-S., Kelly, J.M., 2002. Design and manufacturing of fiber reinforced elastomeric isolator for seismic isolation. Journal of Materials Processing Technology 130, 145–150.

Morgan, T., Whittaker, A.S., Thompson, A., 2001. Cyclic behaviour of high-damping rubber bearings, in: Proc. 5th World Congress on Joints, Bearings and Seismic Systems for Concrete Structures. American Concrete Institute Rome, Italy, pp. 7–11.

Naeim, F. (Ed.), 2001. The Seismic Design Handbook, second edition. ed. Springer US, Boston, MA. https://doi.org/10.1007/978-1-4615-1693-4

Naeim, F., Kelly, J.M., 1999. Design of seismic isolated structures: from theory to practice. John Wiley & Sons.

Nassar, M., Guizani, L., Nollet, M.-J., Tahan, A., 2022. Effects of temperature, analysis and modelling uncertainties on the reliability of base-isolated bridges in Eastern Canada, in: Structures. Elsevier, pp. 295–304.

Nobari Azar, F.A., Karimzadeh Naghshineh, A., Sen, M., 2022. Preparation and characterization of natural rubber–based new elastomers for high-damping base isolation systems. Journal of Elastomers & Plastics 54, 959–974. https://doi.org/10.1177/00952443221075505

Oh, J., Kim, J.H., 2017. Prediction of long-term creep deflection of seismic isolation bearings. Journal of Vibroengineering 19, 355–362.

Olivier, G., Adamou, S., Arnaud, B., Patrick, P., 2014. Détermination des états limites des appuis et des isolateurs de ponts dans une approche basée sur la performance sismique (Rapport final de projet de recherche exécuté par l'Université de Sherbrooke pour le Ministère des Transports du Québec No. Numéro de référence : MTQ-R716 Numéro de rapport : CRGP-2014/01). Université de Sherbrooke, Département de génie civil, 2500 Boulevard Université J1K 2R1 Sherbrooke (Qc) Canada.

Pianese, G., Van Engelen, N., Toopchi-Nezhad, H., Milani, G., 2024. High-damping fiber-reinforced elastomeric seismic isolator in different boundary conditions: An experimental insight. Engineering Structures 300, 117199. https://doi.org/10.1016/j.engstruct.2023.117199

Qayyum, B., 2016. Low temperature performance of elastomeric bearings in a full size field experimental bridge (M.S.). State University of New York at Buffalo, United States -- New York.

Rutherford, A., 2012. ANOVA and ANCOVA: A GLM Approach. Wiley.

Schaefer, R.J., 2010. Mechanical properties of rubber. Harris' Shock and Vibration Handbook, Sixth edition, A. Piersol, T. Paez (Eds), McGraw-Hill Companies Inc 33.1-33.18.

Shirazi, A., 2010. Thermal degradation of the performance of elastomeric bearings for seismic isolation. University of California – San Diego.

Taylor, A.W., Igusa, T., 2004. Primer on Seismic Isolation, Books. https://doi.org/10.1061/9780784407516

Taylor, A.W., Lin, A.N., Martin, J.W., 1992. Performance of Elastomers in Isolation Bearings: A Literature Review. Earthquake Spectra 8, 279–303. https://doi.org/10.1193/1.1585682

Thompson, A.C.T., Whittaker, A.S., Fenves, G.L., Mahin, S.A., 2000. PROPERTY MODIFICATION FACTORS FOR ELASTOMERIC SEISMIC ISOLATION BEARINGS.

Toopchi-Nezhad, H., Ghotb, M.R., Al-Anany, Y.M., Tait, M.J., 2019. Partially bonded fiber reinforced elastomeric bearings: Feasibility, effectiveness, aging effects, and low temperature response. Engineering Structures 179, 120–128.

Treloar, L.G., 1975. The physics of rubber elasticity.

Wu, D., Li, C., Yang, Z., Liu, Y., Xiong, Y., Jiang, G., 2022. Probability Distribution Characteristics of Horizontal and Vertical Mechanical Properties of Rubber Bearings. Materials 15, 8031.

Yakut, A., 2000. Performance of elastomeric bridge bearings at low temperatures. The University of Texas at Austin.

Yura, J.A., National Research Council (U.S.), American Association of State Highway and Transportation Officials, National Cooperative Highway Research Program (Eds.), 2001. Elastomeric bridge bearings: recommended test methods, NCHRP report. National Academy Press, Washington, D.C.

Zhang, R., Li, A., 2022. Probability distribution characteristics and statistical parameters of the horizontal stiffness of rubber isolation bearings. Journal of Earthquake Engineering 26, 2437–2449.

Zhang, Z., Zhou, Y., 2023. Experimental and analytical investigations on horizontal behaviour of full-scale thick rubber bearings. Soil Dynamics and Earthquake Engineering 174, 108202. https://doi.org/10.1016/j.soildyn.2023.108202

Zhou, Y., Zhang, Z., 2022. Experimental and analytical investigations on compressive behaviour of thick rubber bearings for mitigating subway-induced vibration. Engineering Structures 270, 114879. https://doi.org/10.1016/j.engstruct.2022.114879